

# **Acute Focal Micro Injury induces microglial driven activation and proliferation in CNS astrocytes**

**Dissertation zur Erlangung des Grades  
Doktor der Naturwissenschaften**

Am Fachbereich Biologie  
der Johannes-Gutenberg-Universität Mainz

Miriam Johanna Schillner  
Geboren in Vorwerk am 17.10.1992

Mainz, 2022

Dekan:

1. Gutachter\*in:

2. Gutachter\*in:

Tag der mündlichen Prüfung: 21.06.2022



**„Science is a horizon to search for – not a prize to hold in your hand”**

Shion Takeuchi, Matt Chapman, Alex Hirsch

Gravity Falls, 2014, “Little Gift Shop of Horrors”



# I Table of contents

I	Table of contents .....	i
II	Abbreviations .....	iv
III	Summary .....	viii
IV	Zusammenfassung .....	ix
V	Publications .....	xi
VI	Acute Focal Micro Injury induces microglial driven activation and proliferation in CNS astrocytes .....	1
1	Introduction .....	1
1.1	Multiple Sclerosis .....	1
1.1.1	From the “outside in” or from the “inside out” – where does it all start? .....	2
1.2	Astrocytes .....	4
1.2.1	Homeostasis – CNS maintenance .....	4
1.2.2	Damage and Disease – The spectrum of reactive astrogliosis.....	5
1.2.3	The glial scar – Dr. Jekyll or Mr. Hide? .....	6
1.3	Microglia.....	9
1.3.1	Homeostasis – CNS surveillance.....	9
1.3.2	Damage and disease – Fire fighter or fire starters? .....	10
1.3.3	Microglia priming.....	13
1.4	Focal laser injury.....	14
1.5	Astrocyte and microglia crosstalk in neuroinflammation .....	15
1.6	Designer Receptor Exclusively Activated by Designer Drugs .....	17
1.7	Project aim .....	19
2	Material & Methods .....	20
2.1	Material .....	20
2.1.1	Laboratory equipment.....	20
2.1.2	Microscopes.....	20
2.1.3	Consumables.....	21
2.1.4	Chemicals and reagents .....	22
2.1.5	Buffers, solutions and media .....	23
2.1.6	Kits and magnetic beads .....	24
2.1.7	Cytokines .....	24
2.1.8	Antibodies.....	25

2.1.9	Mouse strains .....	27
2.1.10	Software.....	28
2.2	Methods.....	29
2.2.1	Mice .....	29
	Generation of the CSF1R <sup>Cre</sup> x DREADDGq.mCitrine mouse line .....	29
2.2.2	Organotypic hippocampal slice culture (OHSC).....	29
2.2.3	Astrocytic labelling for live cell imaging in OHSCs.....	30
2.2.4	Acute Focal Micro Injury (AFMI) on OHSCs .....	30
2.2.5	Two-photon microscopy.....	31
2.2.6	Murine T cell cultures.....	31
	Isolation of APCs .....	31
	Isolation of naïve CD4 <sup>+</sup> T cells .....	32
	CD4 <sup>+</sup> T cell differentiation.....	32
	Assessment of cytokine production.....	33
2.2.7	OHSC and T cell co cultures .....	34
2.2.8	Microglia depletion in OHSC.....	34
2.2.9	Cell proliferation assay in OHSC .....	34
2.2.10	Chemogenetic activation of microglia in OHSC .....	35
2.2.11	Immunohistochemistry .....	35
2.2.12	Microscopy .....	36
	Keyence microscopy .....	36
	Confocal microscopy.....	37
2.2.13	Image analysis .....	37
	Longitudinal whole field MFI analysis .....	37
	Astrocyte and microglia MFI analysis .....	37
	Astrocyte proliferation analysis .....	38
	Colocalization analysis.....	38
	Microglia morphology analysis.....	38
2.2.14	Statistics.....	39
3	Results .....	40
3.1	Development of a laser injury model to study glial cell reaction under non-inflammatory conditions .....	40
3.2	Astrocytes and microglia show different temporal reaction patterns in response to an acute focal laser injury.....	45

3.3	Astrocytic proliferation is increased within and around the glial scar 7 days after AFMI.....	48
3.4	Astrocytic response is further elevated by inflammatory injury.....	52
3.5	DREADD-activated microglia display a shift towards a rod-like phenotype.....	57
4	Discussion .....	62
VII	References .....	71
VIII	Appendix .....	85
1	List of figures .....	85
2	List of tables .....	86
3	Curriculum vitae.....	87
IX	Acknowledgements .....	<b>Fehler! Textmarke nicht definiert.</b>



## II Abbreviations

$\mu$	micro
$\mu\text{g}$	microgram
$\mu\text{l}$	microliter
$\mu\text{m}$	micrometer
ACh	Acetylcholine
AD	Alzheimer's Disease
ADP	Adenosine Diphosphate
AF	Alexa Fluor
AFMI	Acute Focal Micro Injury
Aldh1L1	Aldehyde dehydrogenase 1 family member L1
ALS	Amyotrophic Lateral Sclerosis
ANOVA	Analysis of variance
APC	Antigen Presenting Cell
ara-C	cytosine arabinoside
ATP	Adenosine Triphosphate
BBB	Blood-Brain Barrier
BDNF	Brain Derived Neurotrophic Factor
BME	Basal Medium Eagle
BSA	Bovine Serum Albumin
C1q	Complement Component Subunit 1q
$\text{Ca}^{2+}$	Calcium
CCL	C-C motif Chemokine Ligand
CCR	C-C motif Chemokine Receptor
CD	Cluster of Differentiation
CHRM3	wildtype human muscarinic 3 receptor
CNO	Clozapine-N-oxide
CNS	Central Nervous System
$\text{CO}_2$	Carbon Dioxide
CSF1R	Colony Stimulating Factor 1 Receptor
CSPG	Chondroitin Sulfate Proteoglycan
$\text{CuSO}_4$	Copper(II) sulfate
CX3CR1	C-X3-C chemokine receptor 1
CXCL	C-X-C motif Chemokine Ligand
DAM	Disease-Associated Microglia
DAMP	Damage-Associated Molecular Pattern
DAPI	4',6-Diamidino-2-phenylindole dihydrochloride
DIV	Days <i>in vitro</i>
DMSO	Dimethylsulfoxid
DMT	Disease-Modifying Treatment
dpi	days post injury
DREADD	Designer Receptor Activated by Designer Drug

EAAT	Excitatory Amino Acid Transporter
EAE	Experimental Autoimmune Encephalitis
ECM	Extracellular Matrix
EdU	5-ethynyl-2'-deoxyuridine
EGF	Epidermal Growth Factor
eGFP	Enhanced Green Fluorescent Protein
ET	Endothelin
EtOH	Ethanol
FACS	Fluorescence-Activated Cell Sorting
FBS	Foetal Bovine Serum
FBS	Foetal Bovine Serum
FELASA	Federation for Laboratory Animal Science Association
FGF	Fibroblast Growth Factor
FN	Fibronectin
Foxp3	forkhead box P3
g	gram
G	centrifugal force
GABA	$\gamma$ -Aminobutyric Acid
GDNF	Glial-cell line Derived Neurotrophic Factor
GFAP	Glial Fibrillary Acidic Protein
GFP	Green Fluorescent Protein
GIRK	G-protein Inwardly Rectifying Potassium channels
GLAST	Glutamate and Aspartate Transporter
GLT	Glutamate Transporter
GPCR	G-Protein-Coupled Receptors
h	hour
H <sub>2</sub> O <sub>2</sub>	Hydrogen Peroxide
HEPES	4-(2-hydroxyethyl)-1-piperazineethanesulfonic acid
hM3Dq	modified human muscarinic receptor 3
hM4Di	modified human muscarinic receptor 4
Iba1	Ionized calcium-binding adapter molecule 1
IFN	Interferon
IGF	Insulin-like Growth Factor
IHC	Immunohistochemistry
IL	Interleukin
IP <sub>3</sub> R	Inositol Triphosphate Receptor
KHCO <sub>3</sub>	Potassium bicarbonate
KORD	$\kappa$ -Opioid-Derived DREADD
L	Litre
LCN2	Lipocalin 2
LPS	Lipopolysaccharide
M	Mol
MACS	Magnetic Activated Cell Sort

MBP	Myelin Basic Protein
MEM	Minimum Essential Medium
MFI	Mean Fluorescent Intensity
Mg <sup>2+</sup>	Magnesium
MHC	Major Histocompatibility Complex
min	minute
ml	millilitre
MM	Mouse Medium
mm	millimeter
MOG	Myelin Oligodendrocyte Glycoprotein
MS	Multiple Sclerosis
mW	Milliwatt(s)
Na <sub>2</sub> EDTA	EDTA disodium salt dehydrate
Na <sub>2</sub> HPO <sub>4</sub> *2H <sub>2</sub> O	Sodium phosphate dibasic dihydrate
NaH <sub>2</sub> PO <sub>4</sub> *2H <sub>2</sub> O	Sodium dihydrogen phosphate dihydrate
NaHCO <sub>3</sub>	Sodium bicarbonate
NAWM	Normal-Appearing White Matter
NF-κB	Nuclear Factor κ-light-chain-enhancer of activated B cells
NG	Nerve/Glia Antigen
NGS	Normal Goat Serum
NH <sub>4</sub> Cl	Ammonium chloride
nm	nanometer
NO	Nitric Oxide
ns	not significant
OHSC	Organotypic Hippocampal Slice Culture
OPC	Oligodendrocyte Progenitor Cell
ORM2	Orosomucoid-2
p	postnatal
P/S	Penicillin / Streptomycin
PAMP	Pathogen-Associated Molecular Pattern
PB	Phosphate Buffer
PBS	Phosphate Buffered Saline
PBSTx	Phosphate Buffered Saline with Triton X-100
PDGF	Platelet-Derived Growth Factor
PFA	Paraformaldehyde
PLP	Proteolipid Protein
PLX3377	Pexidartinib
PMT	Photon Multiplier Tube
PP	Polypropylene
R	Roundness
RM	Repeated Measures
RNA	Ribonucleic Acid

ROCK	Rho-associated Kinase
ROI	Region Of Interest
ROS	Reactive Oxygen Species
RPMI	Roswell Park Memorial Institute
RRMS	Relapsing Remitting Multiple Sclerosis
RyR	Ryanodine Receptor
s	second
SCM	Slice Culture Medium
SEM	Standard Error of the Mean
SOCE	Store Operated Calcium Entry
SPF	Specifically Pathogen Free
SPM	Slice Preparation Medium
SPMS	Secondary Progressive Multiple Sclerosis
SR101	Sulforhodamine 101
TARC	Translational Animal Research Center
TBI	Traumatic Brain Injury
TGF	Transforming Growth Factor
Th cell	T helper cell
TLR	Toll-Like Receptor
TNF	Tumor Necrosis Factor
T <sub>reg</sub>	Regulatory T cell
VEGF	Vascular Endothelial Growth Factor
WM	Wash Medium
β-ME	β-Mercaptoethanol

### III Summary

Multiple Sclerosis (MS) is a severe autoimmune disease, characterized by demyelination and neurodegeneration of the central nervous system (CNS). The cause of the disease is still debated with theories claiming that it is either initiated by autoreactive T cells invading the CNS (outside-in hypothesis) or by events within the CNS followed by infiltration (inside-out hypothesis). While the exact mechanisms of the disease development are unclear, disease progression has been demonstrated to be driven by the crosstalk of the adaptive and innate immune system. The present thesis is focused on the crosstalk between astrocytes and microglia in CNS damage and a modulation of their interaction by encephalitogenic T cells. A focal laser injury model was established producing a consistent and reproducible non-inflammatory injury in intact organotypic hippocampal slice cultures (OHSCs). A distinct temporal response pattern was observed for both microglia and astrocytes, with microglia being the first responders towards the damage and subsequently driving the ensuing astrocyte reaction. The astrocytic response consisted either in parts of the formation of a glial scar entirely through spatial rearrangements in the absence of microglia or aided by cellular proliferation driven by microglia signalling. Infiltration of pro-inflammatory Th17 cells increased astrogliosis and astrocytic proliferation, underlining the role of immune cell invasion in modulating glial activation. In a next step, the chemogenetic Designer Receptor Exclusively Activated by Designer Drugs (DREADD) model – as a non-invasive way to chronically activate cells in their intact cellular environment – was successfully established in microglia in OHSCs. Stable expression of the modified receptor hM3Dq under the *CSF1R* promotor could be shown in Iba1<sup>+</sup> microglia. DREADD-mediated activation led to a significant increase in microglia displaying a rod-like morphology potentially signifying a primed microglia phenotype. Overall, the present thesis underlines a prominent role of microglia in driving astrocytic activation and proliferation under both inflammatory and non-inflammatory conditions. Furthermore, it demonstrates the occurrence of an elusive microglia phenotype after chemogenetic manipulation.

## IV Zusammenfassung

Multiple Sklerose (MS) ist eine schwerwiegende Autoimmunerkrankung, die durch Demyelinisierung und Degeneration von Nervenzellen des zentralen Nervensystems (ZNS) gekennzeichnet ist. Die Ursache der Erkrankung wird bis heute debattiert und es wird vermutet, dass es zwei mögliche Auslöser gibt. Der Erste sind autoreaktive T Zellen, die in das ZNS Parenchym einwandern („outside-in“ Hypothese). Der Zweite, dass Vorgänge im ZNS selbst dafür verantwortlich sind und die T Zell Infiltration nachgeschaltet passiert („inside-out“ Hypothese). Während die Entstehung der Erkrankung bis heute unklar ist, konnte gezeigt werden, dass das Zusammenspiel des angeborenen und adaptiven Immunsystems für das Fortschreiten der Krankheit maßgeblich verantwortlich ist. Die vorliegende Arbeit beschäftigt sich mit der Interaktion zwischen Astrozyten und Mikroglia und deren Modulation durch ZNS-reaktive T Zellen im Kontext von ZNS Schädigung. Hierfür wurde in organotypischen hippocampalen Schnittkulturen (OHSCs) ein fokales Laser-Schaden-Modell entwickelt, welches eine konsistente und reproduzierbare nicht-inflammatorische Schädigung des Gewebes hervorruft. Astrozyten und Mikroglia zeigten ein klares zeitliches Reaktionsmuster in Bezug auf die Gewebsverletzung. Mikroglia reagierten als erstes auf den Schaden und steuerten die anschließende astrozytäre Antwort. Neben anderen Mechanismen ist das Bilden einer Glia Narbe ein wichtiger Teil der astrozytären Reaktion auf Schädigungen des ZNS Gewebes. Dies geschah hier in Abwesenheit von Mikroglia vollständig durch eine Neuordnung der Astrozyten in räumlicher Nähe zur Verletzung und in Anwesenheit der Mikroglia zusätzlich durch Zellteilung der involvierten Astrozyten. Die Infiltration peripherer pro-inflammatorischer T Zellen trug zur starken Erhöhung des Anteils sich teilender Astrozyten bei. Somit konnte gezeigt werden, dass das Eindringen von Immunzellen einen großen Einfluss auf die Modulation der Aktivierung von Gliazellen hat. Im nächsten Schritt wurde das chemogenetische DREADD Modell erfolgreich in Mikroglia in OHSCs etabliert. Diese Technik erlaubt es, Zellen auf eine nicht-invasive Art in ihrem intakten Zellverbund chronisch zu aktivieren. Der modifizierte hm3Dq Rezeptor zeigte unter der Kontrolle des *CSF1R* Promotors eine stabile Expression in Iba1<sup>+</sup> Mikroglia. Die Aktivierung der Mikroglia über das DREADD Konstrukt führte zu einem signifikanten Anstieg einer stäbchenförmigen Morphologie, welche möglicherweise eine Form prä-aktivierter (primed) Mikroglia darstellen. Insgesamt unterstreicht die hier vorliegende Arbeit eine wichtige Rolle von Mikroglia in der Steuerung der Aktivierung und Proliferation von Astrozyten unter inflammatorischen und nicht-inflammatorischen Bedingungen.

Weiterhin konnte eine bislang wenig erforschte Mikroglia Morphologie im Zusammenhang mit chemogenetischer Manipulation nachgewiesen werden.

## V Publications

- (1) **Miriam Schillner\***; Beatrice Wasser\*; Julia Loos, Katrin Pape; Julian T. Löffel; Falk Steffen; Federico Marini; Arthur Liesz; Matthias Klein; Tobias Bopp; Frauke Zipp; Stefan Bittner. *Regulatory T cells target CNS myeloid cells to control established neuroinflammation*. (in submission) \*equally contributing
- (2) Catherine Larochelle; Beatrice Wasser; H el ene Jamann; Julian T. L offel; Qiao-Ling Cui; **Miriam Schillner**; Dirk Luchtman; J er ome Birkenstock; Albrecht Stroh; Jack Antel; Stefan Bittner; Frauke Zipp. *Pro-inflammatory T-helper 17 directly harm oligodendrocytes in neuroinflammation*. 2021. PNAS. doi: 10.1073/pnas.2025813118
- (3) Julia Loos; Samantha Schmaul; Theresa Noll; Magdalena Paterka; **Miriam Schillner**; Julian T. L offel; Frauke Zipp; Stefan Bittner. *Functional characteristics of Th1, Th17 and ex-Th17 cells in EAE revealed by intravital two-photon microscopy*. 2020. J Neuroinflammation. doi: 10.1186/s12974-020-02021-x
- (4) Kerstin M uller; Andrea Schnatz; **Miriam Schillner**; Simone Woertge; Christina M uller; Ilse von Graevenitz; Ari Waisman; Jan van Minnen; Christina F Vogelaar. *A predominantly glial origin of axonal ribosomes after nerve injury*. 2018. Glia. doi: 10.1002/glia.23327





# **VI Acute Focal Micro Injury induces microglial driven activation and proliferation in CNS astrocytes**

## **1 Introduction**

### **1.1 Multiple Sclerosis**

Multiple sclerosis (MS) is a chronic autoimmune disease, characterized by inflammation, demyelination, and neuronal degeneration in the central nervous system (CNS) <sup>1,2</sup>. It affects mostly people with disease onset between 20 and 40 years and is one of the major causes of disability in younger patients <sup>3</sup>. Disease course as well as manifestation of clinical symptoms are very heterogenous and dependent largely on where the inflammatory lesions occur. About 85 % patients display a relapsing-remitting (RRMS) disease course where phases of disease progression (relapse) and recovery (remission) alternate in varying intervals. Over time, remission becomes more and more incomplete and a substantial proportion of patients transition into a secondary progressive (SPMS) disease course, where symptoms and disability gradually worsen. Clinical symptoms include visual and sensory disturbances, muscle weakness, vertigo, ataxia as well as fatigue and depression <sup>3-5</sup>.

Hallmarks of the disease are infiltration of autoreactive T cells, breakdown of the blood-brain barrier (BBB), de- and remyelination as well as neurodegeneration, axonal loss and gliosis. The interplay of these events results in typical demyelinated lesions surrounded by a glial scar that occur within white and grey matter areas throughout the CNS <sup>5-7</sup>. The CNS is capable of restoring the myelin sheath and even repairing damaged axons to a certain extent, which explains the phases of remission seen in RRMS patients <sup>8</sup>. With increasing numbers of lesions (“lesion load”) and more extensive damage to axons and neuronal soma, repair mechanisms become insufficient, thus resulting in disability progression <sup>9-11</sup>.

The factors contributing to MS pathogenesis are as heterogeneous as the disease course and symptoms displayed by patients. These range from environmental factors to genetic predispositions as well as previous viral infections <sup>12-15</sup>. Several pathways and cellular processes have been identified in connection with MS neurodegeneration so far, like mitochondrial dysfunction, accumulation of intracellular calcium, sodium and potassium channels, and glutamate excitotoxicity <sup>3,9,10,16-20</sup>. Most of these findings have been made in animal models of MS that mimic different parts of the disease depending on the exact model.

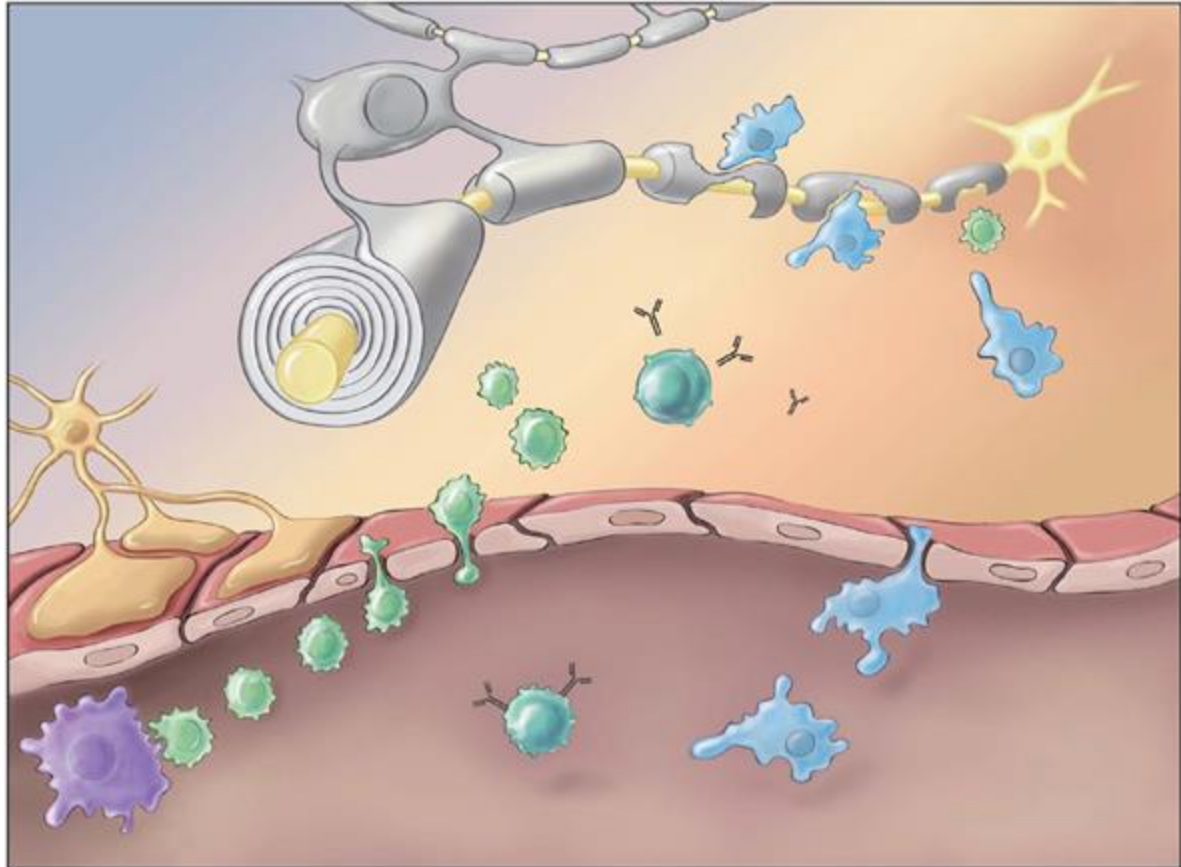


**Figure 1: Interplay of CNS resident and invading peripheral immune cells in MS.** Infiltration of autoreactive T cells into the CNS via the BBB and reactivation by antigen presentation. Mediation of demyelination and axon damage by T cells and microglia. Colour coding; grey: oligodendrocytes; yellow: neurons; green: T cells; blue: macrophages; orange: astrocytes; red: endothelial cells; purple: antigen-presenting cells, turquoise: B cells/plasma cells. Adapted from Bittner et al., 2013 <sup>18</sup>.

The most common is experimental autoimmune encephalomyelitis (EAE), in which autoreactivity is induced against one of the main proteins of the myelin sheath (myelin oligodendrocyte glycoprotein (MOG), myelin basic protein (MBP) or proteolipid protein (PLP)) <sup>21,22</sup>.

### 1.1.1 From the “outside in” or from the “inside out” – where does it all start?

While it is undisputed that CNS demyelination and oligodendrocyte injury are at the core of the MS pathology, it is unclear whether they are the cause or the consequence of neuroinflammation.

A long-standing hypothesis postulates the infiltration of autoreactive cluster of differentiation (CD) 4<sup>+</sup> T cells primed in the periphery, breaching into the CNS via the BBB where they are reactivated to perpetrate neuroinflammatory damage. Thereby recruiting the innate immune system, causing oligodendrocyte injury, demyelination and subsequently axonal loss<sup>23</sup>. The fact that focal inflammatory lesions are observed predominantly early in the disease indicates that MS develops from an outside attack.<sup>7,24,25</sup> This “outside-in” hypothesis is further supported by both the current disease-modifying treatments (DMTs), which reduce demyelinating lesions through modification of peripheral immunity and by genome-wide association studies<sup>26,27</sup>.

Another theory is that the initial damage occurs years before manifestation of symptoms from within the CNS directed to oligodendrocytes and possibly neurons. Resulting myelin debris is transported into the periphery, where it is used for antigen-presentation and priming of myelin-specific autoreactive T cells<sup>28,29</sup>. These T cells then enter the CNS, inflicting an inflammatory attack on oligodendrocytes and the myelin sheath resulting in neurodegeneration and axonal loss<sup>30</sup>. Evidence for this “inside-out” hypothesis is the occurrence of oligodendrocyte and axonal degeneration before inflammation in some types of MS lesions<sup>31</sup>, in the absence of an adaptive immune response<sup>32-34</sup> and the continuing disease progression under treatment with immunomodulatory drugs<sup>35</sup>.

Both hypotheses are linked to a number of theories suggesting a first and second hit phenomenon, where either a viral infection of the thymus<sup>13,36</sup> or a direct trauma to the brain<sup>37,38</sup> are considered a first hit that leads to immune cell activation and development of MS. Those theories are still controversial and have partially been refuted<sup>39-41</sup>. However, one could argue that especially the “inside-out” hypothesis represents a form of first and second hit.

Both theories are supported by independent lines of evidence and are to this day extensively debated<sup>27,42-44</sup>. However, there is still no conclusive answer to the question of what initially causes MS.

## 1.2 Astrocytes

### 1.2.1 Homeostasis – CNS maintenance

Astrocytes (named by Camillo Golgi for their stellar appearance) represent a heterogeneous group that fulfils many functions within the CNS network<sup>45-47</sup>. They can be derived from either neural progenitor cells, nerve/glial antigen (NG) 2 cells that also give rise to oligodendrocyte progenitor cells (OPCs) or radial glia<sup>48-50</sup>. Astrocytes typically possess several branched processes organized around the cell soma. They form tightly regulated non-overlapping domains and are interconnected creating the astrocytic syncytium<sup>46,51-54</sup>. Within the syncytium, astrocytes are connected via gap junctions and transport molecules from one astrocyte to another. Through their extensive processes astrocytes are capable of contacting and enveloping all synapses within the CNS to ensure regular neuronal functioning<sup>46</sup>. They take up and release molecules like glutamate, adenosine triphosphate (ATP) and  $\gamma$ -aminobutyric acid (GABA) in response to synaptic activity and modulate neuronal excitation and transmission. This function is called the tripartite synapse and is considered crucial for information processing and integration in the neuronal network<sup>55-57</sup>. Glutamate uptake by astrocytes via the excitatory amino acid transporters (EAAT) -1 and -2 serves several functions, like the supply of glutamine converted from glutamate to the neurons to ensure proper network function, but also the prevention of glutamate excitotoxicity by removing excess glutamate from the extracellular space<sup>58</sup>. Besides regulating neuronal signalling, astrocytes have been shown to aid axonal and dendritic growth by direct physical contact<sup>59</sup>.

Astrocytes perform further essential roles in the homeostatic brain such as maintaining the BBB and providing metabolic support for neurons, as well as modulation of myelination<sup>58,60,61</sup>.

The BBB is a physical barrier that restricts the entrance into the CNS parenchyma via the blood vessels. It is formed by endothelial cells, perivascular pericytes and the astrocytic endfeet<sup>62-64</sup>. While astrocytes are not strictly necessary for BBB formation they play a crucial role in its maintenance<sup>64</sup>. Furthermore, their contact with the vasculature serves a second purpose as they can take up glucose from the blood, distribute it along the syncytium and store it in glycogen granules. Upon hypoglycaemic conditions or high neuronal activity, astrocytes have been shown to supply glucose metabolites to neurons to ensure proper neuronal function<sup>65-68</sup>.

Astrocytes facilitate oligodendrocyte function from OPC proliferation and differentiation<sup>69-71</sup>, to maturation of oligodendrocytes<sup>72</sup> and enhancement of myelination<sup>73-75</sup>.

### 1.2.2 Damage and Disease – The spectrum of reactive astrogliosis

Astrocytes show a distinct reactivity towards CNS damage and disease, called reactive astrogliosis, that has long been believed to be functionally passive and merely an indicator of diseased tissue<sup>46</sup>. Extensive research has proven astrogliosis to contribute to numerous diseases and pathologies from traumatic injury to neurodegeneration and has shown that it is far from a homogeneous all or nothing response<sup>76-81</sup>. It represents a spectrum of changes on molecular, cellular and functional levels that depend on the form and severity of the injury and is regulated by various internal and external signalling molecules<sup>82</sup>. The definitions of reactive gliosis as well as the related terminology, while generally defined, have been used in a broad sense and inconsistently over the years<sup>83</sup>. This can be attributed to the complex nature of astrocytes and the diversity of triggers they encounter in different diseases and from different cell types (Figure 2). On the basic molecular level, reactive astrogliosis is often defined by an increase in expression of the intermediate filaments vimentin or glial fibrillary acidic protein (GFAP).

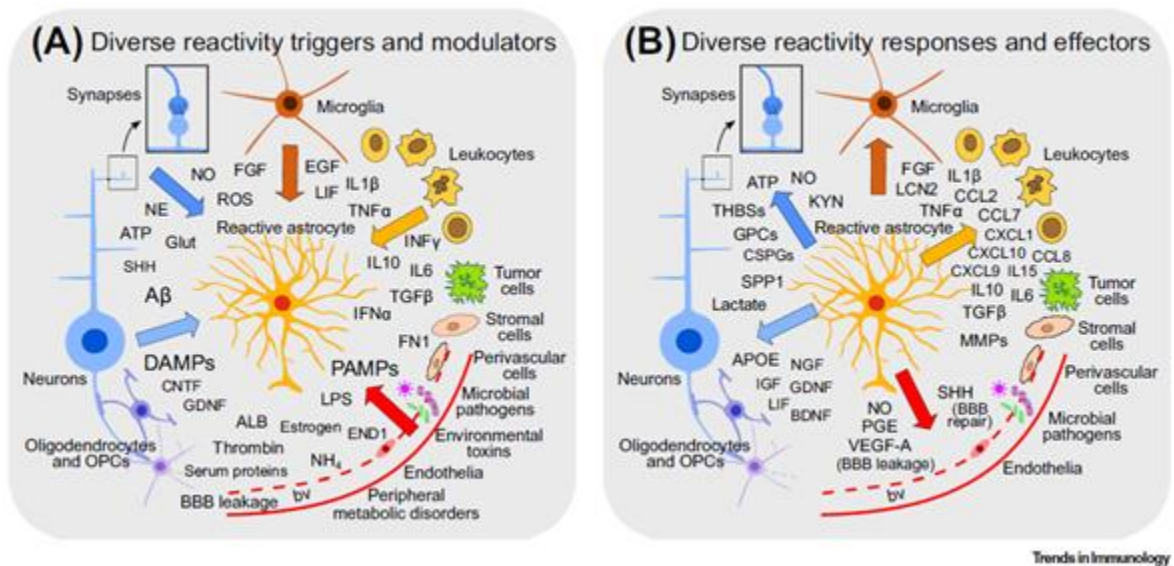


**Figure 2: Diversity of astrocytic triggers and responses.** Astrocyte reaction is modulated and shaped by a plethora of factors secreted by a variety of cell types from the CNS and the periphery. In turn, astrocytes themselves interact with those cell types shaping their reaction. Adapted from Sofroniew, 2020<sup>84</sup>.

The latter being the most commonly used marker to identify reactive astrocytes although it is not expressed uniformly by all astrocytes<sup>85</sup>. It marks mild to moderate astrocyte reaction and is observable in MS both around lesions and in normal-appearing white and grey matter<sup>86</sup>.

The consequences of reactive astrocytes in the context of MS have been linked to disease progression over the expression of the key inflammatory pathway nuclear factor  $\kappa$ -light-chain-enhancer of activated B cells (NF- $\kappa$ B) leading to myelin damage and impaired remyelination, breakdown of the BBB and the increased expression of lipocalin2 (LCN2) in EAE. This has also been shown in other disease models to increase microglia activation and recruitment of peripheral immune cells via C-C motif chemokine ligand (CCL) -2 and C-C motif chemokine receptor (CXCL) -10<sup>79,80,87,88</sup>.

The factors secreted by various cell types of the innate and adaptive immune system drive the astrocytes towards a more severe reaction marked by elongation of the cells and the formation of a glial scar around the lesion site. This is accompanied by proliferation and only occurs in a subset of astrocytes on the lesion border. Therefore, within the spectrum of astrocyte reactivity a new concept for reactive astrocyte subtypes has been proposed<sup>84</sup>. Classifying astrocytes into specific subtypes has been tried numerous times starting with the first differentiation into protoplasmic and fibrous astrocytes based on morphological characteristics that has been long standing<sup>46,89</sup>, but in recent years found to be outdated<sup>2,47</sup>. Later years saw a rise in classification of astrocytes into neuroprotective vs neurotoxic, culminating in the A1 and A2 classifications based on transcriptomic analysis<sup>90,91</sup>, which was found to be too simplistic and has now been widely rejected by astrocyte researchers<sup>92</sup>. The new proposed classification is based on the proliferation or absence thereof and separates reactive astrocytes into proliferative, border-forming reactive astrocytes and nonproliferative reactive astrocytes. While the function of proliferative reactive astrocytes seems rather clear and will be discussed in more detail in the next section, nonproliferative astrocytes are described as maintaining their position and exhibit variable levels of molecular changes in response to injury. Their activation can be transient and has the potential to be resolved in acute injury<sup>84</sup>.

### **1.2.3 The glial scar – Dr. Jekyll or Mr. Hide?**

As mentioned before, astrocytes around the lesion site undergo morphological and functional changes by forming a dense and permanent glial scar or border to separate the damaged and inflamed from the healthy tissue<sup>82,93,94</sup>. This is closely associated with proliferation of the astrocytes involved and it appears that a substantial number of border-forming astrocytes stems from cell division<sup>94,95</sup>. As proliferation rarely occurs in healthy tissue<sup>76,95,96</sup>, it can be considered a marker for reactive astrogliosis and an astrocytic subtype<sup>84</sup>.

Several molecules have been characterized that induce astrocytic proliferation including the trophic factors fibroblast growth factor (FGF), brain-derived neurotrophic factor (BDNF), glial-cell line-derived neurotrophic factor (GDNF), epidermal growth factor (EGF) and vascular endothelial growth factor (VEGF), as well endothelin-1 (ET-1) and ATP<sup>96-102</sup> secreted by various cell types. Astrocytes forming the glial border also undergo changes with increased expression of adhesion molecules, antigen presentation molecules, cytokines, growth factors and other molecules that modify the composition of the extracellular matrix (ECM)<sup>61,84</sup>.

The prevailing opinion on glial scar formation, especially in the context of demyelinating disease, is that it is detrimental and exacerbates neurodegeneration and axonal loss. While reactive astrocytes on the edge of MS lesions show increased expression of chemoattractant molecules like CXCL1, CXCL8 and CXCL10 that induces OPC migration towards the demyelinated lesion, the glial scar presents a physical barrier that the OPCs cannot overcome<sup>103-107</sup>. Furthermore, reactive astrocytes are capable of secreting ECM-modifying molecules like chondroitin sulfate proteoglycans (CSPG), which inhibits OPC differentiation and adhesion via rho-associated kinase (ROCK) and anosmin-1, thereby inhibiting oligodendrocyte differentiation<sup>108,109</sup>. Moreover, an indirect effect of reactive astrocytes on oligodendrocyte and neuronal damage is excitotoxicity. In EAE, glutamate transporters along with enzymes needed to convert the glutamate into glutamine are downregulated leading to accumulation of extracellular glutamate and excitotoxic injury<sup>110</sup>.

This view has, however, been challenged as the glial scar formation also aids in reforming the BBB and prevents further immune cell invasion into the CNS. Inhibition or attenuation of the glial scar *in vivo* have been shown to have detrimental consequences with spreading of inflammation, increased lesion size, reduced demyelination, neuronal loss, and prevention of axonal regrowth<sup>76,77,95,111-113</sup>. Therefore, astrocytes and the glial scar aid in protecting the healthy tissue from secondary degeneration by released excitotoxic molecules, nitric oxide (NO) and reactive oxygen species (ROS)<sup>114,115</sup>. In a recent study, reactive scar-forming astrocytes were found to aid regenerative efforts by preventing premature OPC differentiation in demyelination via fibronectin (FN) -1 as well as supporting OPC survival and proliferation during remyelination by secretion of insulin-like growth factor (IGF)<sup>116</sup>.



Overall, it can be said that glial scar formation is not inherently detrimental but represents a beneficial mechanism aimed at protecting the uninjured tissue and facilitating repair and regeneration. However, it is a complex system that depends on the expression of different factors at precise time points to exert its neuroprotective functions properly<sup>116</sup>. The increasing lesion load as well as the crosstalk between astrocytes, invading T cells and microglia likely disturbs this balanced mechanism resulting in the detrimental outcome of reactive astrogliosis that is observed in MS and EAE. Gaining a better understanding of glial scar formation and the influence of astrocytic interactions in the context of neuroinflammatory injury still presents a valuable research topic for therapeutic targets in the future.

## 1.3 Microglia

### 1.3.1 Homeostasis – CNS surveillance

From their first discovery in the 20<sup>th</sup> century microglia have been found in a number of pathological conditions and to be a heterogeneous group of cells involved in many CNS functions. In contrast to astrocytes, microglia do not originate from the neuroectoderm but from mesodermal progenitors in the yolk sac <sup>117</sup>. During homeostatic conditions they mostly exhibit a surveying or ramified phenotype with a small soma and many fine processes that dynamically extend or retract and form transient protrusions. Through this behaviour, microglia are constantly scanning their environment clearing metabolic products and degrading tissue components by phagocytosis <sup>118,119</sup>. As part of their surveying functions, microglia also exhibit short (~5 minutes) but frequent contacts with other CNS elements such as astrocytes, neurons and blood vessels <sup>118</sup>.

They play a key role in shaping neuronal circuits and networks by removing synapses and dendritic spines in a process termed synaptic stripping. Microglia respond to neuronal activity in a bimodal manner with contacts increasing in neuronal hypo- as well as hyperexcitability accompanied by increased microglial calcium ( $\text{Ca}^{2+}$ ) signalling <sup>120-123</sup>.

Microglia  $\text{Ca}^{2+}$  signalling is mediated by the internal  $\text{Ca}^{2+}$  storage release by both ryanodine receptors (RyRs) and inositol triphosphate receptors ( $\text{IP}_3\text{Rs}$ ) <sup>124</sup>. The intracellular  $\text{Ca}^{2+}$  release is followed by an influx of extracellular  $\text{Ca}^{2+}$  via the store operated calcium entry (SOCE) mechanism <sup>125</sup>. Since spontaneous  $\text{Ca}^{2+}$  signalling is nearly absent in surveying/ramified microglia its increase is considered an activation mechanism signifying a change in microglial state <sup>126-128</sup>.

Their role in myelination under homeostatic conditions has not been analyzed extensively as most studies focus on their involvement in neuroinflammatory pathologies, which will be discussed in the next section. Microglia-oligodendrocyte co-cultures have shown that microglia stimulate expression of MBP and PLP in oligodendrocytes <sup>129</sup>. Several studies using conditioned medium from non-activated microglia demonstrated a positive effect on OPC survival and maturation through platelet-derived growth factor (PDGF) - $\alpha$  and NF- $\kappa\text{B}$ , as well as OPC differentiation through galactin-1 and oligodendrocyte survival via IGF-2 <sup>130-132</sup>.

It should be noted however, that similar to astrocytes, the extraction of microglia from the tissue network elicits a change in their state of activation making the claim of non-activated microglia questionable<sup>84,133</sup>. Furthermore, the term “activated microglia” can be misleading as surveying microglia also present a dynamic and activated state<sup>121,134</sup>.

### 1.3.2 Damage and disease – Fire fighter or fire starters?

Through their constant surveillance of the environment and ability to recognize a broad range of molecules, microglia are prepared to respond to any type of pathological stimulus classified as damage-associated molecular patterns (DAMPs) or pathogen-associated molecular patterns (PAMPs) and shift towards an active or reactive phenotype<sup>134</sup>. Since microglia encounter cellular debris or intracellular components as part of their homeostatic surveillance and this does not elicit a change in activation, it has become clear that the microglial response is very finely regulated. Microglia possess a specific array of receptors called the sensome<sup>135</sup> and react to intracellular components if they are present in an unusually high amount. Furthermore, they are also equipped to react towards unknown stimuli like microbial components, abnormal structures like protein aggregates or stimuli indicative of a specific functional state like immunoglobulin-antigen complexes<sup>134,136,137</sup>.

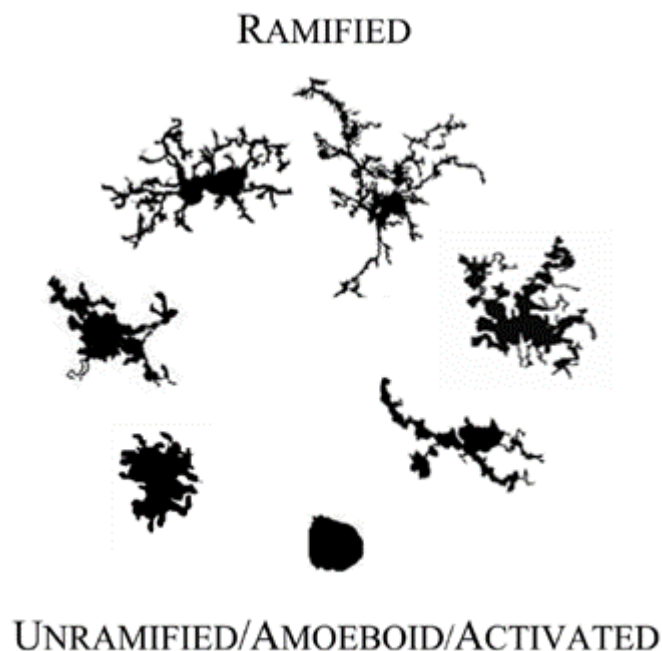


**Figure 3: Diversity of microglia morphologies found in the human CNS.** Microglia shapes even within classified descriptions are variable and cells are able to shift between them. Adapted from Karperien et al., 2013<sup>138</sup>.

Depending on the stimulus encountered, activation of microglia results in diverse phenotypes and diverse functionality<sup>134</sup>. Common microglia functions associated with a reaction towards injury include antigen-presentation, phagocytosis and secretion of both pro- and anti-inflammatory factors<sup>139</sup>.

Upon encountering a DAMP or PAMP, microglia extend more processes to the site of the damage before starting to reshape their morphology and moving towards the damage<sup>118,119</sup>. Morphological changes often consist of processes thickening and retracting to the point of them adopting an ameboid shape, which is considered a stereotypical response<sup>124,140</sup>. However, there are many more morphological shapes that have been described, as well as the ability of microglia to shift between them<sup>141</sup>. Described morphologies include bushy, activated, hyper-activated, hyper-ramified and rod-like microglia<sup>138,142</sup>. Those classifications are used inconsistently and researchers frequently fail to disclose the exact phenotypic characteristics they associate with the morphological definition<sup>138</sup>. Bushy, activated and hyper-activated microglia are often used interchangeably to describe the intermediate stages between ramified and ameboid microglia, characterized by a larger cell body and shorter processes<sup>124</sup>. Hyper-ramified microglia on the other hand show a more extensive number of branched processes and have, for example, been linked to stress responses<sup>143</sup>. Rod-like microglia still present a mystery as they have been described very early on in the context of infectious diseases, but little is known about their function<sup>141,144</sup>. They possess an elongated cell body and a bipolar distribution of their processes<sup>145</sup> and have over time been linked to a variety of CNS diseases and injuries as well as ageing<sup>141</sup>. While morphological changes in microglia have been consistently linked to pathological conditions, it is unclear to what extent they associate with microglia function and changes on a molecular level<sup>146</sup>. Moreover, a study in individuals without history of neurological, psychiatric or neuroinflammatory disease found the presence of ramified as well as ameboid and other reactive phenotypes<sup>147</sup>.

The emergence of molecular technologies like ribonucleic acid (RNA) sequencing and other omic methods have increased the understanding of microglial heterogeneity and function in the context of neuroinflammatory disease and MS. Single cell mass cytometry identified a homeostatic gene signature for microglia that undergoes disease-specific changes in EAE and APP-PS1, a murine model of Alzheimer's disease (AD)<sup>148</sup>.

Comparing the genetic phenotypes of microglia from APP-PS1, EAE and mSOD1, a murine model for amyotrophic lateral sclerosis (ALS), mice revealed common homeostatic genes like P2RY12, TMEM119, CSF1R, HEXB, MERTK and CX3CR1 that are lost during disease and identified a disease-associated microglia (DAM) gene signature with shared upregulation of inflammatory genes such as APOE, ITGAX, CCL2, CLEC7a and AXL <sup>149</sup>.

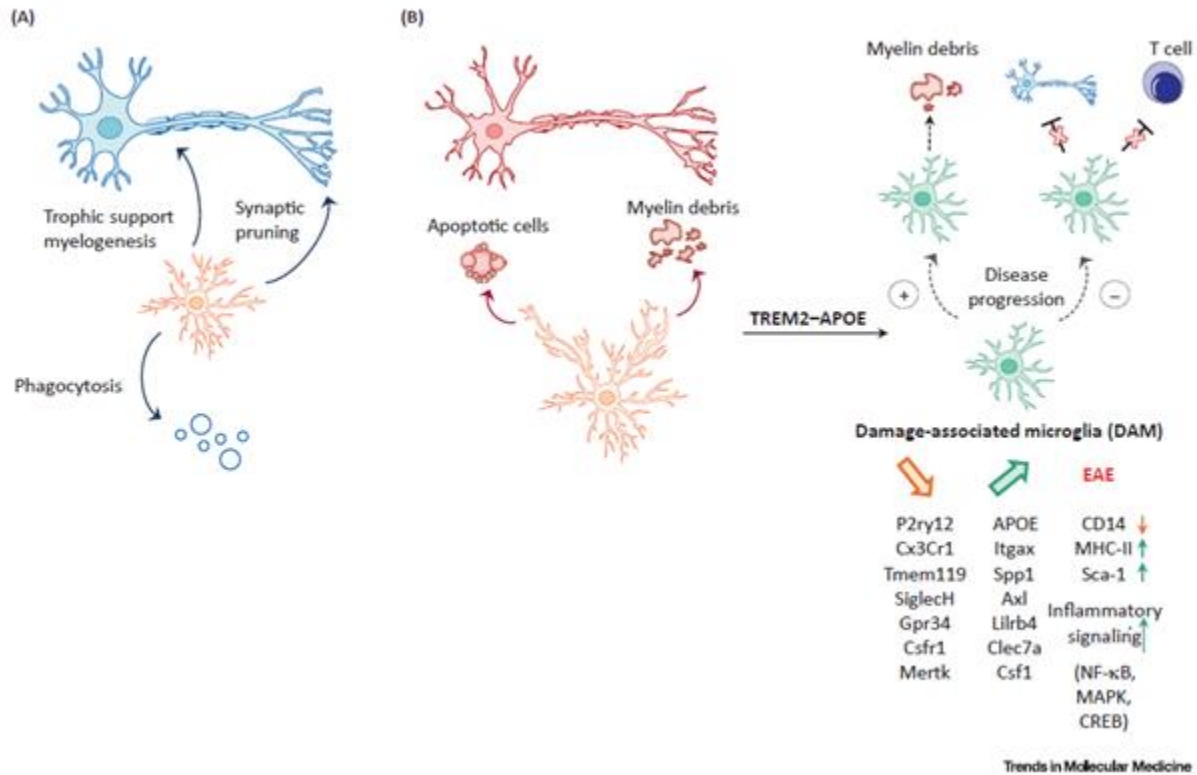


**Figure 4: Microglia function under homeostatic conditions and MS.** In homeostasis, microglia provide support to neurons and remove cellular debris by phagocytosis. In MS pathology, they lose their homeostatic signature and adopt a DAM phenotype dependent on TREM2-APOE pathways. Adapted from Voet et al., 2019 <sup>150</sup>.

Generally, microglia exhibit many functions considered detrimental in MS disease progression. Reactive microglia are found in MS lesions as well as normal-appearing white matter (NAWM), where they can form clusters. These clusters are associated with damaged axons without demyelination and T cell infiltration and are considered pre-active lesions <sup>151</sup>. Microglia in early active and chronic lesions show a phagocytic phenotype associated with tissue damage. Furthermore, they express pro-inflammatory cytokines as well as chemokines relevant for antigen-presentation, T cell recruitment and reactivation as well as oxidative injury <sup>150-152</sup>. On the other hand, they have also been shown to secrete anti-inflammatory cytokines inducing protective Th2 and regulatory T cells (T<sub>regs</sub>) or enhancing oligodendrogenesis.

Their phagocytotic capabilities also have a beneficial role in clearance of myelin debris and remyelination as well as capture of living pro-inflammatory T cells <sup>153-156</sup>. Many pathogens contain a mannosyl motive and are recognized and removed via the microglial mannose receptor. Expression levels of the mannose receptor are upregulated after anti-inflammatory interleukin (IL) -4 and downregulated after pro-inflammatory interferon (IFN) - $\gamma$  signalling further underlining a supportive role for microglial phagocytosis <sup>157</sup>.

### **1.3.3 Microglia priming**

A concept that is often brought up and discussed in relation to development and progression of neurodegenerative disease is microglia priming. It is defined as an exaggerated response to a pathological stimulus that exceeds the reaction of naïve ramified microglia. While there are conflicting reports about morphological differences compared to ramified microglia, differences on the molecular level include expression of MHCII, CD68, AXL, CD11C and LGALS3 <sup>142,158,159</sup>. Neuronal damage is considered a trigger that transiently activates microglia and leaves them in a primed state after the damage has been resolved. A secondary stimuli then triggers the enhanced response characterized by synthesis of pro-inflammatory cytokines <sup>159</sup>. Interestingly the cluster of microglia found in MS NAWM considered to be pre-active lesions have been shown to represent a primed phenotype connecting this phenomenon to disease progression in MS <sup>160</sup>.

## 1.4 Focal laser injury

A tool that has been widely used to study microglial responses in live cell imaging is the focal laser injury, where a two-photon laser beam with a high intensity is focused on small tissue area to create a localized damage resembling traumatic CNS injury. There are several advantages of using laser injury in comparison to mechanical injury. First, it allows for almost continuous live cell imaging before and after the damage at the exact same site without the need for moving the tissue to perform a mechanical injury. Second, it creates a more stable and consistent injury as the targeted area and injury depth can be set precisely, therefore reducing variability between different experiments. Lastly, when applied *in vivo* it can be used via a thinned skull window, which prevents an initial microglia activation through craniotomy, making the study of surveying microglia and the rapid changes that occur when facing damage possible. Developing this technique, Nimmerjahn and colleagues were the first ones to demonstrate the highly dynamic behaviour of surveying microglia previously called resting microglia and their rapid response upon CNS damage <sup>118</sup>. Further studies were able to show that microglia chemotaxis depends on purinergic P2Y12 receptors responding to adenosine diphosphate (ADP) or ATP released from neurons <sup>119,161</sup>. Moreover, it was shown that the laser injury-induced reaction was similar to mechanical injury further solidifying the method <sup>119</sup>. Purinergic receptors were also demonstrated to mediate intracellular increases in Ca<sup>2+</sup> in microglia processes during movement <sup>128</sup>.

**Table 1: Laser injury model parameters in published literature.** – indicates missing information. The publication from Haynes and colleagues did not specify any parameters but referred to both the Nimmerjahn and Davalos papers, therefore, it is assumed their parameters aligned with theirs.

Publication	Targeted area	Injury size	Laser power	Laser time
Nimmerjahn et al 2005 <sup>118</sup>	6 – 13 $\mu\text{m}$	-	20 – 60 mW	20 – 40 s
Davalos et al, 2005 <sup>119</sup>	$\sim 1 \mu\text{m}$	15 – 20 $\mu\text{m}$	60 – 80 mW	1 – 3 s
Haynes et al 2006 <sup>161</sup>	-	-	-	-
Pozner et al 2015 <sup>128</sup>	8 $\mu\text{m}$	10 – 15 $\mu\text{m}$	80 – 100 mW	90 s

## 1.5 Astrocyte and microglia crosstalk in neuroinflammation

Astrocyte and microglia both perform crucial functions in the CNS under homeostatic conditions and are in constant communication, not only with neurons, but also with one another. This finely balanced, bidirectional crosstalk becomes especially clear when having a look at how it contributes to neuroinflammation and -degeneration.

Microglia are the first responders to any CNS damage through their constant surveillance of the parenchyma and their reaction subsequently drives the astrocytic response. They secrete transforming growth factor (TGF)  $\alpha$  acting via the ErbB1 receptor and VEGF-B initiating FLT-1 signalling in astrocytes during EAE pathogenesis. Both signalling pathways regulate NF- $\kappa$ B in astrocytes. Knock-down of TGF- $\alpha$  on microglia exacerbated, while VEGF-B knock-down attenuated EAE suggesting a tight regulation of pro-inflammatory astrocyte responses depending on microglia signalling<sup>97</sup>. Combined secretion of IL-1 $\alpha$ , tumor necrosis factor (TNF)  $\alpha$  and complement 1q (C1q) induces upregulation of pro-inflammatory signalling in astrocytes as well as loss of phagocytotic capabilities and leads to cell death of neurons and oligodendrocytes<sup>91,162</sup>. Microglia-derived IFN- $\alpha/\beta$  has been shown to lead to a downregulation of astrocytic chemokine signalling and subsequent immune cell infiltration, signifying a protective mechanism<sup>163</sup>.

While pro-inflammatory signalling from microglia mostly drives an equally pro-inflammatory reaction in astrocytes, it can also induce the expression and secretion of orosomucoid2 (ORM2). ORM-2 acts upon the microglia C-C-motif receptor (CCR) -5 blocking microglial activation and migration thereby exerting anti-inflammatory effects<sup>164</sup>. Contrasting this mechanism, microglia are also capable of inducing LCN2, which opposes ORM2 function and has been discussed earlier as a pro-inflammatory modulator of EAE<sup>87</sup>. What determines the expression of either ORM2 or LCN2 in astrocytes after microglia signalling has so far not been answered. Reactive astrocytes are able to recruit microglia to CNS lesion sites via CXCL10 signalling for removal of myelin debris. A process that is beneficial for remyelination and regeneration as discussed earlier<sup>165</sup>.

In summary, the question if astrocyte-microglia crosstalk is detrimental or beneficial is not easily answered as it is a highly complex conversation that can be both depending on the context.



To dissect how one cell type influences the response of the other it is often necessary to be able to selectively trigger activation in only one cell type. The bacterial endotoxin lipopolysaccharide (LPS) has long been thought to be a selective activator of microglia and has been used extensively in experimental paradigms. It acts via the Toll-like receptor (TLR) -4, that is expressed on both microglia and astrocytes and was shown to also activate astrocytes<sup>166,167</sup>.

## 1.6 Designer Receptor Exclusively Activated by Designer Drugs

The need for specific and selective activation/deactivation of cell types or a subpopulation of cells have led to the development of chemical genetic or chemogenetic models using engineered proteins (for an overview of chemogenetic models in general see <sup>168</sup>). Of those, the Designer Receptor Exclusively Activated by Designer Drugs (DREADDD) model is the most commonly used <sup>169</sup>. Here, ligand-dependent G-protein-coupled receptors (GPCRs) are modified to only respond to specific pharmacologically inert compounds creating a lock-and-key system <sup>170</sup>. Several different DREADDDs have been engineered so far, that can broadly be categorized into four categories: Gq-, Gi and Gs- and  $\beta$ -Arrestin-DREADDDs <sup>169</sup>.

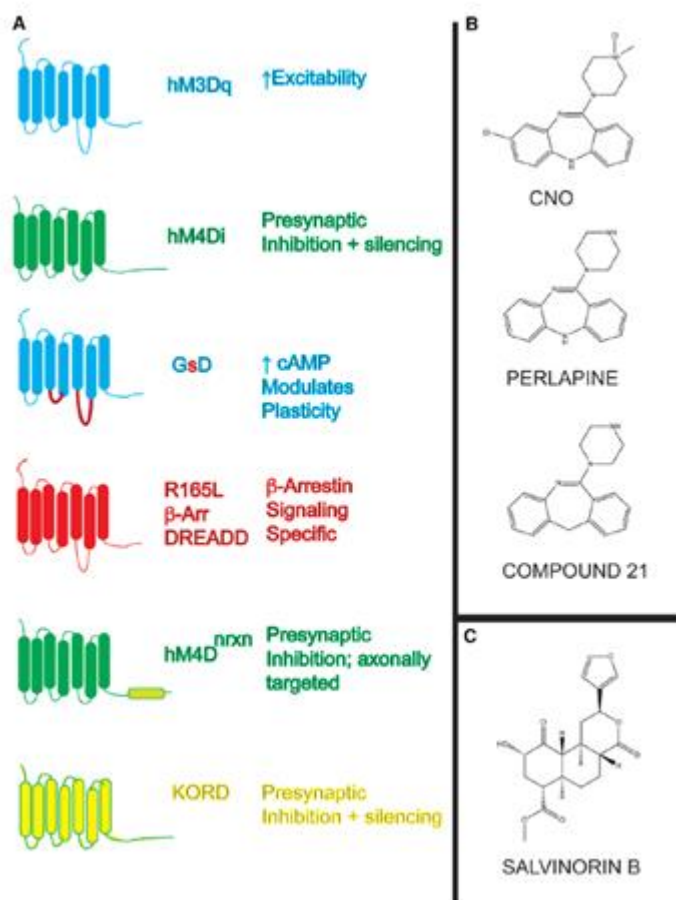


**Figure 5: Available DREADDD constructs and their ligands.** Adapted from Roth, 2016 <sup>169</sup>.

Gq-DREADDDs are excitatory constructs used to intrinsically activate cells by increasing intracellular  $\text{Ca}^{2+}$  <sup>170</sup>. They are modified human muscarinic receptors and of the three originally created only human muscarinic receptor 3 (hM3Dq) is frequently used <sup>169</sup>.

Gi-DREADDs are inhibitory constructs used to intrinsically deactivate or silence cells by using G-protein inwardly rectifying potassium channels (GIRKs) <sup>170</sup>. There are three types available, of which two are modified human muscarinic receptor with hM4Di being the most commonly used one. The third uses the  $\kappa$ -opoid-receptor DREADD (KORD) <sup>169</sup>. Gs-DREADDs are based on rat muscarinic receptor 3 <sup>171</sup>, while the  $\beta$ -Arrestin-DREADD signals exclusively via  $\beta$ -arrestin <sup>172</sup>.

Gq-, Gi-, Gs- and  $\beta$ -Arrestin-DREADDs are all able to be targeted by the inert compounds clozapine-N-oxide (CNO), perlapine and compound 21, while KORDs are only activated by salvinorin B. CNO is the most widely used ligand for DREADDs shown to be effective even in small doses and able to penetrate the BBB. It has potential for back-metabolism to clozapine but the rate and consequences of that are still debated <sup>169,173</sup>. Compound 21 or perlapine present alternatives to CNO use. Compound 21 has been shown to be a potent agonist for both hM3Dq and hM4Di <sup>173,174</sup>, while perlapine has so far only been tested on hM3Dq <sup>174</sup>.

The majority of studies have used DREADDs to enhance or silence neuronal activity of specific subpopulations or in specific regions of the CNS <sup>169,175</sup>, but there is an increasing number of publications on astrocytes <sup>176</sup> and microglia <sup>123,177</sup> in recent years.

## 1.7 Project aim

The present thesis aims to investigate the crosstalk of astrocytes and microglia as well as their interactions with encephalitogenic T cells in CNS damage. More specifically, it is focused on how the microglial activation influences the astrocytic response towards a CNS insult and how this is modified by invading T cells.

The first step was to analyze the extent and time frame of responses of both astrocytes and microglia to a non-inflammatory injury. Therefore, a focal laser injury model was established to obtain consistent and reproducible results. Utilizing this model *in vitro* in OHSCs, parameters for astrocyte and microglia activation like upregulation of specific markers and morphological changes, as well as cell migration and proliferation were analyzed at different time points after the injury.

The next step was to investigate how the innate immune system modulates the responses and interactions of astrocytes and microglia. Therefore, different types (pro- and anti-inflammatory) of CNS-antigen specific CD4<sup>+</sup> T cells were introduced to OHSCs after focal laser injury and glial responses were analyzed.

Lastly, a microglia-specific DREADD model was established within the framework of this thesis to further investigate how microglia influence and modulate astrocytic functions and responses.

## 2 Material & Methods

### 2.1 Material

#### 2.1.1 Laboratory equipment

Table 2: Laboratory equipment

Instrument	Company
Analog Vortex Mixer	VWR International GmbH, Darmstadt (Germany)
Autoclave Heraeus	Thermo Fisher Scientific, Waltham (USA)
BD FACS Canto II	BD Bioscience, Franklin Lakes (USA)
Cell Counting Chamber Neubauer improved	Brand, Wertheim (Germany)
Cell Culture Incubator	Binder GmbH, Tuttlingen (Germany)
Centrifuge Heraeus Fresco 21	Thermo Fisher Scientific Inc., Waltham (USA)
Centrifuge Multifuge Heraeus XIR	Thermo Fisher Scientific Inc., Waltham (USA)
Dissection tools	Fine Science Tools Inc., Heidelberg (Germany)
Eppendorf Research Adjustable-Volume Pipettes	Eppendorf GmbH, Wesseling-Berzdorf (Germany)
Gammacell Irradiator 2000	Institute for Virology, University Medical Center Mainz
Horizontal Laminar Flow Hood Heraguard	Thermo Fisher Scientific Inc., Waltham (USA)
IKAMAG® REC-G Magnetic Stirrer	IKA-Werke, Staufen im Breisgau (Germany)
Magnetic stand MACS	Miltenyi Biotec GmbH, Bergisch Gladbach (Germany)
McIlwain Tissue Chopper	Campden Instruments LTD, Loughborough (UK)
MidiMACS and QuadroMACS Separators	Miltenyi Biotec GmbH, Bergisch Gladbach (Germany)
Pipetus	Hirschmann Laborgeräte GmbH & Co.KG, Eberstadt (Germany)
Vertical Laminar Flow Hood SAFE 2020	Thermo Fisher Scientific Inc., Waltham (USA)
Vibratome Microm HM 650V	Thermo Scientific
Water bath Aqualine AL18	Lauda GmbH & CO. KG, Lauda-Königshofen (Germany)

#### 2.1.2 Microscopes

Table 3: Microscopes

Instrument	Company
Binocular Microscope Leica 56D	Leica Mikrosysteme Vertrieb GmbH, Wetzlar (Germany)
Keyence BZ-X710 all-in-one fluorescence microscope	Keyence Corporation, Osaka (Japan)
SP8 Confocal Microscope 6000 DM CS	Leica Mikrosysteme Vertrieb GmbH, Wetzlar (Germany)

**Table 4: MP5 two photon microscope set up**

Instrument	Company
<b>HCX IRAPO L 25×/0.95 W, FWD 2.5 mm objective</b>	Leica Mikrosysteme Vertrieb GmbH, Wetzlar (Germany)
<b>Ludin enclosure</b>	Leica Mikrosysteme Vertrieb GmbH, Wetzlar (Germany)
<b>TCS-MP5 upright multi-photon system</b>	Leica Mikrosysteme Vertrieb GmbH, Wetzlar (Germany)

### 2.1.3 Consumables

**Table 5: Laboratory consumables**

Product	Company
<b>6, 12, 24, 48-Well Multiwell Culture Plate</b>	Greiner Bio-one GmbH, Frickenhausen (Germany)
<b>Coverslips 24x60mm, 24x50mm</b>	Thermo Fisher Scientific Inc., Waltham (USA)
<b>Eppendorf tubes 0.5, 1.5, 2 ml</b>	Eppendorf GmbH, Wesseling-Berzdorf (Germany)
<b>Centrifuge Tubes, polypropylene (PP), 15 mL + 50 mL</b>	Greiner Bio-one GmbH, Frickenhausen (Germany)
<b>Microscope glass slides</b>	Thermo Fisher Scientific Inc., Waltham (USA)
<b>Filter pipette tips 10 µl, 100 µl 200 µl, 1000 µl</b>	Starlab, Hamburg (Germany)
<b>Serological pipettes 5, 10, 25, 50 ml</b>	Starlab, Hamburg (Germany)
<b>Razor Blades</b>	Wilkinson
<b>Cell strainer, nylon mesh 100 µm</b>	BD Bioscience, Franklin Lakes (USA)
<b>MACS LS Columns</b>	Miltenyi Biotec GmbH, Bergisch Gladbach (Germany)
<b>Cling film</b>	Carl Roth GmbH, Karlsruhe (Germany)
<b>Gloves Size S, M</b>	Starlab, Hamburg (Germany)
<b>Nalgene Rapid-Flow Filter Unit, 250 ml, 500 ml</b>	Thermo Fisher Scientific Inc., Waltham (USA)
<b>Pipette tips</b>	VWR International GmbH, Darmstadt (Germany)
<b>Pre-Separation Filters, 30 µm</b>	Miltenyi Biotec GmbH, Bergisch Gladbach (Germany)
<b>Millicell Cell Culture Insert, 30 mm, hydrophilic PTFE, 0.4 µm</b>	Merck Millipore, Billerica (USA)
<b>Scalpels</b>	B. Braun AG, Melsungen (Germany)
<b>Netwell Inserts 74 µm, Ø 15 mm</b>	Sigma-Aldrich Corp., St Louis (USA)
<b>Cell Culture Dish, polystyrene, Ø 60 mm + 100 mm</b>	Greiner Bio-One GmbH, Frickenhausen (Germany)

## 2.1.4 Chemicals and reagents

Table 6: Chemicals and reagents

Chemical/ reagent	Company
<b>4',6-Diamidino-2-phenylindole dihydrochloride (DAPI)</b>	Thermo Fisher Scientific, Waltham (USA)
<b>Albumin bovine fraction V (bovine serum albumin, BSA)</b>	Serva Electrophoresis GmbH
<b>Ammonium chloride (NH<sub>4</sub>Cl)</b>	Sigma-Aldrich Corp., St Louis (USA)
<b>Aqua bi. dest. sterile</b>	B. Braun AG, Melsungen (Germany)
<b>Brefeldin A</b>	Sigma-Aldrich Corp., St Louis (USA)
<b>Clozapine-N-oxide (CNO)</b>	Sigma-Aldrich Corp., St Louis (USA)
<b>D-Glucose</b>	Carl Roth GmbH, Karlsruhe (Germany)
<b>Dimethylsulfoxide (DMSO)</b>	Carl Roth GmbH, Karlsruhe (Germany)
<b>EDTA disodium salt dehydrate (Na<sub>2</sub>EDTA) solution (0.5 M)</b>	Sigma-Aldrich Corp., St Louis (USA)
<b>Ethanol 70 % (v/v) (EtOH)</b>	AppliChem GmbH, Darmstadt (Germany)
<b>Foetal Bovine Serum, heat inactivated (FBS)</b>	Biochrom AG, Berlin (Germany)
<b>Histoacryl</b>	B. Braun AG, Melsungen (Germany)
<b>Horse Serum, heat inactivated</b>	Thermo Fisher Scientific, Waltham (USA)
<b>L-Glutamine (200 mM)</b>	Sigma-Aldrich Corp., St Louis (USA)
<b>Low melt agarose</b>	Carl Roth GmbH, Karlsruhe (Germany)
<b>Minimum essential medium (MEM)</b>	Thermo Fisher Scientific, Waltham (USA)
<b>Normal Goat Serum (NGS)</b>	Vector Laboratories, Burlingame (USA)
<b>Paraformaldehyd (PFA)</b>	Carl Roth GmbH, Karlsruhe (Germany)
<b>Penicillin / Streptomycin (P/S) (10,000 units penicillin and 10 mg streptomycin per ml)</b>	Sigma-Aldrich Corp., St Louis (USA)
<b>Pexidartinib (PLX3377)</b>	Plexxikon Inc., Berkeley (USA)
<b>Potassium bicarbonate (KHCO<sub>3</sub>)</b>	Carl Roth GmbH, Karlsruhe (Germany)
<b>ProLong Gold Antifade Mountant</b>	Thermo Fisher Scientific, Waltham (USA)
<b>Saponine</b>	Carl Roth GmbH & Co. KG, Karlsruhe (Germany)
<b>Sodium bicarbonate (NaHCO<sub>3</sub>)</b>	Carl Roth GmbH, Karlsruhe (Germany)
<b>Sodium dihydrogen phosphate dihydrate (NaH<sub>2</sub>PO<sub>4</sub>*2H<sub>2</sub>O)</b>	Carl Roth GmbH & Co KG
<b>Sodium phosphate dibasic dihydrate (Na<sub>2</sub>HPO<sub>4</sub>*2H<sub>2</sub>O)</b>	Carl Roth GmbH & Co KG
<b>Sulforhodamine 101 (SR101)</b>	Thermo Fisher Scientific, Waltham (USA)
<b>Triton X-100</b>	Sigma-Aldrich Corp., St Louis (USA)
<b>Type F Immersion Liquid</b>	Leica Mikrosysteme Vertrieb GmbH, Wetzlar (Germany)
<b>β-Mercaptoethanol (β-ME)</b>	Sigma-Aldrich Corp., St Louis (USA)

## 2.1.5 Buffers, solutions and media

**Table 7: Commercially obtained buffers, solutions and media**

Buffer/ Media	Company
<b>4-(2-hydroxyethyl)-1-piperazineethanesulfonic acid (HEPES)</b>	Life Technologies Corp., Carlsbad (USA)
<b>Basal Medium Eagle (BME)</b>	Life Technologies Corp., Carlsbad (USA)
<b>Dulbecco's Phosphate-buffered saline without Ca<sup>2+</sup> &amp; Mg<sup>2+</sup> (PBS [-])</b>	Sigma-Aldrich Corp., St Louis (USA)
<b>RPMI 1640 medium</b>	Life Technologies Corp., Carlsbad (USA)

**Table 8: Custom made buffers, solutions and media**

Buffer/ Solution	Ingredients
<b>Blocking solution</b>	5% serum (NGS)+ 1% BSA in PBSTx (0.5%)
<b>BSA (10%)</b>	1 g BSA in 10 ml PBS
<b>CNO (2mM)</b>	5 mg CNO, 36.45 µl DMSO in 7.29 ml PBS
<b>DAPI stock solution</b>	5 µl in 49.5 ml Aqua dest. sterile
<b>EdU reaction cocktail (for one sample, modified for free floating OHSC staining)</b>	1329 µl 1x Click-iT™ reaction buffer + 20 µl CuSO <sub>4</sub> + 1 µl Alexa Fluor® azide 647 + 150 µl 1x reaction buffer additive
<b>FACS Buffer</b>	0.5 % BSA in PBS
<b>Glucose solution (20%)</b>	20 g D-Glucose in 100 ml Aqua dest. sterile
<b>Lysis buffer</b>	8.29 g/l NH <sub>4</sub> Cl, 1 g/l KHCO <sub>3</sub> , 37.2 mg/l Na <sub>2</sub> EDTA in dH <sub>2</sub> O
<b>MACS buffer</b>	0.5 % BSA, 0.5 M EDTA in PBS
<b>MEM (2x)</b>	160.93 g MEM, 0.35 g NaHCO <sub>3</sub> in 5 L dH <sub>2</sub> O
<b>Mouse Medium (MM)</b>	10 % FCS, 1 % P/S, 1 % L-Glutamine, 0.1 % β-mercaptoethanol, 1 % HEPES in RPMI
<b>NH<sub>4</sub>Cl (50 mM)</b>	0.133 g NH <sub>4</sub> Cl in 50 ml PBS
<b>PB</b>	810 ml of solution A (Na <sub>2</sub> HPO <sub>4</sub> *2H <sub>2</sub> O in 2 L dH <sub>2</sub> O) + 190 ml of solution B (NaH <sub>2</sub> PO <sub>4</sub> *2H <sub>2</sub> O in 1 L dH <sub>2</sub> O) in 1 L dH <sub>2</sub> O, pH 7.35-7.4
<b>PBSTx (0.5%)</b>	500 µl Triton-X 100 ml in PBS
<b>Saponine buffer</b>	25 ml Saponine in 475 ml FACS buffer
<b>Slice culture medium</b>	50 ml 2x MEM + 41.8 ml Aqua dest. sterile + 50 ml BME + 50 ml heat inactivated horse serum + 2 ml 200 mM L-Glutamine + 6.25 ml 20 % Glucose, pH 7.2
<b>Slice preparation medium</b>	100 ml 2x MEM + 98 ml Aqua dest. sterile + 1 ml 200 mM L-Glutamine, pH 7.35
<b>Wash Medium (WM)</b>	5 % FCS, 1 % P/S, 1 % HEPES in RPMI



## 2.1.6 Kits and magnetic beads

**Table 9: Commercial kits**

Kit	Company
<b>Click-iT™ EdU Cell Proliferation Kit for Imaging, Alexa Fluor® 647 dye</b>	Thermo Fisher Scientific, Waltham (USA)
<b>CD4 T cell isolation kit</b>	Miltenyi Biotec GmbH, Bergisch Gladbach (Germany)
<b>eBioscience™ Foxp3 / Transcription Factor Staining Buffer Set</b>	Invitrogen, Carlsbad (USA)

**Table 10: Magnetic beads**

Kit	Isotype	Company
<b>CD62L MicroBeads</b>	rat- $\alpha$ -mouse monoclonal IgG2a	Miltenyi Biotec GmbH, Bergisch Gladbach (Germany)
<b>CD90.2 MicroBeads</b>	rat- $\alpha$ -mouse monoclonal IgG2b	Miltenyi Biotec GmbH, Bergisch Gladbach (Germany)

## 2.1.7 Cytokines

**Table 11: Cell culture cytokines**

Cytokines	Company
<b>human TGF-<math>\beta</math></b>	R&D Systems, Minneapolis (USA)
<b>IL-12</b>	BioXCell, West Lebanon (USA)
<b>IL-18</b>	MBL, Woburn (USA)
<b>IL-2</b>	R&D Systems, Minneapolis (USA)
<b>IL-23</b>	R&D Systems, Inc., Minneapolis (USA)
<b>IL6</b>	R&D Systems, Minneapolis (USA)
<b><math>\alpha</math>CD28</b>	BD Bioscience, Franklin Lakes (USA)
<b><math>\alpha</math>CD3</b>	BD Bioscience, Franklin Lakes (USA)
<b><math>\alpha</math>IFN<math>\gamma</math></b>	BioXCell, West Lebanon (USA)
<b><math>\alpha</math>IL12</b>	BioXCell, West Lebanon (USA)
<b><math>\alpha</math>IL4</b>	BioXCell, West Lebanon (USA)

## 2.1.8 Antibodies

**Table 12: Immunohistochemistry – primary antibodies**

Antibody	Species	Dilution	Company
<b><math>\alpha</math>GFAP</b>	rabbit	1:1000	Merck Millipore, Billerica (USA)
<b><math>\alpha</math>GFAP</b>	mouse	1:1000	Sigma-Aldrich Corp., St Louis (USA)
<b><math>\alpha</math>GFP</b>	mouse	1:1000	Synaptic Systems GmbH, Göttingen (Germany)
<b><math>\alpha</math>Iba1</b>	rabbit	1:500	FUJIFILM Wako Pure Chemical Corporation, Osaka (Japan)

**Table 13: Immunohistochemistry – secondary antibodies**

Antibody	Species	Dilution	Company
<b><math>\alpha</math>Mouse Alexa Fluor® 488</b>	goat	1:1000	Invitrogen, Carlsbad (USA)
<b><math>\alpha</math>Mouse Alexa Fluor® 488</b>	donkey	1:1000	Invitrogen, Carlsbad (USA)
<b><math>\alpha</math>Mouse Alexa Fluor® 568</b>	goat	1:1000	Invitrogen, Carlsbad (USA)
<b><math>\alpha</math>Mouse Alexa Fluor® 647</b>	goat	1:1000	Invitrogen, Carlsbad (USA)
<b><math>\alpha</math>Mouse Alexa Fluor® 647</b>	donkey	1:1000	Invitrogen, Carlsbad (USA)
<b><math>\alpha</math>Rabbit Alexa Fluor® 488</b>	goat	1:1000	Invitrogen, Carlsbad (USA)
<b><math>\alpha</math>Rabbit Alexa Fluor® 488</b>	donkey	1:1000	Invitrogen, Carlsbad (USA)
<b><math>\alpha</math>Rabbit Alexa Fluor® 568</b>	goat	1:1000	Invitrogen, Carlsbad (USA)
<b><math>\alpha</math>Rabbit Alexa Fluor® 568</b>	donkey	1:1000	Invitrogen, Carlsbad (USA)

**Table 14: FACS antibodies**

Antibody	Clone	Isotype	Concentration	Company
<b><math>\alpha</math>CD16/ <math>\alpha</math>CD32 (FC-block)</b>	2.4G2	rat- $\alpha$ -mouse monoclonal IgG2b, $\kappa$	0.5 mg/ml	BD Bioscience, Franklin Lakes (USA)
<b><math>\alpha</math>CD4-PECy7</b>	RM4-5	rat- $\alpha$ -mouse polyclonal IgG	0.2 mg/ml	BD Bioscience, Franklin Lakes (USA)
<b><math>\alpha</math>CD62L-APC</b>	MEL-14	rat- $\alpha$ -mouse monoclonal IgG2a, $\kappa$	0.2 mg/ml	BD Bioscience, Franklin Lakes (USA)
<b><math>\alpha</math>FoxP3-PECy7</b>	FJK-16s	rat- $\alpha$ -mouse monoclonal IgG2a, $\kappa$	0.2 mg/ml	Thermo Fisher Scientific, Waltham (USA)
<b><math>\alpha</math>IFN-<math>\gamma</math>-Horizon (V450)</b>	XMG1.2	rat- $\alpha$ -mouse monoclonal IgG1, $\kappa$	0.2 mg/ml	BD Bioscience, Franklin Lakes (USA)
<b><math>\alpha</math>IL-17A-APC</b>	eBio17B7	rat- $\alpha$ -mouse monoclonal IgG2a, $\kappa$	0.2 mg/ml	Thermo Fisher Scientific, Waltham (USA)
<b><math>\alpha</math>TNF-<math>\alpha</math>-AF700</b>	MP6- XT22	rat- $\alpha$ -mouse monoclonal IgG1, $\kappa$	0.2 mg/ml	BD Bioscience, Franklin Lakes (USA)
<b><math>\alpha</math>V<math>\beta</math>11-FITC</b>	RR3-15	rat- $\alpha$ -mouse monoclonal IgG2b, $\kappa$	0.1 mg/ml	BD Bioscience, Franklin Lakes (USA)

## 2.1.9 Mouse strains

Table 15: Laboratory mouse strains

Strain	Genetic modification	Origin	Reference
<b>C57BL/6</b>	None (wildtype)	Janvier Labs, Laval (France)	-
<b>B6.Tg(Aldh111-EGFP,-DTA)D8Rth/J (Aldh111-eGFP)</b>	Astrocyte specific expression of eGFP	Jackson Laboratory (#026033)	Tsai et al., 2012 <sup>178</sup>
<b>B6.2D2</b>	MOG <sub>35-55</sub> specific CD4 <sup>+</sup> T cells	in house breeding	Bettelli et al., 2003 <sup>179</sup>
<b>B6.2D2.RFP</b>	MOG <sub>35-55</sub> specific CD4 <sup>+</sup> T cells labeled with red fluorescent protein	in house breeding	B6.2D2 x B6.acRFP
<b>C57BL/6-Tg(Csf1r-cre)1Mnz/J</b>	Expression of Cre recombinase under the <i>Csf1r</i> promotor	Jackson Laboratory (#029206)	Loschko et al., 2016 <sup>180</sup>
<b>B6N;129-Tg(CAG-CHRM3*,-mCitrine)1Ute/J</b>	Floxed HA- and mCitrine-tagged hM3Dq mutant receptor	Jackson Laboratory (#026220)	Zhu et al., 2016 <sup>181</sup>
<b>CSF1R<sup>Cre</sup> x DREADD<sub>Gq</sub>.mCitrine</b>	Expression of a mutant hM3Dq construct under the CSF1R promotor	in house breeding	Loschko et al., 2016 <sup>180</sup> , Zhu et al. 2016 <sup>181</sup>

## 2.1.10 Software

**Table 16: Software**

Software	Application	Company
<b>Adobe Illustrator CS 6</b>	Figure layout	Adobe Systems Inc.
<b>Endnote X7</b>	Citation management	Clarivate, Boston (USA)
<b>FACS Diva</b>	FACS analysis	BD Bioscience, Franklin Lakes (USA)
<b>Fiji (ImageJ) <sup>182</sup></b>	Image analysis*	National Institutes of Health, Bethesda (USA)
<b>GraphPad Prism 9</b>	Statistical analysis	GraphPad Software, Inc., La Jolla (USA)
<b>Keyence BZ-X710 software</b>	Keyence image acquisition	Keyence Corporation, Osaka (Japan)
<b>LAS-X</b>	Two-photon and confocal image acquisition	Leica GmbH, Wetzlar (Germany)
<b>Office 2016</b>	Document and table writing	Microsoft Corp., Redmond (USA)

\*The following FIJI plugins were used for image analysis: Colocalization threshold, Particle Analysis, Cell counter.

## 2.2 Methods

### 2.2.1 Mice

All experiments were conducted under the German Animal Welfare Law, approved by local authorities and in accordance with the guidelines of the Federation for Laboratory Animal Science Associations (FELASA). Animals were kept under specifically pathogen free (SPF) conditions in the animal housing facility of the Translational Animal Research Center (TARC) Mainz and the University Medical Center of the Johannes Gutenberg University Mainz. Mice were housed in groups of 2-5 animals in ventilated cages with food and water ad libitum. A stable 12 h dark/ light cycle was maintained.

#### **Generation of the CSF1R<sup>Cre</sup> x DREADD<sub>Gq</sub>.mCitrine mouse line**

The CSF1R<sup>Cre</sup> x DREADD<sub>Gq</sub>.mCitrine was generated by crossbreeding of two mouse lines: the C57BL/6-Tg(Csf1r-cre1)Mnz/J mouse line, which expresses a Cre recombinase protein under the colony stimulating factor 1 receptor (CSF1R) promoter, and B6N;129-Tg(CAG-CHRM3\*,-mCitrine)1Ute/J, a mouse line, that has a floxed modified hM3Dq (also called CHRM3\*) together with a mCitrine fluorescent tag. The hM3Dq receptor was modified from the wildtype human muscarinic 3 receptor (CHRM3) by targeted mutagenesis of two amino acids. The mutation resulted in complete abolishment of affinity for acetylcholine (ACh, natural ligand) and introduced a new affinity for the small molecule CNO, which has no endogenous target within the organism. This effectively creates a receptor that can only be activated by a molecule that is normally inert within the body or more specifically a “Designer Receptor Exclusively Activated by Designer Drug” (DREADD) as the construct has been named by its developers<sup>183</sup>. Crossbreeding of the two mouse lines results in the removal of the floxed stop cassette by the Cre recombinase and expression of the hM3Dq receptor in CSF1R expressing myeloid cells.

### 2.2.2 Organotypic hippocampal slice culture (OHSC)

OHSCs were prepared using a modified version of the protocol developed by Gogolla et al.,<sup>184,185</sup>. For all experiments, mouse pups between the postnatal age of 3 to 7 days (p3-7) were used. Before tissue collection, 6-well culture plates were prepared by placing cell culture inserts in each well containing 1.2 ml slice culture medium (SCM). Culture plates were placed in the incubator for pre-warming of the medium and to ensure CO<sub>2</sub> saturation. Small petri-dishes were filled with 5 ml slice preparation medium (SPM) and kept at 4 °C. Two petri-dishes per animal were prepared.

To avoid contamination all tissue collection was performed under a horizontal laminar flow semi-sterile hood. A Leica 56D binocular microscope was used for magnification. Dissection tools were sterilized using dry heat (200 °C for 2 h) between slice culture preparations and cleaned with 70 % EtOH during preparation. Pups were sacrificed and their brains collected in a petri dish with cold SPM. Brain hemispheres were cut along the longitudinal fissure and separated from the midbrain. After removal of the meninges, hippocampi with parts of the entorhinal cortices were extracted and put on to a McIlwain tissue chopper. Hippocampal tissue was cut into 300 µm thick slices and transferred into a fresh petri dish with cold SPM. Slices being intact, showing clear hippocampal structures and having some entorhinal cortex attached were transferred to the previously prepared cell culture membranes. Depending on the experiment, different numbers of slices per membrane were cultured: 6 for immunohistological stainings and 3 for two-photon microscopy. All slice preparation steps were performed in 15 minutes or less to avoid tissue degeneration and cell death. Slices were cultured at 37 °C with 95 % humidity and 5 % CO<sub>2</sub>. SCM was changed 24 hours after slice preparation and every two to three days after that.

### **2.2.3 Astrocytic labelling for live cell imaging in OHSCs**

For *ex vivo* slice imaging of astrocytes, a counterstaining was used to ensure sufficient astrocytic labelling in cultures from heterozygous Aldh1L1-eGFP litters. Counterstaining was performed using the live cell fluorescent dye SR101, which is a widely used compound for *in* and *ex vivo* astrocytic labelling<sup>186-190</sup>. After applying SR101, the dye is taken up by astrocytes and transported via gap junctions throughout the astrocytic syncytium<sup>191,192</sup>. SR101 stock solution (1 mM) was diluted in SCM to a working concentration of 1 µM and added on top of and under the slice culture insert to ensure uniform coverage. OHSCs were incubated for 20 minutes and washed with fresh SCM for 8 minutes before two photon microscopic imaging. OHSCs from homozygous Aldh1L1-eGFP litters were not labelled with SR101.

### **2.2.4 Acute Focal Micro Injury (AFMI) on OHSCs**

Cell culture inserts from OHSCs were transferred to a small cell culture dish (60 mm) filled with pre-warmed SCM and placed into the specimen stage of the TCS MP5 two photon microscope. The microscope enclosure was heated (37 °C), humidified and gas perfused (95% O<sub>2</sub>, 5% CO<sub>2</sub>) to ensure survival of cells and tissue sections during the procedure. The selected area of the hippocampus was the CA1 region. Upper and lower limits of the slice were determined and the focal plane was set to the middle of the slice.

A laser beam with a wavelength of 850 nm was focused on an area 30x30  $\mu\text{m}$  and the photon multiplier tube (PMT) shutters were closed to prevent them from being damaged. Laser power intensity and duration of laser application were varied to determine optimal parameters (see results 3.1). To make sure the injury procedure worked, a z-stack of the entire slice was taken and checked for appearance of a typical bright autofluorescent sphere at the injury site. Control slices were handled the same way as AFMI slices except for the laser injury. After performing laser injury on all slices present on the cell culture inserts, they were placed back into their cell culture well containing fresh, pre-warmed SCM or used immediately for further experimental steps.

### **2.2.5 Two-photon microscopy**

AFMI development over time was analyzed by longitudinal two-photon microscopy. Slices that received an AFMI and control slices were transferred to the MP5 two-photon microscope as described above (see methods 2.2.4) and z-stacks covering the entire slice were acquired at 850 nm using a HCX IRAPO L 25x/0.95 W, FWD 2.5 mm objective. Z-stacks were obtained 1 and 7 days post injury (dpi).

### **2.2.6 Murine T cell cultures**

For all T cell cultures used in the experiments, naïve T cells and antigen presenting cells (APCs) were obtained using magnetic activated cell sort (MACS) and co-cultured as follows. Centrifugation steps were performed at 550 G for 5 minutes at 4 °C unless specified otherwise.

#### **Isolation of APCs**

C57BL/6J mice (6-12 weeks old) were sacrificed by cervical dislocation. Spleens were collected and transferred to 5 ml WM in a 15 ml falcon tube. To create a single cell suspension, spleens were meshed through a 100  $\mu\text{m}$  cell strainer. After centrifugation, 10 ml lysis buffer was added to the cells to break down the erythrocytes present in the cell suspension. Lysis was stopped with 5 ml of WM and cells were centrifuged. The cell pellet was resuspended in an appropriate amount of MACS buffer and cells were counted manually using a Neubauer counting chamber to determine the necessary reagent volume for the bead-based MACS. Another centrifugation step was performed, cells were resuspended in 95  $\mu\text{l}$  MACS buffer and 5  $\mu\text{l}$  CD90.2 magnetic beads for every  $10^7$  cells and incubated for 15 minutes at 4 °C. The CD90.2 beads were used to label splenic lymphocytes, which possess no antigen presenting capacities and were subsequently fixated in the magnetic field between magnet and LS column and removed during the magnetic cell sort.



Unlabelled APCs collected in the flow-through of the sort were centrifuged and resuspended in 10 ml sterile filtered MM. APCs were irradiated with 3000 rad using a gamma irradiator to prevent their proliferation in the co-culture. After irradiation, cells were centrifuged, resuspended in an appropriate amount of MM and cell numbers were determined.

### **Isolation of naïve CD4<sup>+</sup> T cells**

B6.2D2 or B6.2D2.RFP mice (6 to 12 weeks old) were sacrificed by cervical dislocation. Spleens were collected and transferred into 5 ml WM in a 15 ml falcon tube. To create a single cell suspension, spleens were meshed through a 100 µm cell strainer. After centrifugation 10 ml lysis buffer was added to the cells to break down the erythrocytes present in the cell suspension. Lysis was stopped with 5 ml of WM and cells were centrifuged. The cell pellet was resuspended in an appropriate amount of MACS buffer and cells were counted manually using a Neubauer counting chamber to determine the necessary reagent volume for the bead-based MACS. Magnetic cell sort was performed using the Miltenyi CD4 isolation kit to obtain CD4<sup>+</sup>CD62L<sub>hi</sub> cells according to manufacturer's instructions. After centrifugation, untouched cells were resuspended in 40 µl MACS buffer and 10 µl CD4 T cell biotin antibody for every 10<sup>7</sup> cells and incubated for 10 min at 4 °C. Next, 30 µl MACS buffer, 20 µl anti-biotin microbeads and 5 µl CD8.Ly2 microbeads were added and incubated for 5 min at 4 °C. CD8 microbeads were used to reduce CD8<sup>+</sup> T cell contamination in the culture. After the untouched sort, CD62L magnetic beads were used to perform a positive sort on the CD4<sup>+</sup> T cells. 960 µl MACS buffer and 40 µl CD62L beads were added to the cells and incubated for 10 min at 4 °C. Efficacy of the T cell isolation was assessed by flow cytometry. For this, small sample was stained with αCD4-PeCy7 (1:1000), αCD62L-APC (1:200) and αVβ11-FITC (1:100) antibodies.

### **CD4<sup>+</sup> T cell differentiation**

Naïve T cells were differentiated into T helper cell (Th) -17, -1 or T<sub>reg</sub> cells by co-culturing them in 2 ml MM with irradiated CD90.2-depleted APCs and stimulation with specific cytokines in a 24-well plate.

Th17 cells were differentiated using a 1:10 T cell to APC ratio and adding 2 µg/ml αCD3e, 3 ng/ml huTGF-β, 20 ng/ml IL-23, 20 ng/ml IL-6, 10 µg/ml α-IL-4 and 10 µg/ml α-IFNγ. Cells were split and fed on day 3 of the culture (d3) with 50 U/ml 10 ng/ml IL-23.

Th1 cells were differentiated using a 1:5 T cell to APC ratio and received 2 µg/ml αCD3e, 25 µg/ml IL-18, 10 µg/ml IL-12 and 10 µg/ml α-IL-4. Cells were split and fed on d2 and d4 with 100 U/ml IL-2.

T<sub>reg</sub> cells were differentiated using a 1:5 T cell to APC ratio and received 2 µg/ml αCD3e, 3 ng/ml huTGF-β, 10 µg/ml α-IFN $\gamma$  and 10 µg/ml α-IL-12. Cells were split and fed on d2 and d4 with 100 U/ml IL-2.

All T cell cultures were used d5 or d6 for co-culturing experiments with OHSCs.

### **Assessment of cytokine production**

Quality of culture was checked by assessing the cytokine production of the T cell cultures before harvesting for co-culture experiments. Prior to the cytokine check, a 48-well plate was coated with αCD3e and αCD28 antibodies in PBS. For each culture, one well was coated with 120 µl PBS, 3 µg/ml αCD3e and 2.5 µg/ml αCD28 and the plate was wrapped in cling film decontaminated by 70 % ethanol before incubation at 4 °C overnight. T cells were stimulated by removing the αCD3e/ αCD28 coating and adding 1 ml of cell suspension to the well. The remaining 1 ml of the same T cell culture well was transferred to an uncoated well and used as a control. To prevent secretion of cytokines, 5 µg/ml of Brefeldin A, which blocks the Golgi complex, was added to each well and cells were incubated for 4 h at 37 °C with 95 % humidity and 5 % CO<sub>2</sub>. Cells were washed with FACS buffer and centrifuged (600 G, 5 min, 4 °C) before performing extracellular staining of surface antigens. All incubation steps were performed at 4 °C in the dark. Th17 and Th1 cells were stained with 100 µl CD4-PECy7 (1:1000) in PBS for 10 min, while T<sub>reg</sub> cells were stained with 100 µl CD4-Horizon (1:400) and CD25-APC (1:200) in permeabilization buffer (eBioscience™ Foxp3 / Transcription Factor Staining Buffer Set) for 10 min. To stain intracellular markers, cells were fixated using either 2 % PFA (500 µl of 4 % PFA in 500 µl PBS) for 20 min (Th17 and Th1) or with eBioscience Fixation/ Permeabilization Concentrate and Diluent for at least 30 min (T<sub>regs</sub>). Cells were washed and centrifuged (1000 G, 5 min, 4 °C) with either saponine buffer (Th17/ Th1) or permeabilization buffer (T<sub>regs</sub>). Th17 and Th1 intracellular staining was performed with IL17-APC (1:200), TNFα-AF700 (1:200) and IFN $\gamma$ -V450 (1:200) in saponine buffer for 20 min. T<sub>reg</sub> intranuclear staining was performed with FoxP3-PECy7 (1:200) in permeabilization buffer for 20 min. Cells were analyzed using flow cytometry.

### **2.2.7 OHSC and T cell co cultures**

OHSCs were co-cultured with MOG-specific 2D2 or 2D2.RFP CD4 T cells after 11 days *in vitro* (DIV). T cells were harvested after 5 to 6 days in culture, counted and 10  $\mu$ l MM containing 100.000 T cells were added on top of each slice. For control slices, 10  $\mu$ l of MM were added. OHSCs were incubated with T cells for 2 days before fixation.

### **2.2.8 Microglia depletion in OHSC**

OHSCs were treated with 10  $\mu$ M of Pexidartinib (PLX3377, hereafter referred to as PLX) after 3 DIV to deplete microglia by inhibiting CSF1R signalling upon which microglia rely for survival<sup>193-195</sup>. PLX stock solution (20mM in DMSO) was diluted to working concentration in SCM. Medium in culture wells was removed and replaced by SCM with PLX. Control wells received DMSO in SCM. After 72 hours of incubation, medium was replaced by fresh SCM.

### **2.2.9 Cell proliferation assay in OHSC**

OHSCs were treated with 20  $\mu$ M of 5-ethynyl-2'-deoxyuridine (EdU), a nucleoside analog of thymidine containing an alkyne group. EdU stock solution (10 mM in DMSO) was diluted to working concentration in SCM. Slices were treated either directly after AFMI or together with T cell treatment and incubated for 20 hours to label the astrocytes that begin proliferation after treatment, since the astrocytic cell cycle has been determined to last approximately 20 h<sup>196</sup>. Slices treated with cytosine arabinoside (ara-C) instead of AFMI and/ or T cell treatment were used as a negative control as ara-C inhibits cell proliferation by inhibiting DNA synthesis<sup>197,198</sup> (**Figure 6**). Medium was exchanged after incubation and slices were either fixated or kept in culture for 1 to 7 more days depending on the experimental set up. After fixation with 4% PFA and sectioning of the slices (see methods 2.2.11), tissue was washed with 3% BSA in PBS and pre-treated for 20 minutes with PBSTx (0.5%) for permeabilization. EdU reaction cocktail was modified (see Table 8) from the Click-iT™ EdU Imaging Kit (stock solutions were prepared according to manufactures instructions). Slices were incubated for 30 minutes in the dark to label EdU that integrated into the DNA of proliferating cells. The fluorescent dye contains an azide group that binds to the alkyne group of the EdU, catalyzed by Copper(II) sulfate (CuSO<sub>4</sub>)<sup>199</sup>. After EdU labelling, slices were stained for astrocytes via immunohistochemistry (see methods 2.2.11).

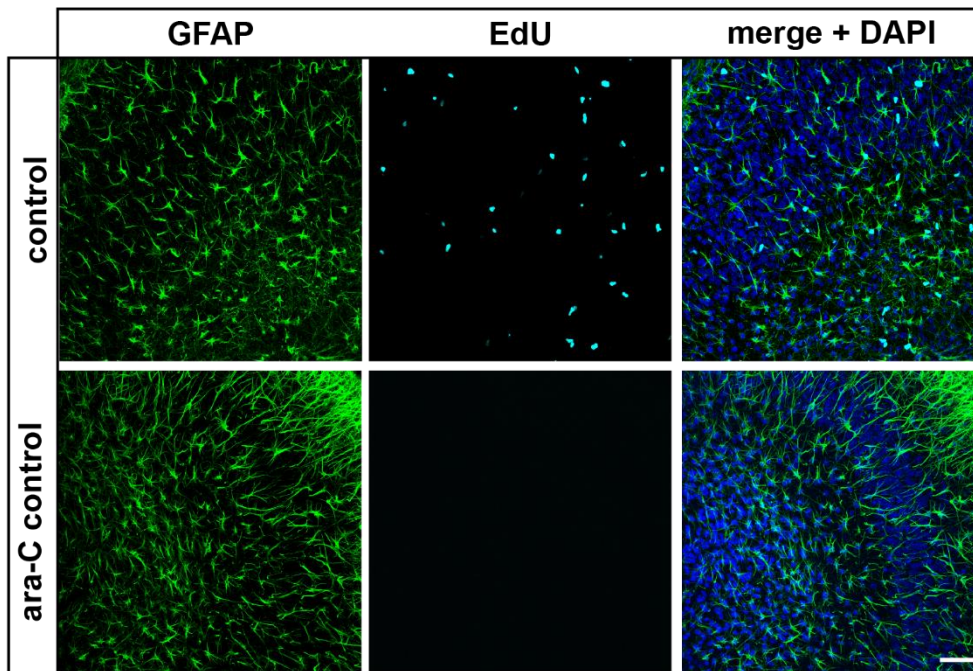


**Figure 6: Ara-C inhibits cell proliferation in all cells in OHSCs.** OHSCs were generated from p3 – 5 mouse pups (Aldh1L1 or B6 mice) and treated with ara-C as a negative control on 5 and 11 DIV. Slices were incubated with EdU (20  $\mu$ M) for 20 h on 11 DIV, before fixation and IHC with GFAP (green), EdU (cyan) and DAPI (blue). Untreated control slices show normal expression of EdU, while ara-C negative controls display no EdU signal. GFAP<sup>+</sup> astrocytes appear normal in number and morphology. Scale: 75  $\mu$ m.

### 2.2.10 Chemogenetic activation of microglia in OHSC

OHSCs from CSF1R<sup>Cre</sup> x DREADD<sub>Gq</sub>.mCitrine pups and B6 pups (control slices) were treated with 1  $\mu$ M CNO after 7 DIV. CNO stock solution (2mM in 0.5% DMSO and PBS) was diluted to working concentration in SCM. Medium in culture wells was removed and replaced by SCM with CNO. Control wells received 0.5% DMSO (in PBS) in SCM. Slices were incubated for 6 h and then fixated with 4% PFA (see methods 2.2.11).

### 2.2.11 Immunohistochemistry

To prepare the OHSCs for free-floating immunofluorescent staining, hippocampal slices were fixed using cold PFA (4 %). SCM was removed from culture wells and replaced by 2 ml of PFA with 1 ml over and under the cell culture insert respectively. Slices were fixated for an hour during which the PFA was changed every 20 minutes. Fixed cultures were washed with PB and either processed immediately or kept in PB at 4 °C.

To ensure optimal staining quality throughout the tissue, slices had to be cut into thinner sections using a method referred to as re-slicing. Membranes were cut out of the cell culture inserts and glued on to an agarose block.

Tissue was sectioned into 50 µm thick slices using a vibratome. Re-sliced sections were transferred into a 12-well plate with netwell inserts in PB using a fine brush. All incubation steps were performed in the dark on an orbital shaker. Washing steps were performed with PBSTx (0.5 %) in between all incubation steps except between blocking and primary antibody incubation. As a first step antigen demasking was performed with NH<sub>4</sub>Cl (50 mM) for 10 min at room temperature, followed by incubation for 1 hour at room temperature with a blocking solution containing 5 % NGS, 1 % BSA and 0.5 % Triton-X, to block non-specific binding sites. Primary antibodies were diluted in blocking solution and re-slices were incubated overnight at 4 °C. Secondary antibody labelling with fluorophore-conjugated antibodies was performed for 1 – 2 hours at room temperature. Nuclear staining was achieved by incubation with DAPI for 12 minutes at room temperature before mounting re-slices on microscopic slides using Prolong Gold. Slices that were only stained with secondary antibodies were used as an internal control to exclude signals originating from unspecific attachment.

### 2.2.12 Microscopy

#### Keyence microscopy

Astrocyte and microglia images used for mean fluorescent intensity (MFI) analysis were acquired on the Keyence BZ-X710 fluorescence microscope using 20X/0.75 NA dry objective. Slices were imaged as mosaics using the XY stitching function. Exposure time was set for each fluorochrome and kept consistent over all experiments, except for DAPI.

**Table 17: Keyence microscope settings**

Fluorescent dye	Emission [nm]	Exposure time [s]
<b>Alexa Fluor® 488</b>	487	1/30
<b>Alexa Fluor® 568</b>	568	1/35
<b>DAPI</b>	405	1/300 – 1/600

## Confocal microscopy

Cell proliferation and DREADD<sup>+</sup> microglia images were acquired on the SP8 confocal microscope using the HC PL APO 20x/0.75 CS2 dry objective. Image resolution was 1024 x 1024 pixel at a frequency of 400 Hz. A frame average of 3 frames per channel was chosen to improve signal-to-noise ratio and image quality.

**Table 18: Confocal microscope settings**

Fluorescent dye	Emission	Absorbance min - max
Alexa Fluor® 488	487	513 – 534
Alexa Fluor® 568	568	592 – 631
Alexa Fluor® 647	647	667 – 688
DAPI	405	444 – 454

### 2.2.13 Image analysis

Images were processed and analyzed with Fiji using base functions, plugins and self-written custom macros.

#### Longitudinal whole field MFI analysis

Maximum projections were created from the z-stacks obtained with the MP5 two-photon microscope. The injured area was manually marked with the free hand tool and added to the region of interest (ROI) manager. Aldh1L1.eGFP MFI was measured and injured area was excluded using the XOR function.

#### Astrocyte and microglia MFI analysis

For analyzing the MFI of astrocytes and microglia, multichannel images were split, maximum projection from z-stacks were obtained, processed with the Subtract Background function (rolling ball radius: 15 pixel) and converted into 8bit format. 8bit grayscale images were converted into binary by using thresholding and binary function Open was used to further separate the cell signals. The analyze particle function was used to add the separated cells to the ROI manager. Particle size was set to 40 – 1000  $\mu\text{m}^2$  for astrocytes and to 30 – 1000  $\mu\text{m}^2$  for microglia to exclude false positive signals. Cell ROIs were then redirected to the original RGB maximum projected image and MFI was measured.

### **Astrocyte proliferation analysis**

Astrocyte cell counts were obtained using the same processing steps as just described (see Astrocyte and microglia MFI analysis), except for the MFI measurements. Maximum projected images of GFAP and EdU channels were merged, and the cell counter tool was used to manually count double positive cells. The GFAP<sup>+</sup> EdU<sup>+</sup> cell count was divided by the total count of GFAP<sup>+</sup> cells to give the amount in percent of GFAP<sup>+</sup> astrocytes. Furthermore, the total number of GFAP<sup>+</sup> EdU<sup>+</sup> cells was divided by the size of the field of view to determine the number of cells per mm<sup>2</sup>.

### **Colocalization analysis**

Iba1 and GFP z-stacks were processed with the Subtract Background function (rolling ball radius: 15 pixels) and analyzed with the colocalization threshold plugin. The resulting output displaying the colocalized pixels between both channels was used for further analysis. After creating a maximum projection, the binary image of the colocalized pixels was processed using the binary function Close and the particle analysis tool. Particle size was set to 10 – 1000 μm<sup>2</sup> to exclude false positive signals. The total amount of Iba1<sup>+</sup> microglia was determined as described in the two previous paragraphs (see Astrocyte and microglia MFI analysis and Astrocyte proliferation analysis). The number of colocalized cells was then divided by the total number of Iba1<sup>+</sup> microglia. Slices with a percentage of colocalized cells higher than 100% were excluded from the analysis.

### **Microglia morphology analysis**

Binary images created during cell number determination of Iba1<sup>+</sup> microglia (see Colocalization analysis) were further processed with the noise reduction function Despeckle and used to extract the shape descriptor roundness (R) as a parameter to analyze microglia morphology. The roundness scale ranges from 0 (no roundness) to 1 (perfect roundness). Cells were classified as rod-like (R: 0.1 – 0.3), ramified (R: 0.4 – 0.7) or ameboid (R: 0.8 – 1) and roundness distributions of treatment groups were analyzed.

#### **2.2.14 Statistics**

All data analysis was performed using GraphPad Prism version 9. Outliers were identified and excluded using the ROUT method with a Q of 1%. Data was tested for normality using Shapiro-Wilk or D'Agostino & Pearson normality test with an  $\alpha$  of 0.05. Parametric data was analyzed using student's t-test (two-tailed), one-way ANOVA or Welch test one-way ANOVA with Tukey's test, Dunnett's test or Dunnett's T3 test for multiple comparisons, as appropriate. Non-parametric data was analyzed using Mann-Whitney U test or Kruskal-Wallis test with Dunn's test for multiple comparisons. Data with more than one dependent variable was analyzed with two-way ANOVA or repeated measures (RM) two-way ANOVA with Šídák's test or Tukey's test for multiple comparisons. The exact statistical test used for any dataset is given in the figure legend. All data is displayed as mean and standard error of the mean (SEM) unless otherwise specified. Significance was defined as  $p < 0.05$ .



### 3 Results

#### 3.1 Development of a laser injury model to study glial cell reaction under non-inflammatory conditions

The first aim of the project was to establish a small and sterile focal injury to model non-inflammatory damage in the CNS. OHSC were used for this injury model as the system provides a cellular network of neurons and glial cells that resembles the *in vivo* situation<sup>184,185,200</sup>. Additionally, it allows for studying CNS-immune system interactions as immune cells (e.g. T cells) can be easily introduced into the tissue due to the absence of the BBB. However, OHSC composition changes over the course of culture, therefore time points for treatments and analysis must be chosen carefully. As the initial preparation of the slices presents a tissue damage there is a strong microglia activation in the first three days *in vitro* (DIV) subsiding around 5 DIV, while the astrocytic activation increases around 7 DIV<sup>201</sup>. OHSCs from hemizygous *Aldh1L1.eGFP* pups (p3-5) stained with SR101 were used to conduct the experiments.

Key parameters were decided upon after reviewing the literature regarding laser injury models<sup>118,119,128,161</sup> (**Table 1**). A target area of 30 x 30  $\mu\text{m}$  was chosen, as ~1 – 13  $\mu\text{m}$  was deemed too small, especially in the context of longitudinal imaging over the course of several days. The laser power settings used in the literature corresponded to 1 – 3 % of total laser power on the MP5 two photon laser, which was lower than the output used for imaging on the MP5 setup. Therefore, it was decided to test 20 – 50 % of total laser power for this model. For duration of laser injury 20, 30 and 60 seconds were chosen which corresponded to literature settings.

First, the different laser power intensities were tested with a duration of 60 seconds to determine the optimal settings for generating a consistently sized injury. Using a laser beam with a wavelength of 850 nm on the target area resulted in localized autofluorescent tissue damage (**Figure 7 A**) that has been described before<sup>119,128</sup>. As laser output power varied between and within experimental sessions, it was closely monitored (**Figure 8**) and power intensities were carefully set to keep conditions consistent. Tested laser power intensities of 20, 30, 40 or 50 % of the total laser power (3526 mW in this experiment), corresponded to 705, 1058, 1411 and 1764 mW.

The orthogonal views show the propagation of the tissue damage through the slice in the xz and yz axis to be rather similar across all tested power levels, which is confirmed by the measurements yielding no significant difference between the mean injury depths of all groups (Figure 7 B).

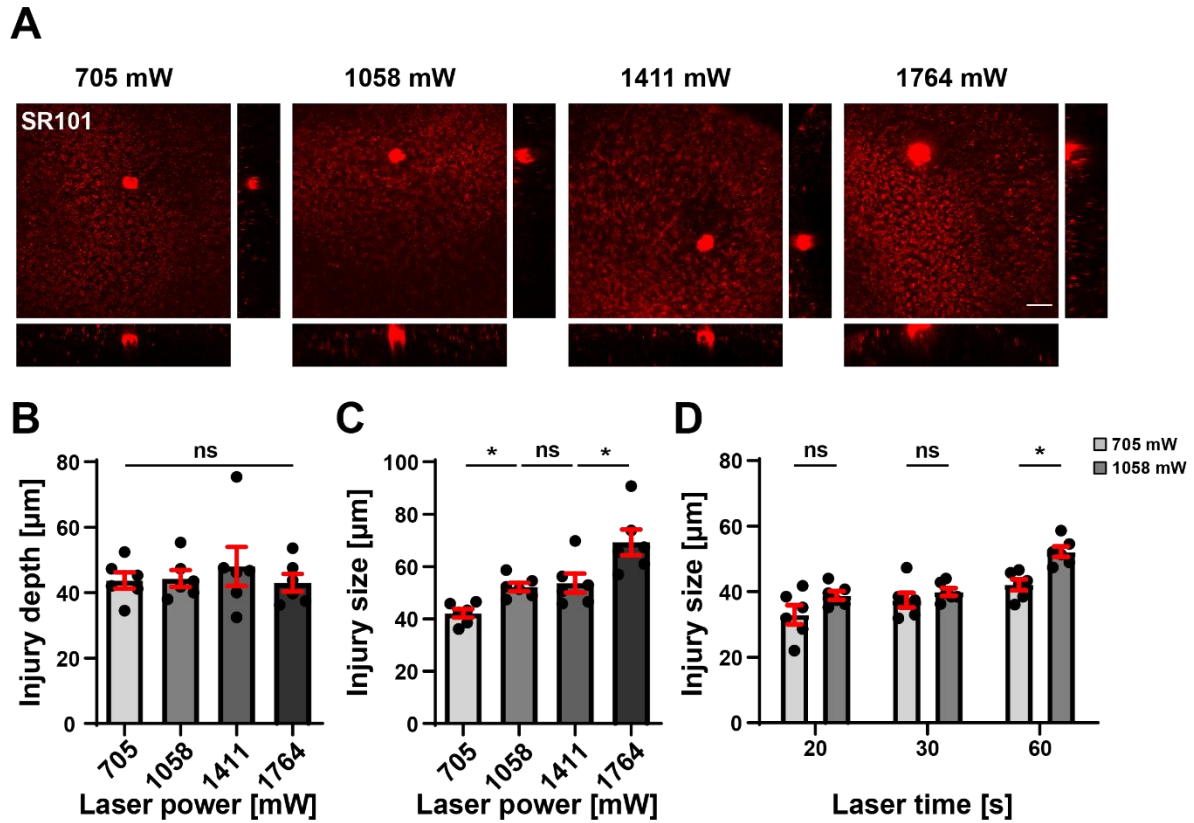


**Figure 7: Injury size but not depth varies between different laser power settings.** Two-photon imaging of laser injuries to establish optimal settings. **A.** Astrocytes in OHSCs from Aldh1L1.eGFP pups p3 – 5 were stained with the live cell dye SR101 (red). A localized injury was created by focusing a two-photon laser beam on a 30 x 30  $\mu\text{m}$  area in the middle of the slice. Images and orthogonal views show larger autofluorescent injuries with increasing laser power. **B-C.** Injury depth measured in the yz plane (**B**) and injury size measured in the xy plane (**C**) in  $\mu\text{m}$  for the different laser powers. Data was analyzed with one-way ANOVA ( $\alpha < 0.05$ );  $n = 6$  for all groups; Main effect:  $F(3,20) = 0.36$ , ns ( $p = 0.79$ ) (**B**); Main effect:  $F(3,20) = 11.91$ , \*\*\* ( $p < 0.001$ ) (**C**). **D.** Differences in mean injury size between 705 and 1058 mW for different laser times. Data was analyzed using two-way ANOVA ( $\alpha < 0.05$ ),  $n = 6$  for all groups; Main effects: Laser power:  $F(1,30) = 15.45$ ,  $p = 0.0005$ , 17.88% of total variation, Laser time:  $F(2,30) = 18.58$ ,  $p < 0.0001$ , 42.98% of total variation; followed by Šídák's multiple comparisons test,  $p$  is reported as multiplicity adjusted  $p$ -value: ns ( $p > 0.05$ ), \*\* ( $p < 0.01$ ). Scale bar: 75  $\mu\text{m}$  (**A**).

Next, the injury size was compared by measuring across the widest part of the injury in the xy plane of the maximum projected image showing a significant impact of laser power on mean injury size (**Figure 7 C**). 1411 and 1764 mW showed larger in-group variance (1411 mW:  $53.67 \pm 3.60$ ; 1764 mW:  $69.28 \pm 4.88$ ), than 705 and 1058 mW (705 mW:  $42.13 \pm 1.68$ ; 1058 mW:  $52.20 \pm 1.64$ ). Furthermore, 1058 and 1411 mW showed only a small difference in mean injury size, therefore additional testing was limited to 705 and 1058 mW laser power.

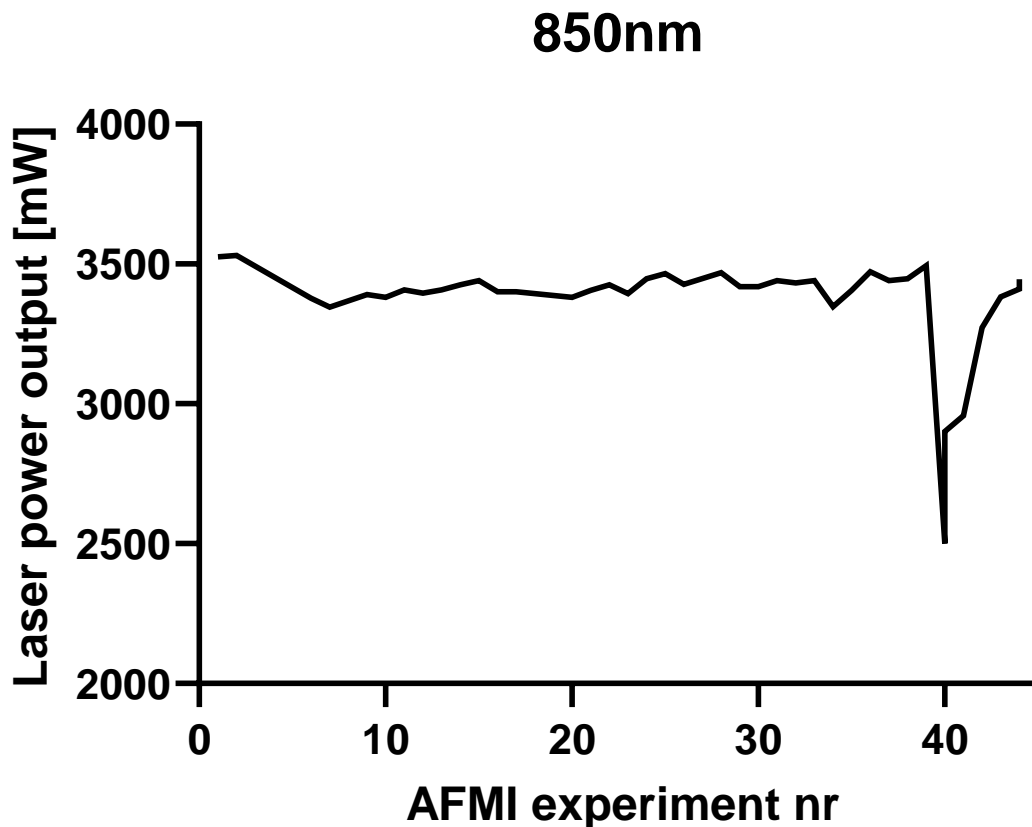


**Figure 8: Fluctuation in MP5 laser power output over the experimental time course.** Laser power output was tracked for each experiment as it varied between as well as within experimental sessions. Power fluctuations mostly occurred between 3300 and 3500 mW but due to cooling system issues output power dropped to 2500 mW in experimental session 40 and slowly recovered in later sessions. Percentage of laser power used for AFMI (~1000 mW) was determined according to initial laser output power.

To test if a shorter laser time would influence injury size and consistency, 705 mW and 1058 mW laser power were tested using 20, 30 and 60 seconds of exposure (**Figure 7 D**). While both laser power and laser time have a significant effect on injury size, multiple comparisons testing only showed a significant difference between 705 and 1058 mW at 60 s of laser time.

Between both laser time conditions 1058 mW showed higher consistency of injury size (20 s:  $38.87 \pm 1.32$ ; 30 s:  $39.97 \pm 1.19$ ; 60s:  $52.20 \pm 1.64$ ) than 705 mW (20 s:  $33 \pm 2.91$ ; 30 s:  $37.4 \pm 2.24$ ; 60 s:  $42.13 \pm 1.69$ ). Therefore, the parameters for inducing AFMI were set to ~1000 mW laser power and 60 seconds of laser time. Due to the software constraints, laser power regulation was limited to 1% increments. Thus, the percentage of total laser power output was set to be as close to 1000 mW as possible for each experimental session and ranged from 28 – 40% (**Table 19**). Mean laser power over all experiments was 1002 mW.

After successfully implementing an AFMI technique to model non-inflammatory tissue damage, the next step was to test the extent of the glial response towards the injury.

**Table 19: Laser power intensities used in AFMI experiments.** The total laser output was carefully recorded for each experimental session to calculate the % of total power needed to achieve an injury laser power as close to 1000 mW as possible.

AFMI experiment	Total laser power output [mW]	% of total power	Injury laser power [mW]
2	3530	28	988.4
5	3416	29	990.64
6	3377	30	1013.1
7	3346	30	1003.8
9	3391	29	983.39
10	3380	29	980.2
11	3408	29	988.32
12	3396	29	984.84
13	3407	29	988.03
14	3426	29	993.54
15	3440	29	997.6
16	3401	29	986.29
17	3400	29	986
20	3381	30	1014.3
21	3405	30	1021.5
22	3426	29	993.54
23	3394	30	1018.2
24	3447	29	999.63
25	3465	29	1004.85
26	3428	29	994.12
28	3469	29	1006.01
29	3419	30	1025.7
30	3419	30	1025.7
31	3441	30	1032.3
32	3432	30	1029.6
33	3441	30	1032.3

34	3347	29	970.63
35	3405	30	1021.5
36	3473	29	1007.17
37	3440	29	997.6
38	3447	29	999.63
39	3494	29	1013.26
40	2500	40	1000
40	2900	32	928
41	2957	34	1005.38
42	3273	31	1014.63
43	3383	30	1014.9
44	3410	30	1023
44	3445	29	999.05

### 3.2 Astrocytes and microglia show different temporal reaction patterns in response to an acute focal laser injury

As described earlier, prior damage to CNS tissue can lead to priming of both microglia and astrocytes and result in the cells remaining in a more activated state. This continuous elevation of activation leads to an exaggerated response to future insults and is a possible mechanism by which chronic neuroinflammation and -degeneration is promoted<sup>142,159,202</sup>. To investigate this idea, the established AMFI method was used as a model to create an initial injury or first hit, since it is a consistent and reproducible method for creating tissue damage. Therefore, the first step for this experimental paradigm was to analyze the extent of glial response to AFMI.

Longitudinal two-photon imaging of OHSCs prepared from Aldh1L1.eGFP mouse pups (**Figure 9 A**) revealed a decrease in injury size and an increase in Aldh1L1.eGFP fluorescence (**Figure 9 B**) over time, signifying a possible resolution of the insult by the glial cells. Both groups, control and AMFI, displayed an increase in fluorescence intensity over time, which was expected due to the general increase of astrocytic reactivity in OHSCs<sup>201</sup>. Aldh1L1.eGFP MFI was also increased by AFMI both 1 and 7 dpi, although the increase was only significant at 7 dpi (**Figure 9 C**). Due to the low resolution, it was not possible to analyze the astrocytic response on a more cellular level. Therefore, OHSCs prepared from either Aldh1L1.eGFP or B6 mouse pups were stained with GFAP, and cellular MFI was analyzed. As expected, astrocytes reacted with formation of a glial scar at the injury site (**Figure 9 D**), although surprisingly already at 1 dpi, as astrocytic scar formation is often reported to start at day 4 – 6 after injury<sup>203-205</sup>. This is however, not reflected in their GFAP reactivity measured as fluorescence intensity on a single cell level, with there being no significant difference in MFI between control and injured slices (**Figure 9 E**). More in line with previous findings is the significant increase in GFAP MFI in injured slices at 7 dpi (**Figure 9 F**).

The microglia response is much faster with what appears to be migration or reorientation of Iba1<sup>+</sup> microglia towards the injury site occurring only minutes after AFMI (**Figure 9 G**). This initial reaction is also reflected in a pronounced significant increase in Iba1 MFI (**Figure 9 H**). At 1 dpi microglia have already dispersed again and MFI levels do not differ significantly from the control group (**Figure 9 I**), which was also observed at later time points (data not shown).

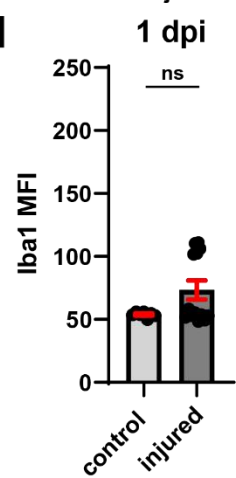
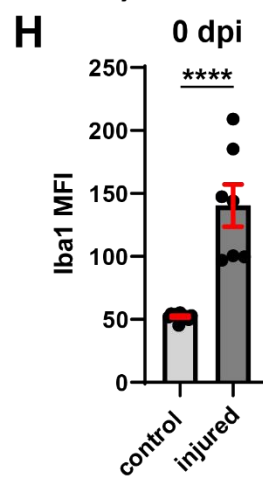
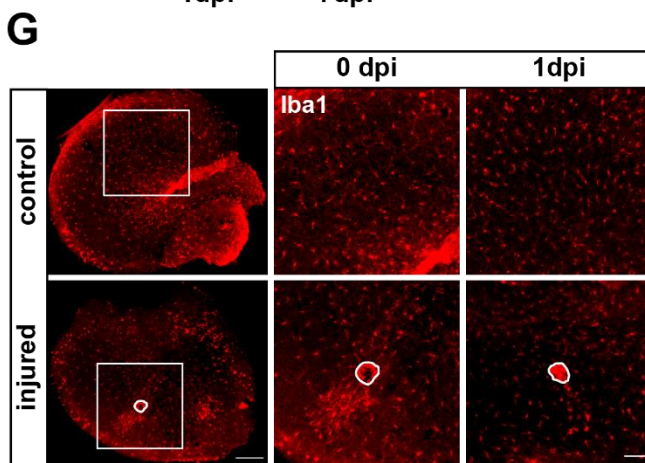
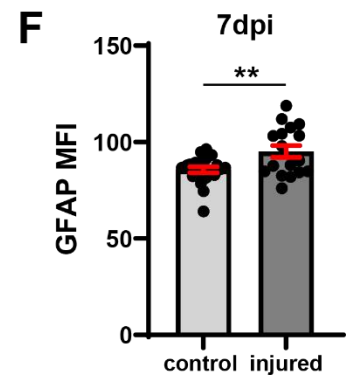
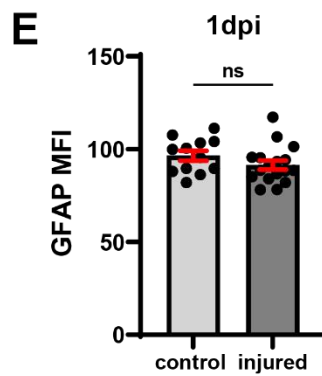
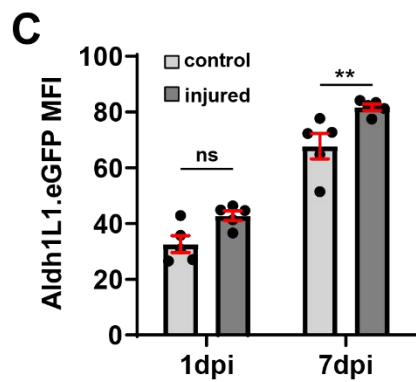
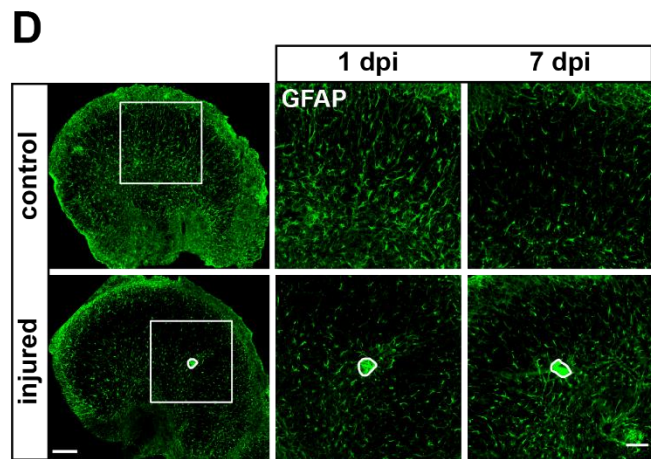
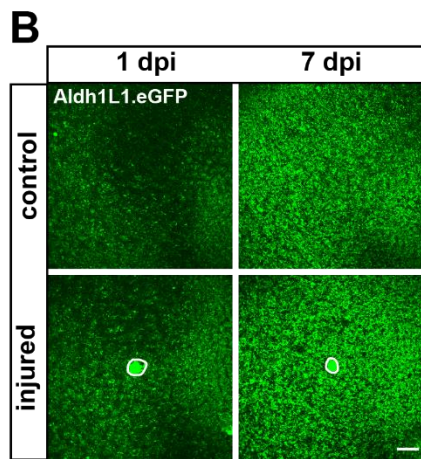
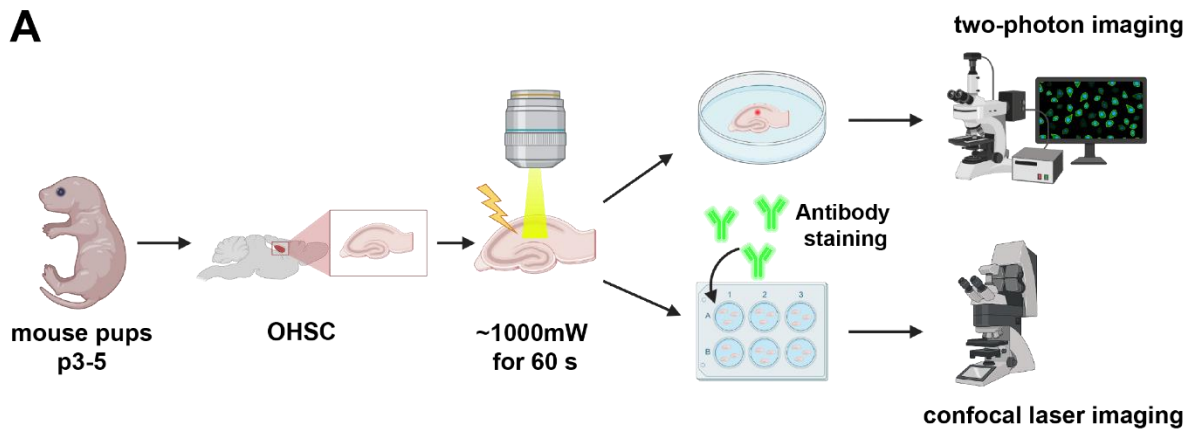


**Figure 9: Glial activation increases in response to AFMI in OHSCs.** **A.** Schematic overview of experimental set up<sup>206</sup>. OHSCs were generated from p3 – 5 mouse pups (Aldh1L1 or B6 mice) and cultured for 5 days before laser injury was performed. Slices were put back into culture for either longitudinal two-photon-imaging or fixation and IHC staining at 1 dpi or 7 dpi. **B.** Longitudinal two-photon imaging of Aldh1L1.eGFP (green) slices at 1 and 7 dpi. Laser injury is marked by white outlines. **C.** Analysis of Aldh1L1.eGFP whole field MFI for control and injured slices at 1 and 7 dpi shows increase of Aldh1L1.eGFP MFI over time and after injury. Two-way RM ANOVA ( $\alpha < 0.05$ ),  $n = 5$  for each group; Main effects: Injury:  $F(1,8)=13.54$ ,  $p=0.0062$ , 8.79% of total variation, dpi:  $F(1,8)=209.9$ ,  $p < 0.0001$ , 82.65% of total variation; followed by Šidák's multiple comparisons test,  $p$  is reported as multiplicity adjusted  $p$ -value: ns ( $p > 0.05$ ), \*\* ( $p < 0.01$ ). **D.** OHSCs were stained for astrocytes with GFAP (green). Laser injury is marked by white outlines. Left panels show overview images of GFAP stained slices with boxed areas being enlarged in the middle panels. GFAP<sup>+</sup> astrocytes 1 dpi (middle) and 7 dpi (right) showing scar formation in response to the laser injury (white outlines, lower panels). MFI of all GFAP<sup>+</sup> astrocytes in a 300  $\mu\text{m}$  radius around the injury site was assessed and used to calculate MFI for each slice. **E.** No difference in mean GFAP MFI between control and injured slices was detected 1 dpi. Two-tailed unpaired  $t$  test ( $\alpha < 0.05$ ); control  $n = 12$ , injured  $n = 17$ , ns ( $p > 0.05$ ). **F.** Significant increase in mean GFAP MFI between control and injured slices at 7 dpi. Two-tailed unpaired  $t$  test ( $\alpha < 0.05$ ), control  $n = 23$ , injured  $n = 17$ , \*\* ( $p < 0.01$ ). **G.** OHSCs were stained for microglia with Iba1 (red). Laser injury is marked by white outlines. Left panels show overview images of Iba1 stained slices with boxed areas being enlarged in the middle panels. Iba1<sup>+</sup> microglia presence is heavily increased around the injury site shortly after the injury (0 dpi, lower middle) and subsides at 1 dpi (lower right). MFI of all Iba1<sup>+</sup> microglia in a 300  $\mu\text{m}$  radius around the injury site was assessed and used to calculate MFI for each slice. **H.** Iba1 MFI increased significantly between control and injured slices 0 dpi. Two-tailed unpaired  $t$  test ( $\alpha < 0.05$ ), control  $n = 13$ , injured  $n = 7$ , \*\*\*\* ( $p < 0.0001$ ). **I.** No significant difference in Iba1 MFI was detected between control and injured slices at 1dpi. Mann-Whitney U ( $\alpha < 0.05$ ), control = 7, injured = 13, ns ( $p > 0.05$ ). Scale bars: 50  $\mu\text{m}$  (A), 200  $\mu\text{m}$  (D & G, left panels), 75  $\mu\text{m}$  (D & G, right panels).

Curiously, a large portion of microglia migrating towards the injury site appear to originate from the border region of the slice as evident by the large group of cells between slice border and injury, as opposed to the much smaller group of cells on the other side of the injury (**Figure G**, lower middle panel). Despite having largely dispersed, remnants of this trend can also be observed at 1 dpi (**Figure 9 G**, lower right panel).

Since the microglia only react to the injury within a short period of time (<24 hours) and appear to return to a more homeostatic phenotype, this indicates that the injury alone is a damage that can be resolved by the astrocytes, but with the potential of serving as a primer for the microglia. Therefore, a next step was to introduce a second insult or second hit to investigate this hypothesis. But before that, the astrocytic response was further characterized to investigate severity of astrogliosis and proliferative capacities of the astrocytes.



### 3.3 Astrocytic proliferation is increased within and around the glial scar 7 days after AFMI

After demonstrating that astrocytes react to AFMI with increased activation and typical glial scar formation at the site of injury, the next aim was to explore whether astrocytic proliferation plays a role in their reaction to AFMI. Depending on the severity of a CNS insult, astrocytic proliferation might occur as normally quiescent astrocytes begin to enter the cell cycle <sup>46,207</sup>.

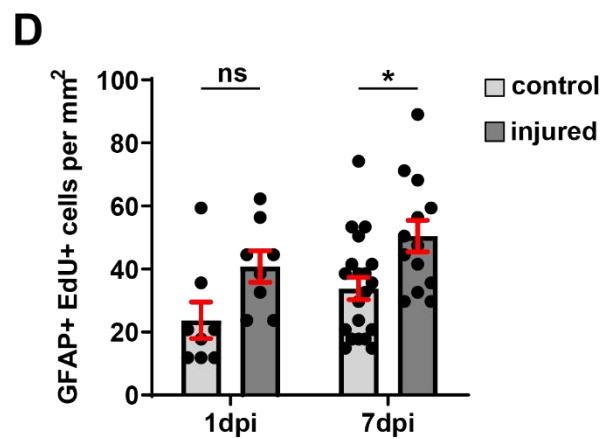
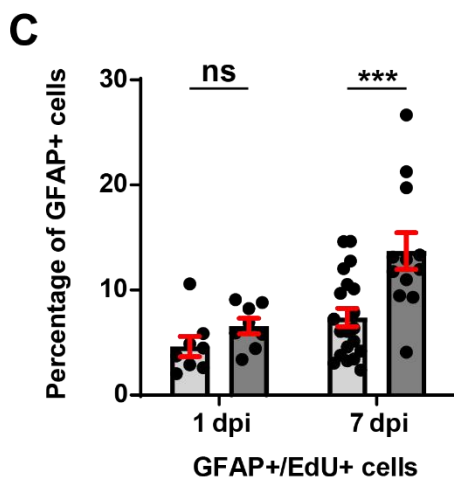
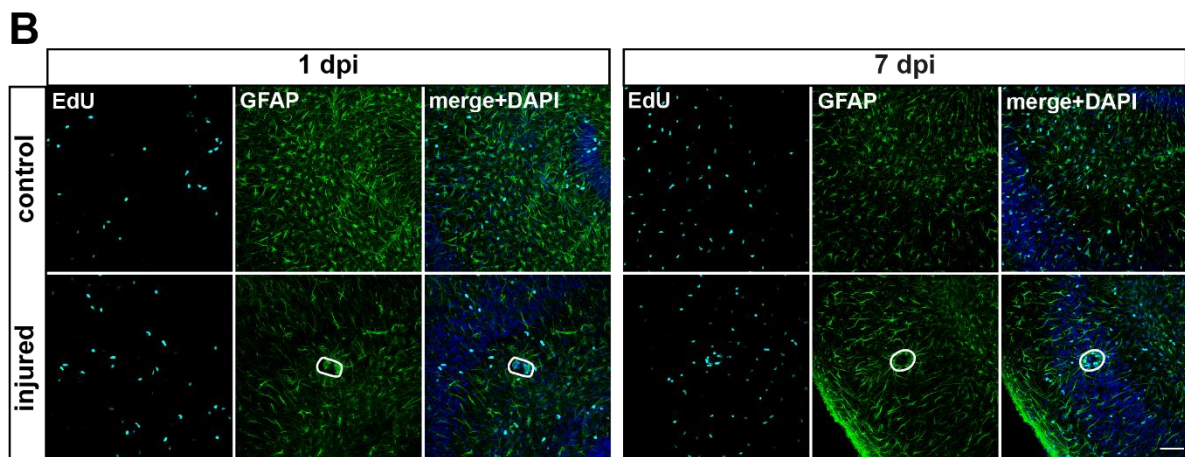
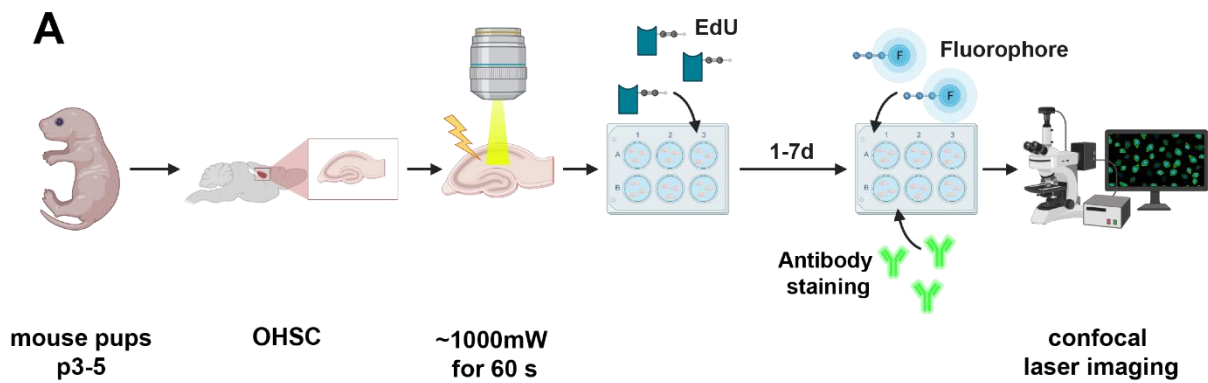


**Figure 10: AFMI induces glial scar formation and increases astrocytic proliferation.** **A.** Schematic overview of experimental set up <sup>206</sup>. OHSCs were generated from p3 – 5 mouse pups (Aldh1L1 or B6 mice) and cultured for 5 days before laser injury was performed. Slices were placed back into culture and incubated with EdU (20  $\mu$ M) for 20 h, before slices were fixated and fluorescently labelled with IHC at 1 and 7 dpi. **B.** OHSCs were stained for EdU (cyan), GFAP (green) and DAPI (blue). Top panels depict control slices, lower panels depict injured slices at 1 dpi (left) and 7 dpi (right). Injured slices show glial scar formation with increase of proliferating cells in the scar area especially at 7 dpi. Laser injury is marked by white outlines. **C-D.** Proliferating astrocytes (GFAP<sup>+</sup>/EdU<sup>+</sup>) increase over time and after injury both in relation to the number of GFAP<sup>+</sup> cells in general (**C**) as well as cells per mm<sup>2</sup> (**D**). Data was analyzed using two-way RM ANOVA ( $\alpha < 0.05$ ), control 1 dpi n = 8, control 7 dpi n = 20, injured 1 dpi n = 8, injured 7 dpi n = 13; Main effects: Injury: F(1,44)=10.02, p=0.0028, 13.90% of total variation; dpi: F(1,44)=14.36, p=0.0005, 19.92% of total variation; followed by Šídák's multiple comparisons test, p is reported as multiplicity adjusted p-value: ns (p > 0.05), \*\*\* (p < 0.001) (**C**); Main effects: Injury: F(1,44)=10.29, p=0.0025, 18.17% of total variation, dpi: F(1,44)=3.027, p=0.089, 5.343% of total variation; followed by Šídák's multiple comparisons test, p is reported as multiplicity adjusted p-value: ns (p > 0.05), \* (p < 0.05) (**D**). Scale bar: 75  $\mu$ m (**B**).

OHSCs treated with EdU after inducing AFMI were used for IHC stainings at 1 and 7 dpi (**Figure 10 A**). EdU is taken up by proliferating cells and incorporated into their DNA, where it can be fluorescently labelled and imaged. Cells continuing to proliferate after the initial EdU pulse has been washed out can also be identified through this method. Both control and injured slices show cell proliferation, with control slices exhibiting an even distribution throughout the slice and increased EdU signals over time (**Figure 10 B**, top panels). Injured slices show a more localized distribution concentrated around the injury, which is especially pronounced at 7 dpi where a lot of EdU<sup>+</sup> cells are located next to and within the glial scar present at the injury site (**Figure 10 B**, lower panels).

Both time and AFMI had a significant effect on the increased percentage of proliferating astrocytes (**Figure 10 C**). Control slices showed a small increase from 1 to 7 dpi with mean percentage being under 10 % in both groups. AFMI slices on the other hand displayed a two-fold increase from 1 to 7 dpi. While the injured slices have a higher percentage of proliferating astrocytes than the control slices, at 1 dpi this difference is not significant. However, at 7 dpi the difference is much more pronounced and highly significant. This reveals a much larger portion of astrocytes continuing to proliferate over time in response to the injury, aiding in the formation of the glial scar. Looking at the abundance of GFAP<sup>+</sup>/ EdU<sup>+</sup> cells it shows that only AFMI has a significant effect on proliferating astrocytes per mm<sup>2</sup> (**Figure 10 D**). Although injured slices show a higher abundance of proliferating astrocytes than control slices, this difference is only significant for 7 dpi.

Generally, EdU<sup>+</sup> cells significantly increase over time in the slices, but when having a closer look at differences between groups only the mean difference between control slices at 1 dpi and AFMI slices at 7 dpi is significant (**Figure 11 A**).

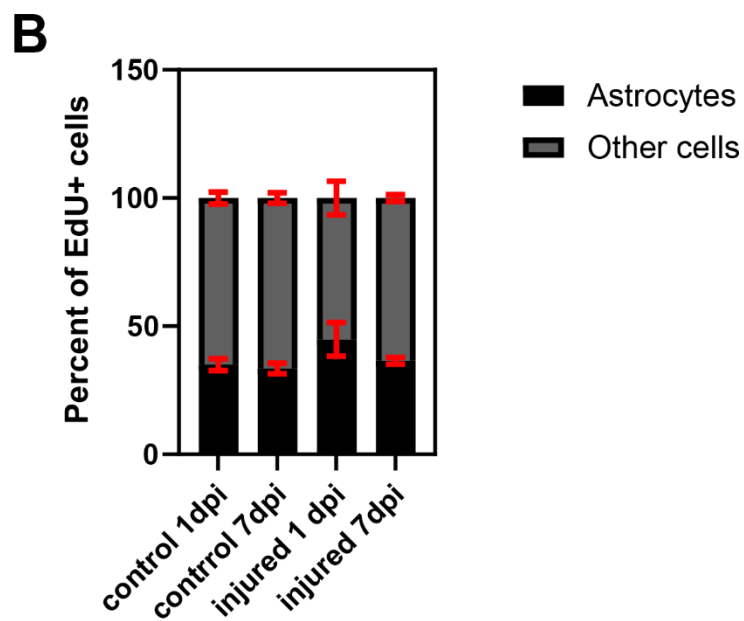
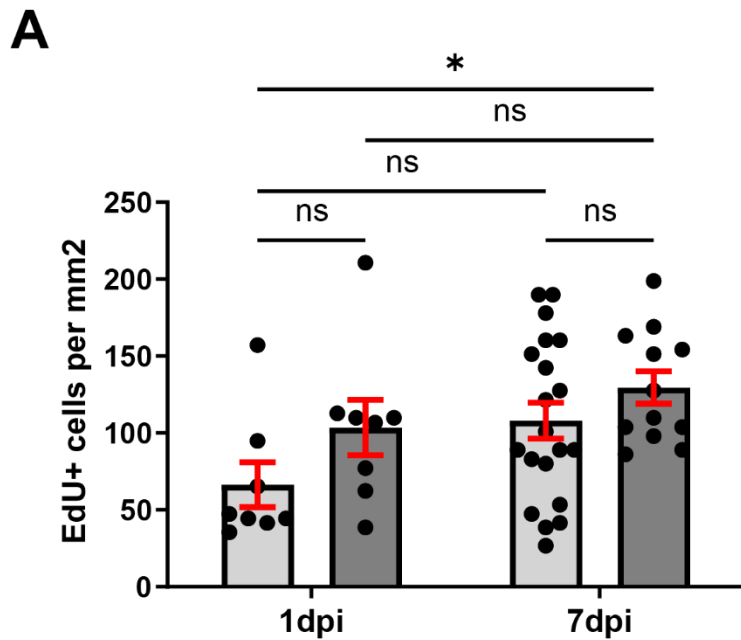


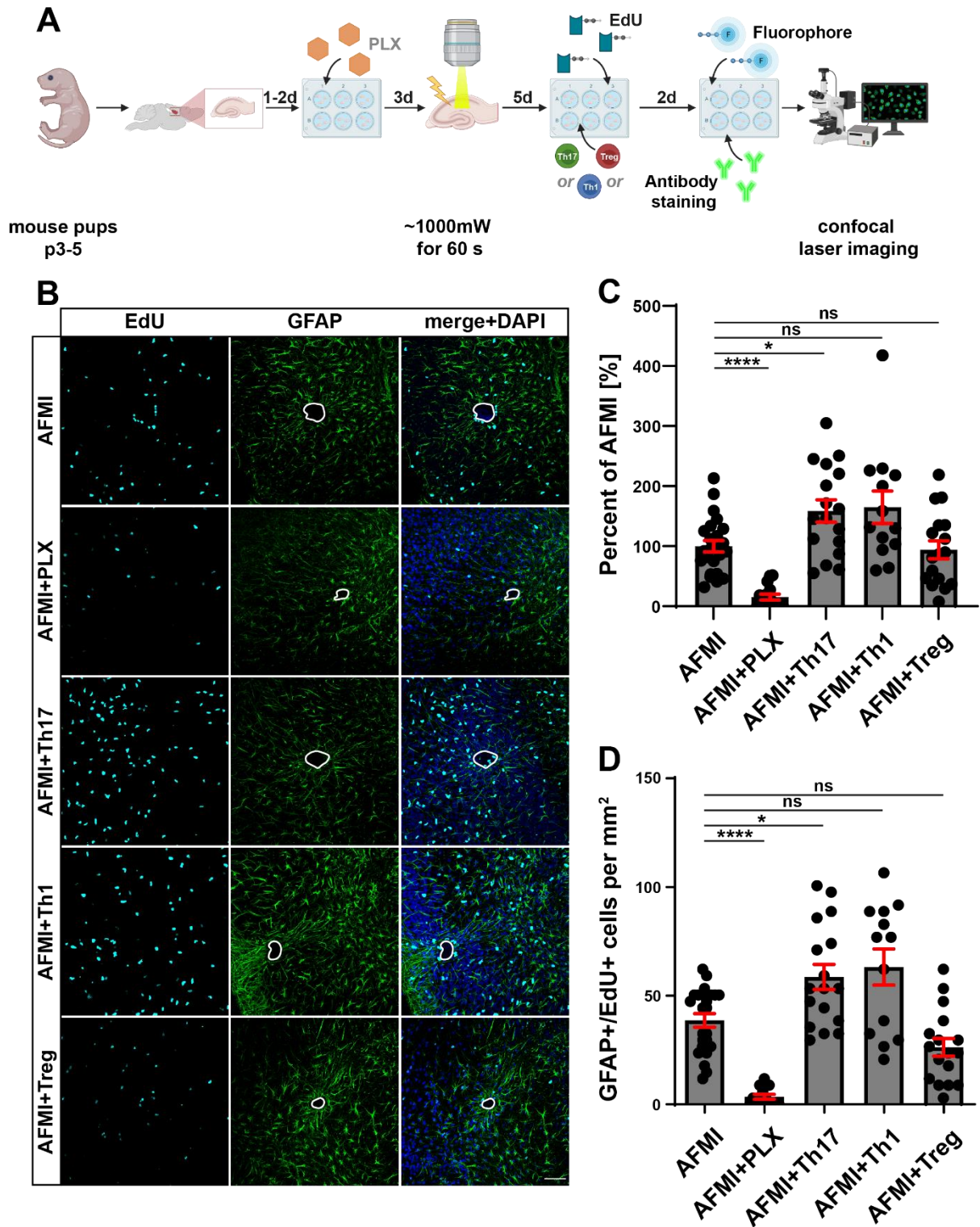
**Figure 11: EdU<sup>+</sup> cells increase in injured slices at 7 dpi.** **A.** Total numbers of EdU<sup>+</sup> cells in OHSCs were analyzed and show no significant differences except between control 1 dpi and AMFI 7 dpi. Data was analyzed using two-way ANOVA ( $\alpha < 0.05$ ), control 1 dpi n = 8, control 7 dpi n = 20, injured 1 dpi n = 8, injured 7 dpi n = 13; Main effects: Injury:  $F(1,44) = 4.050$ ,  $p = 0.0503$ , 7.681 % of total variation; dpi:  $F(1,44) = 5.397$ ,  $p = 0.0249$ , 10.23% of total variation; followed by Tukey's multiple comparisons test, p is reported as multiplicity adjusted p-value: ns ( $p > 0.05$ ), \* ( $p < 0.05$ ). **B.** Proliferating astrocytes (GFAP<sup>+</sup>/EdU<sup>+</sup>) and other cell types displayed as percent of EdU<sup>+</sup> cells. The number of GFAP<sup>+</sup>/EdU<sup>+</sup> cells was divided by the total number of EdU<sup>+</sup> cells and multiplied by 100. Number of proliferating other cell types was determined by subtracting the percent of proliferating astrocytes from 100 %. The fraction of proliferating astrocytes is consistent overall groups with a slight increase in the injured 1 dpi group, that is however, not significant. Data was analyzed using two-way ANOVA ( $\alpha < 0.05$ ), control 1 dpi n = 8, control 7 dpi n = 20, injured 1 dpi n = 8, injured 7 dpi n = 13; Main effects: Cell type:  $F(1,88) = 125.9$ ,  $p < 0.0001$ , 46.14 % of total variation; Treatment:  $F(1,88) = 6.376 \times 10^{-30}$ ,  $p > 0.9999$ ,  $7.008 \times 10^{-30}$  % of total variation; followed by Šidák's multiple comparisons test, p is reported as multiplicity adjusted p-value: ns ( $p > 0.05$ ).

This demonstrated that while cells in OHSCs show a trend towards higher levels of proliferation over time, injury plays a crucial role in elevating proliferative responses. Interestingly, no significant difference could be observed when analyzing the percent of proliferating astrocytes and other cell types from the total amount of EdU<sup>+</sup> cells in the different groups (**Figure 11 B**). This raises the question of which other cell types are proliferating within the tissue and if one of those types is responsible for the significant increase at 7 dpi and AFMI. However, this question is beyond the scope of this thesis.

Interestingly, it appears that while there are a lot of proliferating astrocytes in the glial scar around the AFMI only a few of them are found in the glial scar at the border of the slice (**Figure 10 B**, right lower panels). This may be because those cells have already stopped proliferating at the time of EdU labelling or because the glial scar at the slice border is rather formed by migration and expansion than proliferation of astrocytes in that area.

The presence and increase of proliferating astrocytes in AFMI slices points towards a more severe stage of astrogliosis. Furthermore, EdU labelling of proliferating cells presents a stable read out and was therefore used to analyze the potential effect of primed microglia on the astrocytes.

### 3.4 Astrocytic response is further elevated by inflammatory injury

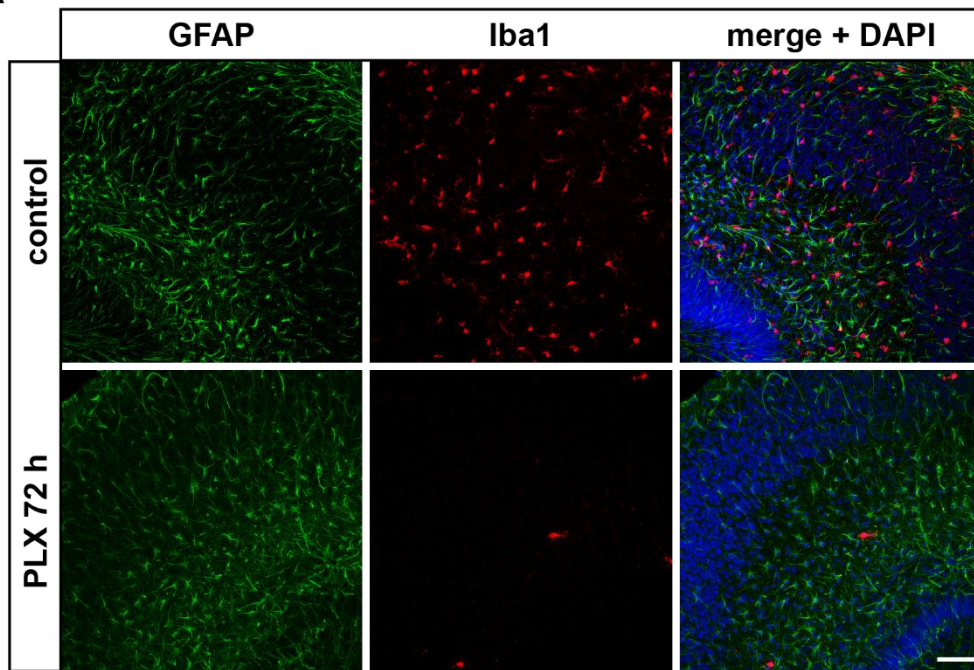
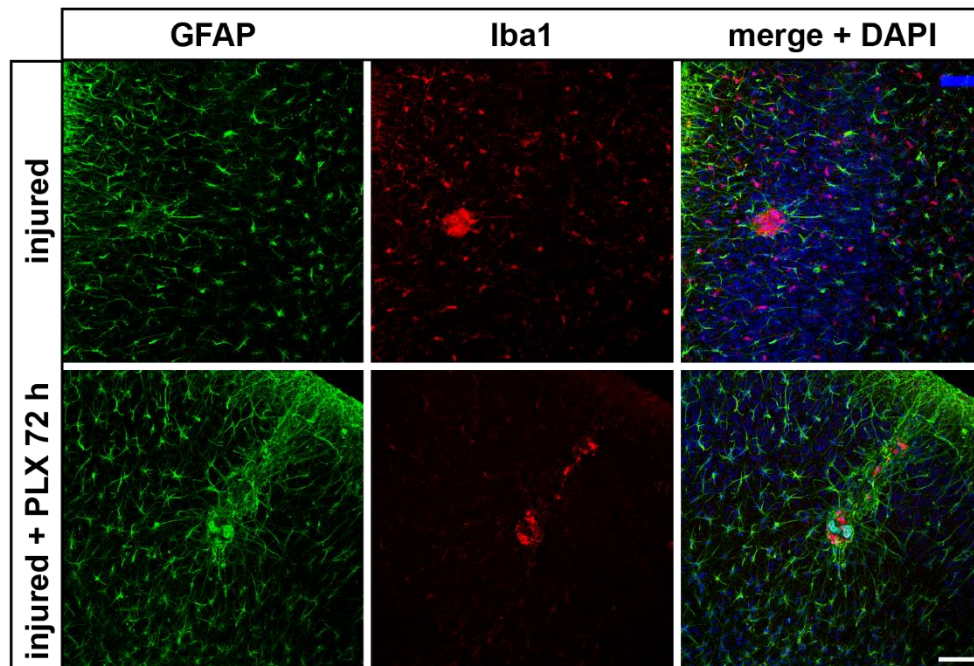


**Figure 12: Influence of microglia depletion and T cell infiltration on astrocytic proliferation after AFMI.**

**A.** Schematic overview of experimental set up<sup>206</sup>. OHSCs were generated from p3 – 5 mouse pups (Aldh1L1 or B6 mice) and cultured for 3 days before treatment with PLX or a vehicle. Laser injury was performed after 3 days and slices were placed back into culture for 5 days, before incubation with EdU (20  $\mu$ M, 20h) and treatment with T cells for 2 days. OHSCs were fixated and stained with IHC. **B.** OHSCs were stained for EdU (cyan), GFAP (green) and DAPI (blue). Slices show reduced proliferative capacities after microglia depletion via PLX, while Th17 and Th1 cells increased overall number of EdU<sup>+</sup> cells. Laser injury is marked by white outlines. **C-D.** GFAP<sup>+</sup>/EdU<sup>+</sup> cells counts (**C**), and abundance (**D**) were analyzed. AFMI treatment was set as baseline and used to normalize proliferating astrocyte (GFAP<sup>+</sup>/EdU<sup>+</sup>) counts of treatment conditions (**C**). PLX treatment drastically reduced EdU<sup>+</sup> astrocyte numbers, while Th17 significantly increased them. Data was analyzed using Welch test one-way ANOVA ( $\alpha < 0.05$ ), AFMI n = 24, AFMI+PLX n = 8, AFMI+17 n = 17, AFMI+Th1 n = 13, AFMI+Tregs n = 17; Main effect:  $W(4,34.25)=47.00$ ,  $p < 0.0001$ , followed by Dunnett's T3 multiple comparisons test, p is reported as multiplicity adjusted p-value: ns ( $p > 0.05$ ), \* ( $p < 0.05$ ), \*\*\*\* ( $p < 0.0001$ ) (**C**); Main effect:  $W(4,33.91)=50.41$ ,  $p < 0.0001$ , followed by Dunnett's T3 multiple comparisons test, p is reported as multiplicity adjusted p-value: ns ( $p > 0.05$ ), \* ( $p < 0.05$ ), \*\*\*\* ( $p < 0.0001$ ) (**D**). Scale bar: 75  $\mu$ m (**B**).

To investigate the possibility of AFMI acting as primer for microglia and their potential in elevating astrocytic response two strategies were used. The first was to deplete microglia from the tissue to see if this would lead to a decrease in astrocytic proliferation. The second was to introduce different types of T cells with either inflammatory (Th17 and Th1) or anti-inflammatory (T<sub>regs</sub>) properties into the culture. For microglia depletion, slices were treated with PLX for 72 hours before AFMI was performed. T cells were introduced 5 days after AFMI and co-cultured with OHSCs for 2 days (**Figure 12 A**). As a quality control, only experiments with a higher number of proliferating astrocytes in AFMI than in untreated control were used for the analysis. PLX treatment appears to have no adverse side effects on astrocytes numbers, appearance (**Figure 13 A**) or glial scarring (**Figure 13 B**). *In vivo*, CNS tissue depleted of microglia is repopulated by infiltration of peripheral macrophages; in OHSCs, which lack a periphery, repopulation has been observed by proliferation of remaining microglia cells as early as day 4 after depletion<sup>208</sup>. However, in the control experiments conducted to confirm depletion and to analyze influence of PLX on astrocytes there were only a few microglia present in the culture at 7 dpi (**Figure 13 B**, lower middle panel) comparable to the situation immediately after depletion (**Figure 13 A**, lower middle panel).

While PLX appears to have no apparent effect on astrocytes, it significantly reduces the abundance of EdU<sup>+</sup> cells (**Figure 12**, **Figure 14**) as well as the number and abundance of proliferating astrocytes (**Figure 12 C and D**) 7 days after AFMI.

**A****B**

**Figure 13: Astrocytes are not affected by PLX mediated microglia depletion.** **A.** OHSCs were generated from p3 – 5 B6 mouse pups and treated with PLX 1 DIV for 72 h before fixation. IHC stainings were GFAP (green), Iba1 (red) and DAPI (blue). Top panels show a control slice containing a larger number of Iba1<sup>+</sup> microglia, while lower panels show a PLX-treated slice containing only a few Iba1<sup>+</sup> cells. GFAP<sup>+</sup> astrocyte numbers are not affected by the treatment. **B.** OHSCs were generated from p3 – 5 B6 mouse pups and treated with PLX 1 DIV for 72 h. AFMI was conducted at 5 DIV and OHSCs were fixated at 7dpi. IHC stainings were GFAP (green), Iba1 (red) and DAPI (blue). Top panels show an injured slice with occurrence of glial scarring and a large number of Iba1<sup>+</sup> microglia distributed throughout the slice. Lower panels show an injured slice treated with PLX displaying glial scarring and a few Iba1<sup>+</sup> microglia within that scar. Scale bar: 75  $\mu$ m (**A – B**).

Infiltration of Th17 cells used as a second hit induces a significant increase in overall abundance of EdU<sup>+</sup> cells (**Figure 14**), but more importantly significantly increases the number and abundance of proliferating astrocytes when compared to AFMI alone (**Figure 12 C and D**). A large number of GFAP<sup>+</sup>/ EdU<sup>+</sup> cells are found in the glial scar surrounding the injury (**Figure 12 B**) pointing towards a negative impact of immune-mediated inflammation on astrocyte activation and glial scar formation.

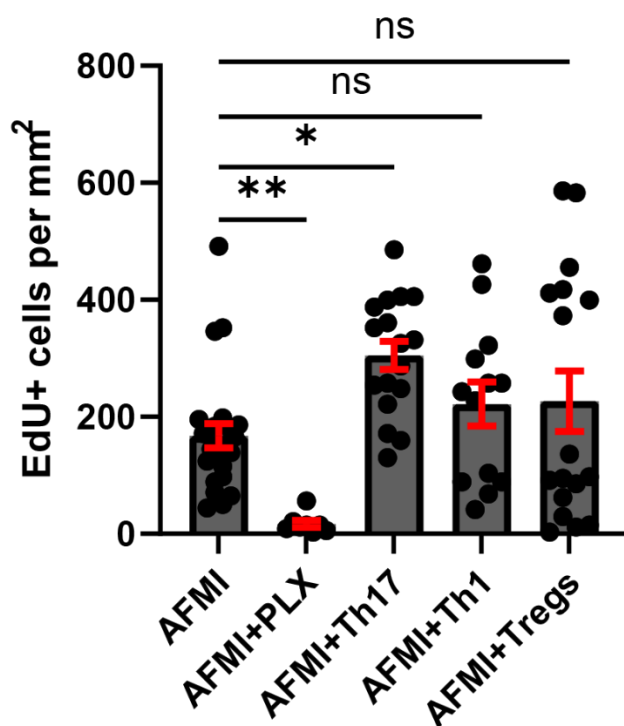




**Figure 14: EdU<sup>+</sup> cells are increased by Th17 cells and decreased by PLX treatment in OHSCs.** OHSCs were generated from p3 – 5 B6 mouse pups and treated with PLX 1 DIV for 72 h. AFMI was conducted at 5 DIV and OHSCs were fixated at 7dpi. PLX treatment significantly reduced abundance of proliferating cells within the slices, while Th17 significantly increased them. EdU<sup>+</sup> cells per mm<sup>2</sup> did not differ between AFMI and Th1/ T<sub>regs</sub> although both groups show a bimodal distribution. Data was analyzed using Kruskal-Wallis test ( $\alpha = 0.05$ ), AFMI n = 24, AFMI+PLX n= 8, AFMI+17 n = 17, AFMI+Th1 n = 13, AFMI+Tregs n = 17, Main effect: p<0.0001, followed by Dunn's multiple comparisons test, each group's mean rank was compared to the mean rank of the AFMI group, \*\* (p<0.01), \* (p<0.05).

Th1 cells infiltrating into the tissue appear to have a similar effect on astrocytic proliferation as Th17 cells. This is however not significant, due to the large variation within and bimodal distribution of the dataset (**Figure 12 C and D**).

Surprisingly, treatment with T<sub>regs</sub> has no impact on number and abundance of proliferating astrocytes (**Figure 12 C and D**) and the slices also display regular formation of glial scarring around the injury site (**Figure 12 B**). This may be because the astrocytes are not a target cell type for the T<sub>regs</sub> in this model.

The decrease of proliferative activity in astrocytes after microglia depletion further strengthens the idea that microglia are the driving force behind the astrocyte response towards injury. Even though PLX appeared to have no discernible effect on the appearance of astrocytes within OHSCs, no statement can be made about functional consequences of the treatment.

### 3.5 DREADD-activated microglia display a shift towards a rod-like phenotype

Since the depletion of microglia had such a profound effect on astrocyte activation, it stood to reason that the continuous activation of microglia is likely to further exacerbate astrogliosis. A stable way to activate and prime microglia is treatment with the bacterial endotoxin LPS<sup>142</sup>. However, LPS – which works via the TLR-4 – also activates astrocytes<sup>166,167</sup>. To clearly dissect the crosstalk between both cell types and the role microglial activity plays on astrocytes, one needs a model where microglia can be intrinsically activated or deactivated. Therefore, the next aim of the project was to establish the genetically encoded chemogenetic tool DREADD in microglia cells.

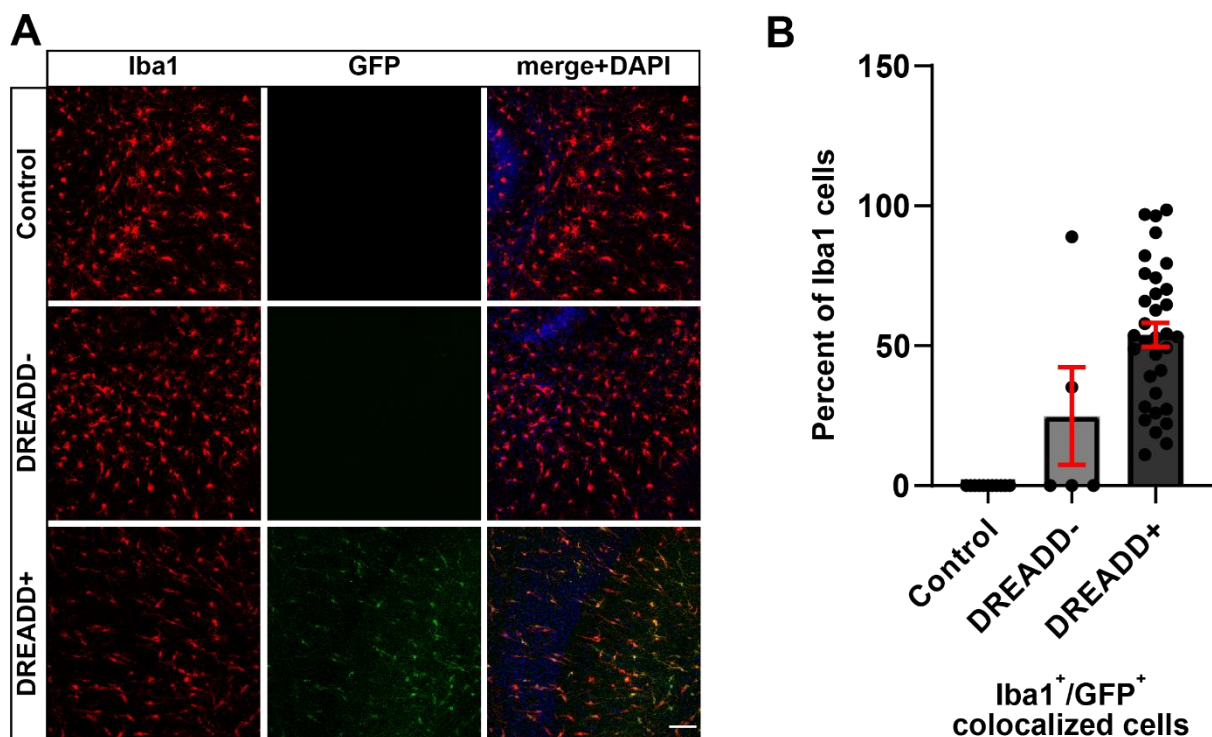


**Figure 15: Characterization of a chemogenetic DREADD<sub>Gq</sub> construct expressed under a CSF1R promoter.** **A.** OHSCs prepared from p7 mouse pups (B6 or CSF1R<sup>Cre</sup> x DREADD<sub>Gq</sub>-mCitrine) were treated with CNO (1 μM) for 6 h and stained for Iba1 (red) and GFP (green) after fixation. **B.** Iba1<sup>+</sup>/GFP<sup>+</sup> cells shown as percent of total amount of Iba1 cells. In a few Cre<sup>-</sup> DREADD<sub>Gq</sub> (DREADD-) slices GFP signals and colocalization with Iba1 were observed, which are considered artifacts and not relevant, Slices prepared from B6 pups displayed no signals. Cre<sup>+</sup> DREADD<sub>Gq</sub> (DREADD+) exhibit consistent GFP staining ranging from 11 to almost a 100% colocalization with Iba1. Control n = 11, DREADD- n = 5, DREADD+ n = 33. No statistical analysis was performed due to large differences in sample size. Scale bar: 75 μm (A).

OHSCs were prepared from mice expressing the activating DREADD hMD3q under the CSF1R promoter. To ensure correct expression of the DREADD construct in microglia cells and determine the level of expression, OHSCs from CSF1R<sup>Cre</sup> x DREADD<sub>Gq</sub>.mCitrine mouse pups were treated with CNO and stained for Iba1 to visualize the microglia as well as GFP to relabel the mCitrine tag of the construct, as fluorescent tags often degrade due to PFA fixation. Colocalization analysis of Iba1 and GFP revealed that all slices from Cre<sup>+</sup> DREADD mice (DREADD<sup>+</sup>) expressed the construct, albeit in varying degrees ranging from 11 to almost a 100 %, with mean expression level being ~54% of Iba1<sup>+</sup> microglia (**Figure 15 A and B**). Low expression rates are likely due to some mice having been hemizygous as the genotyping of the mice does not allow for distinction of hemi- and homozygous animals. Some of the slices from Cre<sup>-</sup> DREADD mice (DREADD<sup>-</sup>) also displayed rare GFP signals and colocalization with Iba1 (**Figure 15 B**), these are however, considered artifacts through poor staining quality and high background fluorescence. Regular B6 mouse pups were used as a negative control and did not display any GFP fluorescent signals (**Figure 15 B**). Although levels of chemogenetically activatable microglia differed between slices, the generation of the model was successful and presents a valuable tool to study microglia activation and interaction with astrocytes in future experiments.

Interestingly, when taking a closer look at the DREADD<sup>+</sup> and CNO-activated microglia a distinct morphological feature becomes apparent. Compared to the DREADD<sup>-</sup> and B6 slices treated with CNO that show mostly ramified and amoeboid microglia, the DREADD<sup>+</sup> slices appear to have a high number of microglia with an elongated cell body bipolar process morphology (**Figure 15 A**). This morphology is called rod-like microglia and still presents a mystery as very little is known about them despite their widespread occurrence in neuropathological conditions<sup>141,145,209</sup>. To examine this phenomenon, distributions of microglia shapes were compared between the control, DREADD<sup>-</sup> and DREADD<sup>+</sup> slices treated with CNO as well as DREADD<sup>+</sup> slices treated with DMSO (DREADD<sup>+</sup> DMSO). Consistent with control and DREADD<sup>-</sup> slices, DREADD<sup>+</sup> DMSO slices appeared to only have sporadic occurrence of rod-like microglia (**Figure 16 A**), thus rejecting the idea that the expression of the DREADD construct or the CNO alone leads to the observed morphological change in microglia. Those findings rather support the hypothesis that the change is a consequence of the microglial activation by the DREADD construct via CNO.

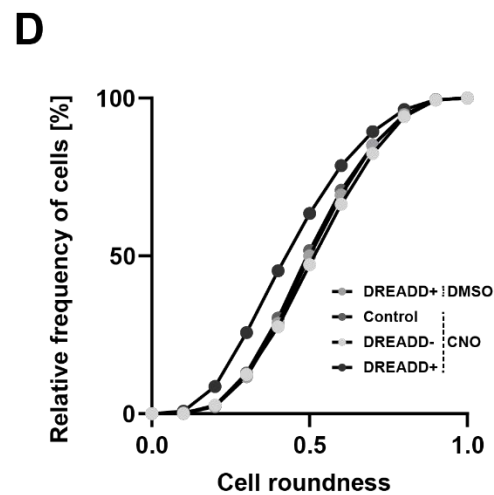
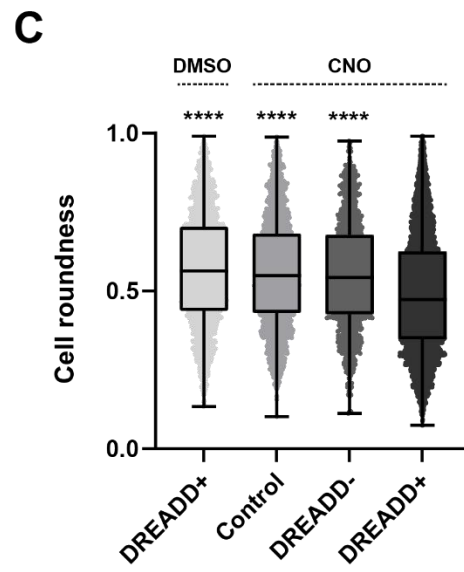
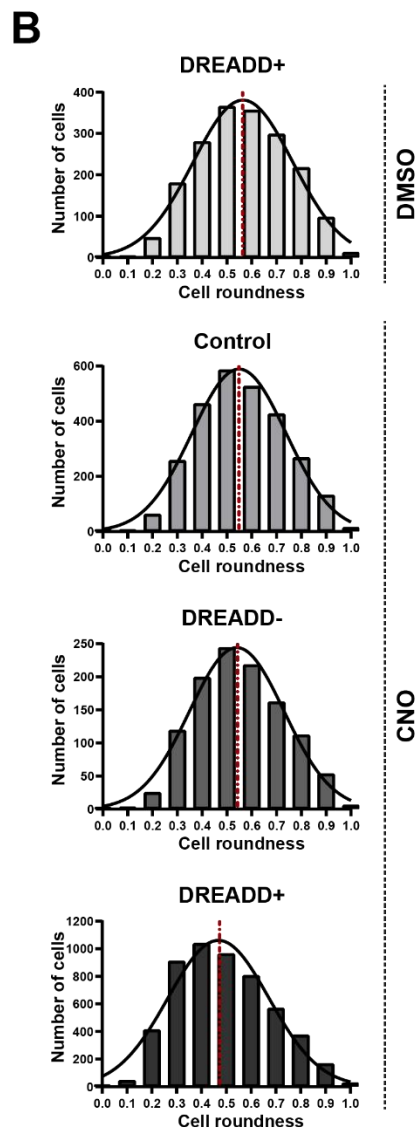
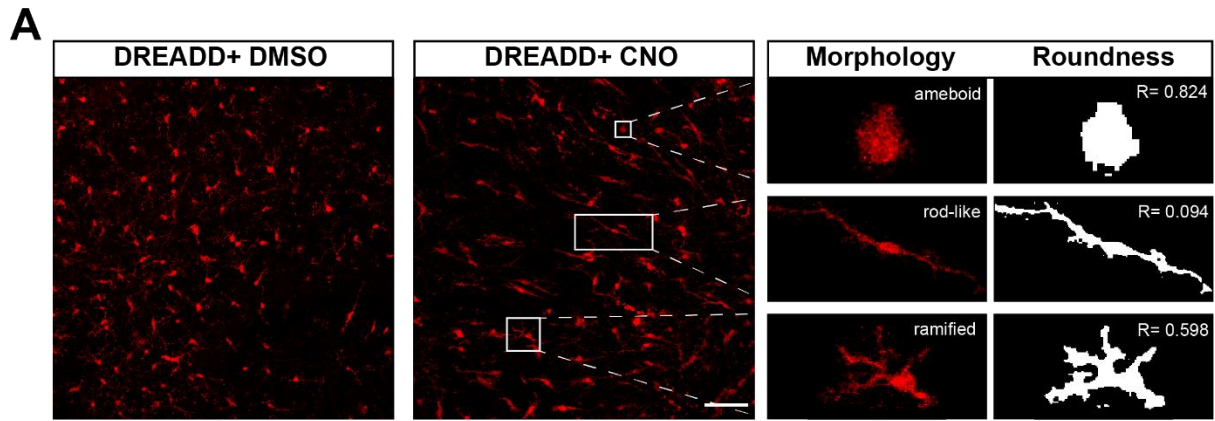


**Figure 16: Morphological changes in DREADD-activated microglia after CNO treatment.** **A.** Left panel: OHSC from p7 Cre<sup>+</sup> DREADD<sub>Gq</sub> pup treated with CNO (1 μM, 6 h) and stained for Iba1 (red). Microglia were categorized morphologically into ameboid, ramified or rod-like microglia (middle panels) and roundness R was determined via particle analysis (right panels). **B.** Frequency distributions of cell roundness for DREADD+ slices treated with DMSO (DREADD+ DMSO) as well as control, DREADD- (DREADD- CNO) and DREADD+ slices treated with CNO (DREADD+ CNO). Cell roundness is given from 0 (not round) to 1 (perfectly round). Black line represents fitting of non-linear gaussian regression. Dotted vertical red line represents median. **C.** Box plot displaying minimum, maximum and distribution of cell roundness with each dot representing one individual cell and black line showing the median. Data was analyzed using Kruskal-Wallis test ( $\alpha < 0.05$ ), DREADD+ DMSO n = 1856, control n = 2732, DREADD- CNO n = 1141, DREADD+ CNO n = 5300; Main effect:  $p < 0.0001$ , followed by Dunn's multiple comparisons test, each group's mean rank was compared to the mean rank of the DREADD+ CNO group, \*\*\*\* ( $p < 0.0001$ ). **D.** Cumulative frequency distribution of cell roundness. DREADD+ CNO curve displays a shift to the left compared to all other curves. Scale bar: 75 μm (**A**).

To support these findings, based solely on visual examination of the slice images, quantity and distribution of microglia morphology were analyzed in all four groups. Microglia were classified into three morphologically distinct categories: ameboid, having a round cell body with little to no processes; rod-like, having a long cell body and a few mostly bipolar processes and ramified, having a roundish cell body and processes of varying numbers and configurations (**Figure 16 A**).

**Table 20: DREADD microglia morphology frequencies.** Cell counts and cumulative frequencies of roundness factor R for all groups. Categorization of R ranges into microglia morphologies: 0.1 – 0.3 rod-like, 0.4 – 0.7 ramified, 0.8 – 1 ameboid.

	DREADD+ DMSO			Control CNO		DREADD- CNO		DREADD+ CNO	
	R	Cell counts	Cumulative frequency	Cell counts	Cumulative frequency	Cell counts	Cumulative frequency	Cell counts	Cumulative frequency
rod-like	0	0	0.00	0	0.00	0	0.00	0	0.00
	0.1	3	0.16	1	0.04	3	0.26	44	0.83
	0.2	48	2.75	62	2.31	25	2.45	411	8.58
	0.3	180	12.45	257	11.71	119	12.88	909	25.74
ramified	0.4	280	27.53	463	28.66	199	30.32	1037	45.30
	0.5	365	47.20	585	50.07	244	51.71	963	63.47
	0.6	356	66.38	526	69.33	218	70.82	805	78.66
	0.7	298	82.44	426	84.92	162	85.01	567	89.36
ameboid	0.8	217	94.13	267	94.69	112	94.83	373	96.40
	0.9	97	99.35	131	99.49	53	99.47	165	99.51
	1	12	100.00	14	100.00	6	100.00	26	100.00

Cell roundness (R) was used as a measure to reflect the morphological shapes and was defined for the three groups as follows: rod-like microglia, R 0.1 – 0.3, ramified R 0.4 – 0.7, amoeboid R 0.8 – 1 (**Table 20**). While control, DREADD- and DREADD+ DMSO slices displayed similar distributions of cell roundness, a clear left shift of the distribution was observed in the DREADD+ CNO slices (**Figure 16 B**). Those differences in distributions were also reflected in a lower median for the DREADD+ CNO slices which differed significantly compared to the medians of all other groups (**Figure 16 C**). To correct for the varying numbers of cells in the different groups, cell roundness was also displayed as relative frequency of all cells revealing a higher occurrence of rod-like and ramified microglia in DREADD+ CNO slices compared to the other groups (**Figure 16 D, Table 20**). Taken together these findings underline the hypothesis that chemogenetic activation of microglia leads to a shift in microglia morphology towards a more rod-like phenotype.

## 4 Discussion

The concept that glial cells within the CNS communicate with neurons (neuron-glia interaction) but also among each other (glia-glia communication) both under homeostatic and pathological conditions has long been established<sup>2,61,109,210-212</sup>. Astrocytes and microglia both influence the differentiation of OPCs into myelinating oligodendrocytes depending on their level of activation. Especially in demyelinating diseases like MS these interactions play a critical role in either ameliorating or exacerbating disease progression (for comprehensive reviews see references<sup>61,210</sup> and<sup>2</sup>).

The crosstalk between astrocytes and microglia leading to neuropathological disturbances happens within distinct spatial and temporal patterns. Although the interaction is bidirectional, astrocyte activation is initially driven by microglia, which are quicker to respond to an insult<sup>210</sup>. Activated microglia are able to secrete a plethora of molecules like TNF- $\alpha$ , NO, IFN- $\alpha/\beta$ , H<sub>2</sub>O<sub>2</sub>, IL1- $\alpha$ , C1q, TGF- $\alpha$ , VEGF-B<sup>91,97,163,213-215</sup> and many more<sup>210</sup>. The astrocytic response and differential activation depend in part on the factors secreted by the microglia, with some factors inducing a more neurotoxic reactivity, while others have been linked to induction of neuroprotection<sup>210</sup>. However, there are other mechanisms that influence astrocytic activation by microglia like the presence and recruitment of other cell types and the ability of astrocytes to downregulate the inflammatory response by inhibiting the microglia. Several factors secreted by astrocytes are crucial in regulating microglia activation and thereby the outcome of the inflammatory injury. ORM2<sup>164</sup> and TGF- $\beta$ <sup>216</sup> have both been implicated in downregulating microglia activation, with ORM2 binding to microglial CCR5 and thereby blocking the CXCL4-CCR5 axis that is crucial for microglia activation. LCN2 on the other hand, counteracts ORM2 functions and increases microglial activation<sup>87</sup>. The increase in ORM2 secretion by astrocytes is mediated by pro-inflammatory factors from microglia and builds up over a course of 24 hours after occurrence of CNS damage<sup>210 164</sup>.

Therefore, a major aim of this thesis was the development of a stable and reproducible laser injury model in an intact tissue environment to study glial responses to a non-inflammatory and controlled damaging CNS insult. After successfully establishing the AFMI model in OHSCs microglial and astrocytic responses towards the injury were observed that fit the timeline of interaction described above. The microglia response characterized by increase of Iba1 and increased microglial presence occurred within minutes after the injury, while the astrocytic activation characterized by increased GFAP reactivity manifested itself at day 7.

It can be hypothesized that in the absence of invading immune cells microglia react towards an injury by increasing their presence and activating the astrocytes in the vicinity of the injury. The activated astrocytes likely proceed by downregulation of microglial activation as 24 hours after injury the Iba1 levels are back to control and microglia have dispersed again. Astrocytes continue to slowly increase their level of activation and begin to form a glial scar around the injury site.

In contrast to the microglia, whose increase in numbers around the injury site is due to migratory behaviour, as cell proliferation cannot take place within mere minutes, the increase in astrocytes and the forming of the glial scar relies in part on proliferation.

The capability of astrocytes to form glial scars at the site of injury is a highly debated topic in terms of beneficial or detrimental outcomes on CNS damage and repair. The glial scar functions as a barrier separating the lesion from the healthy tissue<sup>93</sup>. It has been described as having a negative impact on regeneration/remyelination by preventing OPCs to enter demyelinated MS lesions<sup>104,106,107,109,217</sup>. However, it has also been described as neuroprotective by taking up excessive levels of glutamate, containing the spread of invading immune cells and reforming the BBB<sup>112,114,116</sup>. Disruption of glial scar formation in EAE has been linked to widespread inflammation and worsening of symptoms<sup>113</sup>. While the precise impact of glial scar formation depends on the circumstances and possibly the type of injury, it is well described that the occurrence of a compact glial scar in conjunction with proliferating astrocytes is a hallmark of severe astrogliosis<sup>46,82</sup>. At 1 dpi, the forming of a glial scar can already be observed although without a significant increase in proliferating cells signifying a reorientation and possible migration of the astrocytes in the immediate surroundings of the injury. At 7 dpi, the glial scar has extended in size and contains numerous proliferating astrocytes. Depletion of microglia does not ablate glial scar formation but reduces the number of proliferating cells in general as well as proliferating astrocytes specifically. The reduced numbers of proliferating astrocytes shows that their proliferation is dependent on microglia presence and signalling, while glia scar formation is not.



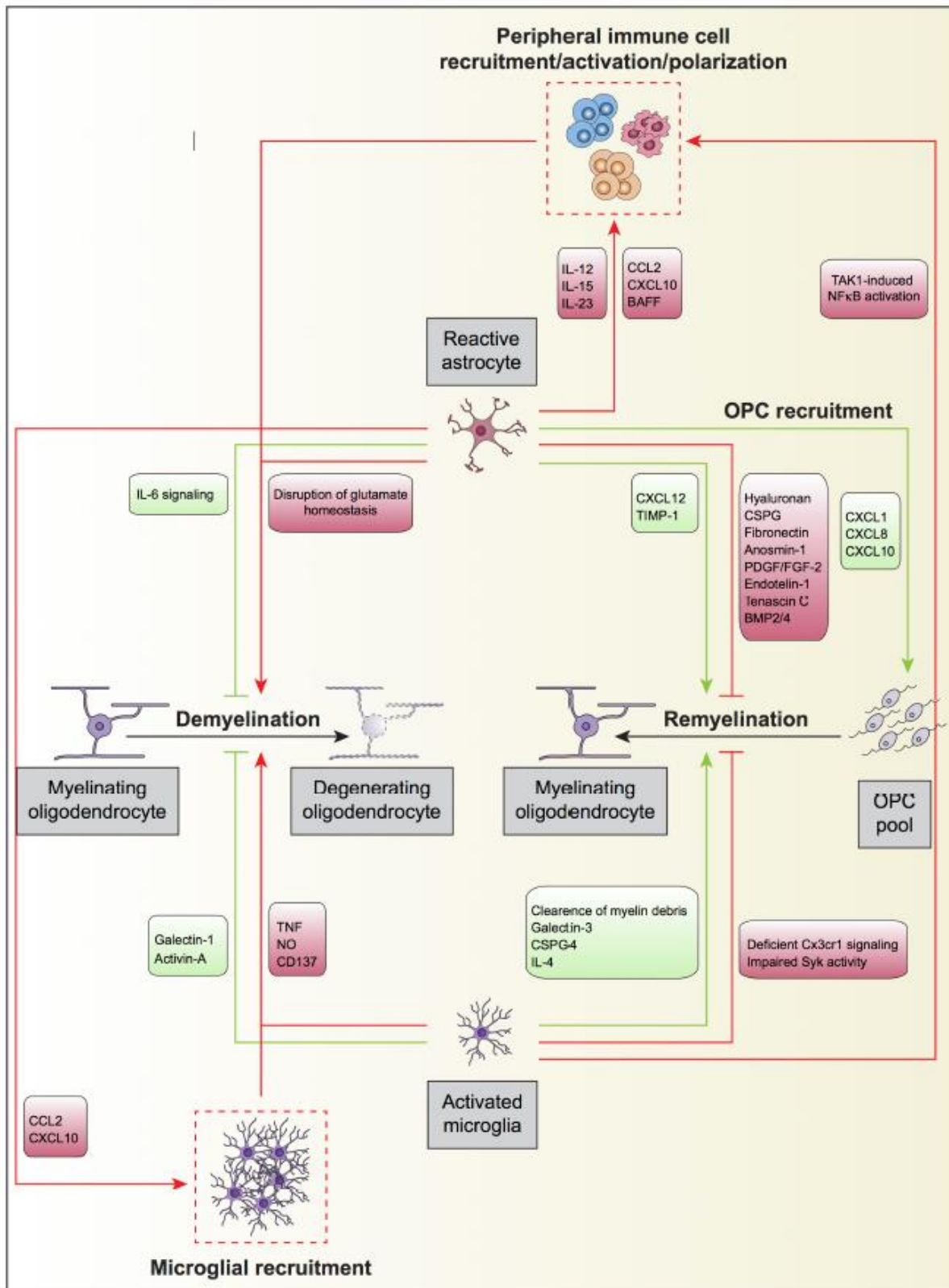


**Figure 17: Influence of microglia and astrocyte crosstalk on immune cell invasion and de-remyelination.** Glial crosstalk in the context of demyelinating and inflammatory disease is highly complex. Adapted from Domingues et al., 2016<sup>61</sup>.

Mature astrocytes are normally quiescent with a low turnover and rate of proliferation but are able to re-enter the cell cycle during scar formation<sup>76,96,207</sup>. Molecular signalling that has been characterized to induce astrocytic proliferation includes trophic factors like FGF, BDNF, GDNF, VEGF<sup>98,99</sup>, as well as EGF<sup>100</sup> and ET-1<sup>96</sup>. Factors like FGF, BDNF, GDNF<sup>101,102</sup> and especially VEGF<sup>97</sup> have been shown to be secreted by microglia. VEGF-B secreted by microglia has been demonstrated to shift astrocytes towards a more neurotoxic phenotype and contributes to EAE pathogenesis<sup>97</sup>. This could indicate a detrimental role of glia scar formation through proliferation after AFMI in the presence of microglia, while scar formation through migratory behaviour without microglia represents a beneficial mechanism protecting the healthy tissue.

The return of microglial cells towards a seemingly surveying phenotype observed 1 day after AFMI hypothesized to be mediated by astrocytic downregulation of activity might be reflective of a primed phenotype rather than a complete return to a surveying state. Microglia residing in a primed state after previous injury are characterized by increased CD68 and MHCII expression and display an exaggerated response towards a second inflammatory stimulus (second hit hypothesis) resulting in hyperactivation<sup>142,159</sup>. After introducing invading pro-inflammatory T cells into the tissue, a further increase of astrocytic proliferation especially within the glial scar was observed. This supports the idea of an exaggerated microglia response driving an exacerbation of astrogliosis and scar formation, which can have both detrimental and beneficial aspects as discussed earlier.

Another explanation for the increased astrocytic reactivity and proliferation is the direct interaction of astrocytes and pro-inflammatory T cells. Especially since the main effect on proliferation found here is by Th17 cells and some studies presented evidence that they are not targeting microglia but only astrocytes in the CNS<sup>218,219</sup>.

Astrocytic interaction with CNS-invading T cells still presents a challenge as it is a highly complex dynamic. Pro-inflammatory NF- $\kappa$ B signalling on astrocytes induces pro-inflammatory T cell phenotypes such as Th17 or Th1<sup>88</sup>, while also possessing the capability of differentiating them into T<sub>reg</sub> cells<sup>220</sup>. The presence of Th17 and Th1 cells in CNS tissue induces an upregulation of a pro-inflammatory response in astrocytes marked by increased expression of inflammatory cytokines like IL6 and chemokines like CCL2, CCL20 and CXCL10<sup>219</sup>.

This presents a mechanism by which astrocytes are further recruiting inflammatory T cells as well as activated microglia, largely considered to exacerbate neuroinflammation<sup>219,221,222</sup>. Although recruitment of microglia can also be associated with increased clearance of debris<sup>165</sup> and CXCL10 expression on astrocytes has also been linked to recruitment of OPCs towards demyelinated areas<sup>103</sup> (**Figure 17**).

Chemically targeting CNS cells either for depletion or activation cells always suffers from unintended side effects. First, because the complete removal of a cell type profoundly disturbs the cellular network and is almost guaranteed to have unintended effects. Second, as mentioned earlier, while the depletion of microglia does not appear to affect astrocytes, consequences on astrocyte function have not been investigated to date.

Selectively activating a cell type within the CNS network proves to be even more difficult. Most studies that investigate the effect of microglia priming and activation use LPS. As mentioned before, LPS also activates astrocytes making it unusable when investigating the influence of microglia activation on astrocytes.

Therefore, the usage of chemogenetic models is a useful tool in investigating astrocyte-microglia crosstalk. The DREADD model that utilizes modified receptors, which can only be activated by specific normally inert small molecules, has mostly been used to target specific populations of neurons and modulate their activity (for a review see<sup>169</sup>). However, the usage of DREADDs to investigate the influence of microglia activation or inhibition *in vitro* and *in vivo* has been slowly increasing over the last years.

Several studies used microglia-specific DREADDs in the context of neuropathic pain, demonstrating that inhibition of microglia activation by hM4Di DREADDs prevents the development of chronic pain in different models<sup>177,223,224</sup>. Furthermore, it could be shown that activation of spinal microglia through hM3Dq DREADDs alone was sufficient to induce hind paw allodynia in rats<sup>177</sup>.

Global expression and activation of hM3Dq under the CX<sub>3</sub>CR<sub>1</sub> promotor resulted in an increase of pro-inflammatory cytokines in the CNS; primary microglia cultures prepared from these mice displayed increased phagocytosis upon activation. Curiously, the combination of continuous DREADD-activation over 4 days resulted in a decreased response towards an inflammatory LPS stimulus<sup>225</sup>.

While it is possible that a prolonged DREADD activation results in a habituation of the microglia, another explanation might be the regulatory effect of astrocytes to counteract microglia activation.

Lastly, a very recent study demonstrated that inhibiting microglial activation via hM4Di DREADDs in OHSC has the same effect on prevention of pro-inflammatory responses in alcohol-induced neuroinflammation as depletion via PLX<sup>208</sup>. Thus, the hM4Di DREADD model is a useful tool to study the astrocytic response without microglial activation and without disrupting the entire cellular network.

All studies utilizing DREADD vector constructs expressed them under the CD68 promotor<sup>177,208,223</sup>, while studies using DREADD mouse models opted for the CX<sub>3</sub>CR<sub>1</sub> promotor<sup>225,226</sup>. In the present study, the hM3Dq DREADD construct was expressed under the CSF1R promotor, since it shows a more selective targeting in the CNS than the CD68 promotor<sup>158,227,228</sup>. For the constitutive CX<sub>3</sub>CR<sub>1</sub> Cre-line, evidence has accumulated that expression of the floxed allele can also occur in neurons<sup>229,230</sup>, while the inducible CX<sub>3</sub>CR<sub>1</sub> Cre-line presents the caveat of having to treat the OHSC with tamoxifen for DREADD expression thereby prolonging the time in culture and increasing glial responses.

None of the existing studies utilizing hM3Dq DREADDs in microglia have reported unusual morphological changes, therefore this study presents the first evidence that DREADD-activated microglia display an increased occurrence of rod-like morphology.

Microglia morphology and its functional consequences are a highly debated topic. Under homeostatic conditions, microglia display a surveying/ramified phenotype characterized by a small cell body and several highly branched processes<sup>118,231</sup>. Upon encountering DAMPs or PAMPs, microglia react by gradually thickening and retracting their processes, while the cell body enlarges. Depending on the extent of those changes, they are classified as bushy, hyper-ramified, active or hyper-active microglia. In their most extreme form, microglia display an ameboid morphology where the processes have completely retracted and only a large round cell soma remains<sup>118,134,232-234</sup>. Morphological changes in microglia are reversible and allow them to shift between states in response to changes in their surroundings (**Figure 18**). While the classifications surveying/ramified and ameboid microglia have been widely accepted and are used consistently, as of yet no uniform system has been established to classify the intermediate ramified microglia states.

Therefore, microglia that displayed neither a rod-like nor an ameboid morphology were collectively classified as ramified microglia in the present study.

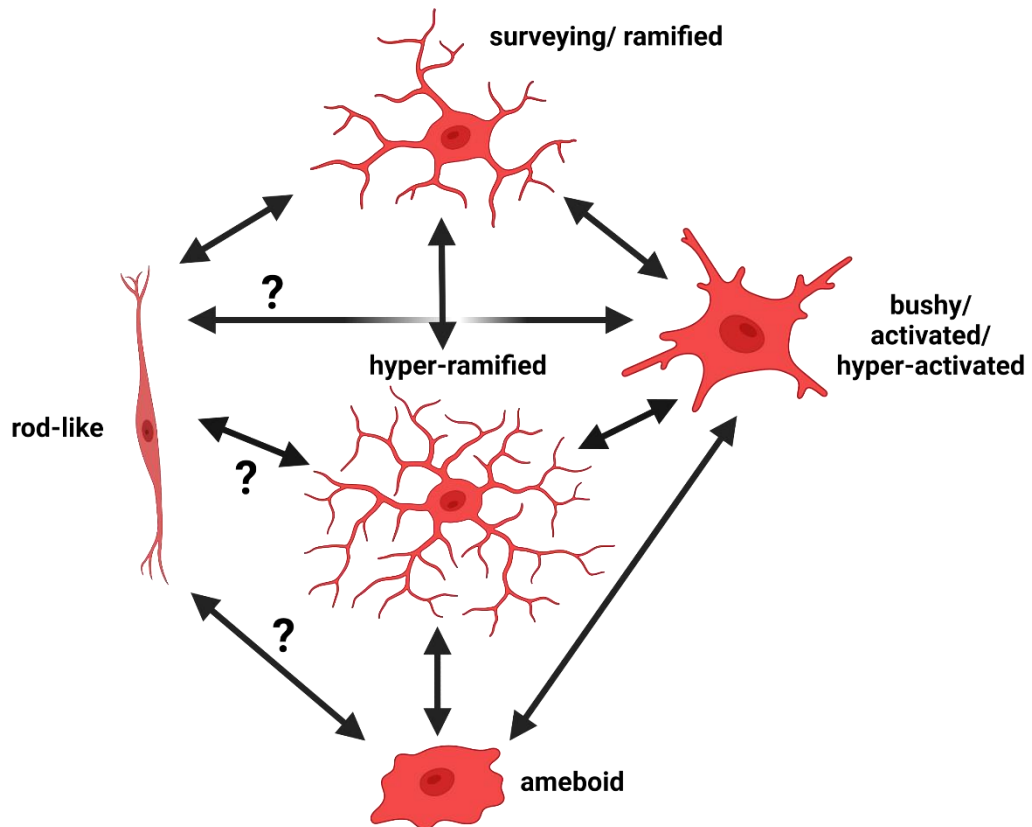


**Figure 18: Schematic representations of microglia morphologies observed in health and disease** <sup>206</sup>. Microglia shift from their homeostatic surveying/ ramified morphology to different phenotypes depending on the activation. Description of phenotype also depends on the classification system used. Morphological shifts do not represent static non-reversible events, but rather fluid changes in state in response to the surroundings. Question marks represent possible events that have not yet been observed and need clarification. Modified from Holloway et al., 2019 <sup>141</sup>.

Rod-like microglia were described as early as 1899 but received sparse attention, since they only appeared infrequently. So far this morphology, which is characterized by an elongated cell body with few bipolar processes, has been linked to infectious diseases, ageing, traumatic brain injury (TBI) and neuroinflammation <sup>145,209,235-238</sup> (for a review see <sup>141</sup>). Rod-like microglia have been observed to form so called trains, which are several cells aligning end-to-end, often appearing to be interconnected.

This has been observed *in vivo* after TBI<sup>145,236,237</sup> and *in vitro* in response to scratched culture plates<sup>239,240</sup>, and is believed to represent an alignment with neuronal structures<sup>241</sup>. Here, neither trains of rod-like microglia nor a specific orientation of the cells, indicative of an alignment with other cell structures, is observable.

Activation via DREADDs presents a stable model to induce a large increase in microglia displaying a rod-like morphology and allows for future analysis of rod-like microglia function. Tentative analyses so far have observed MHCII expression, signifying a role in antigen-presenting and CD68, which is often used as a marker for phagocytosis<sup>236</sup>. Both markers have also been implicated in the characterization of primed microglia<sup>142</sup>. The DREADD hM3Dq exerts its effect by increasing intracellular Ca<sup>2+</sup><sup>169</sup>. While it has been shown that Ca<sup>2+</sup> plays a role in microglia activation, most of the work so far has been done *in vitro* in microglia cell culture<sup>242-245</sup> with some studies reporting the absence of spontaneous Ca<sup>2+</sup> signalling in surveying/ramified microglia *in vivo*<sup>126-128</sup>. About 4 % of microglia display spontaneous Ca<sup>2+</sup> transients in both soma and processes, which increases to 34 % after LPS treatment and 42 % after a focal laser injury *in vivo*. Pre-treating the mice with LPS and performing focal laser injury resulted in 67 % of microglia displaying Ca<sup>2+</sup> transients leading the authors to the conclusion that the cells are primed by LPS and display an exaggerated response towards a second hit represented by the laser injury<sup>128</sup>. As discussed previously, LPS is not exclusively acting upon microglia, therefore it cannot be excluded that astrocytes play a role in the observed microglial reaction. However, the study presents further evidence for the second hit model in the development of neurodegenerative pathologies as well as compelling evidence for a role of intracellular Ca<sup>2+</sup> increase in primed microglia.

Taken together, the findings that primed microglia exhibit CD68 and MHCII expression and increased intracellular Ca<sup>2+</sup> and that the increase of Ca<sup>2+</sup> in microglia via hM3Dq DREADDs leads to a rod-like morphology, which has also been linked to CD68 and MHCII expression, hint at the possibility that the rod-like microglia phenotype represents a form of primed microglia.

Overall, it could be shown that astrocytes and microglia have different timelines of activation in response to a consistent and stable model of laser injury and that the astrocytic response is likely to be driven by microglia. It could be demonstrated that formation of the glial scar is not dependent on microglia as it also occurred in absence of microglia, but the increased formation through proliferating astrocytes is orchestrated by microglia signalling.

Invading pro-inflammatory T cells further increase astrogliosis by elevating astrocytic proliferation. This escalation in astrogliosis is a possible indicator for the switch from a beneficial astrocytic response towards a detrimental one.

Besides establishing a stable model for non-inflammatory CNS injury in intact cellular networks, a second model for chemogenetic activation of microglia could successfully be demonstrated here. The DREADD model provides a way to intrinsically activate microglia for further dissection of glial crosstalk in the CNS. Furthermore, the present study was the first to show that the activation of microglia via elevation of intracellular  $\text{Ca}^{2+}$  leads to a reproducible expression of the largely uncharacterized rod-like phenotype.

There are some questions that remain to be investigated in future studies like what factors are expressed by astrocytes and microglia in the different experimental conditions, as well as the consequences on myelination and axon damage to gain a deeper understanding of the functional ramifications. The successful implementation of the hM3Dq DREADD model provides a powerful tool to further study not only the functional properties of rod-like microglia, but also their role as potentially primed cells as well as the influence on astrocytes in CNS inflammation. Furthermore, it paved the way to implement the hM4Di DREADD model to study the inhibition of microglial activation on astrocytes without profoundly disturbing the cellular network.

## VII References

1. Weiner HL. Multiple Sclerosis Is an Inflammatory T-Cell–Mediated Autoimmune Disease. *Archives of Neurology* 2004; **61**(10): 1613-5.
2. Mayo L, Quintana FJ, Weiner HL. The innate immune system in demyelinating disease. *Immunol Rev* 2012; **248**(1): 170-87.
3. Ellwardt E, Zipp F. Molecular mechanisms linking neuroinflammation and neurodegeneration in MS. *Experimental Neurology* 2014; **262**: 8-17.
4. Lublin FD, Reingold SC, Sclerosis\* NMSSACoCToNAiM. Defining the clinical course of multiple sclerosis. *Results of an international survey* 1996; **46**(4): 907-11.
5. Love S. Demyelinating diseases. *J Clin Pathol* 2006; **59**(11): 1151-9.
6. Kuhlmann T, Ludwin S, Prat A, Antel J, Brück W, Lassmann H. An updated histological classification system for multiple sclerosis lesions. *Acta Neuropathol* 2017; **133**(1): 13-24.
7. Lassmann H. Multiple Sclerosis Pathology. *Cold Spring Harb Perspect Med* 2018; **8**(3).
8. Franklin RJ, Ffrench-Constant C. Remyelination in the CNS: from biology to therapy. *Nat Rev Neurosci* 2008; **9**(11): 839-55.
9. Nikic I, Merkler D, Sorbara C, et al. A reversible form of axon damage in experimental autoimmune encephalomyelitis and multiple sclerosis. *Nat Med* 2011; **17**(4): 495-9.
10. Siffrin V, Radbruch H, Glumm R, et al. In vivo imaging of partially reversible th17 cell-induced neuronal dysfunction in the course of encephalomyelitis. *Immunity* 2010; **33**(3): 424-36.
11. Frohman EM, Racke MK, Raine CS. Multiple sclerosis--the plaque and its pathogenesis. *N Engl J Med* 2006; **354**(9): 942-55.
12. Weiner HL. A shift from adaptive to innate immunity: a potential mechanism of disease progression in multiple sclerosis. *J Neurol* 2008; **255 Suppl 1**: 3-11.
13. Bjornevik K, Cortese M, Healy BC, et al. Longitudinal analysis reveals high prevalence of Epstein-Barr virus associated with multiple sclerosis. *Science* 2022; **375**(6578): 296-301.
14. Hafler DA, Compston A, Sawcer S, et al. Risk alleles for multiple sclerosis identified by a genomewide study. *N Engl J Med* 2007; **357**(9): 851-62.
15. Sadovnick AD, Ebers GC. Epidemiology of multiple sclerosis: a critical overview. *Can J Neurol Sci* 1993; **20**(1): 17-29.
16. Craner MJ, Damarjian TG, Liu S, et al. Sodium channels contribute to microglia/macrophage activation and function in EAE and MS. *Glia* 2005; **49**(2): 220-9.
17. Bittner S, Meuth SG, Göbel K, et al. TASK1 modulates inflammation and neurodegeneration in autoimmune inflammation of the central nervous system. *Brain* 2009; **132**(Pt 9): 2501-16.
18. Bittner S, Meuth SG. Targeting ion channels for the treatment of autoimmune neuroinflammation. *Ther Adv Neurol Disord* 2013; **6**(5): 322-36.
19. Friese MA, Craner MJ, Ezensperger R, et al. Acid-sensing ion channel-1 contributes to axonal degeneration in autoimmune inflammation of the central nervous system. *Nat Med* 2007; **13**(12): 1483-9.
20. Birkner K, Wasser B, Ruck T, et al. beta1-Integrin- and KV1.3 channel-dependent signaling stimulates glutamate release from Th17 cells. *J Clin Invest* 2020; **130**(2): 715-32.



21. Bittner S, Afzali AM, Wiendl H, Meuth SG. Myelin oligodendrocyte glycoprotein (MOG35-55) induced experimental autoimmune encephalomyelitis (EAE) in C57BL/6 mice. *J Vis Exp* 2014; (86).
22. Glatigny S, Bettelli E. Experimental Autoimmune Encephalomyelitis (EAE) as Animal Models of Multiple Sclerosis (MS). *Cold Spring Harb Perspect Med* 2018; **8**(11).
23. Engelhardt B, Carare RO, Bechmann I, Flügel A, Laman JD, Weller RO. Vascular, glial, and lymphatic immune gateways of the central nervous system. *Acta Neuropathol* 2016; **132**(3): 317-38.
24. Nicol B, Salou M, Laplaud DA, Wekerle H. The autoimmune concept of multiple sclerosis. *Presse Med* 2015; **44**(4 Pt 2): e103-12.
25. McFarland HF, Martin R. Multiple sclerosis: a complicated picture of autoimmunity. *Nat Immunol* 2007; **8**(9): 913-9.
26. IMGS C. Multiple sclerosis genomic map implicates peripheral immune cells and microglia in susceptibility. *Science* 2019; **365**(6460).
27. Morgan BP, Gommerman JL, Ramaglia V. An "Outside-In" and "Inside-Out" Consideration of Complement in the Multiple Sclerosis Brain: Lessons From Development and Neurodegenerative Diseases. *Front Cell Neurosci* 2020; **14**: 600656.
28. Fabriek BO, Zwemmer JN, Teunissen CE, et al. In vivo detection of myelin proteins in cervical lymph nodes of MS patients using ultrasound-guided fine-needle aspiration cytology. *J Neuroimmunol* 2005; **161**(1-2): 190-4.
29. Kooi EJ, van Horssen J, Witte ME, et al. Abundant extracellular myelin in the meninges of patients with multiple sclerosis. *Neuropathol Appl Neurobiol* 2009; **35**(3): 283-95.
30. Stys PK, Zamponi GW, van Minnen J, Geurts JJ. Will the real multiple sclerosis please stand up? *Nat Rev Neurosci* 2012; **13**(7): 507-14.
31. Lucchinetti C, Brück W, Parisi J, Scheithauer B, Rodriguez M, Lassmann H. Heterogeneity of multiple sclerosis lesions: implications for the pathogenesis of demyelination. *Ann Neurol* 2000; **47**(6): 707-17.
32. Trapp BD, Peterson J, Ransohoff RM, Rudick R, Mörk S, Bö L. Axonal transection in the lesions of multiple sclerosis. *N Engl J Med* 1998; **338**(5): 278-85.
33. Barnett MH, Prineas JW. Relapsing and remitting multiple sclerosis: pathology of the newly forming lesion. *Ann Neurol* 2004; **55**(4): 458-68.
34. Henderson AP, Barnett MH, Parratt JD, Prineas JW. Multiple sclerosis: distribution of inflammatory cells in newly forming lesions. *Ann Neurol* 2009; **66**(6): 739-53.
35. Ciotti JR, Cross AH. Disease-Modifying Treatment in Progressive Multiple Sclerosis. *Curr Treat Options Neurol* 2018; **20**(5): 12.
36. Haegert DG. The initiation of multiple sclerosis: a new infectious hypothesis. *Med Hypotheses* 2003; **60**(2): 165-70.
37. Poser CM. The role of trauma in the pathogenesis of multiple sclerosis: a review. *Clinical Neurology and Neurosurgery* 1994; **96**(2): 103-10.
38. Poser CM. Trauma to the Central Nervous System May Result in Formation or Enlargement of Multiple Sclerosis Plaques. *JAMA Neurology* 2000; **57**(7): 1074-7.

39. Smatti MK, Cyprian FS, Nasrallah GK, Al Thani AA, Almishal RO, Yassine HM. Viruses and Autoimmunity: A Review on the Potential Interaction and Molecular Mechanisms. *Viruses* 2019; **11**(8): 762.
40. Kurland LT. Trauma and multiple sclerosis. *Ann Neurol* 1994; **36**: 33-7.
41. Martinelli V. Trauma, Stress and multiple sclerosis. *Neurol Sci* 2000; **21**: 849-52.
42. Titus HE, Chen Y, Podojil JR, et al. Pre-clinical and Clinical Implications of “Inside-Out” vs. “Outside-In” Paradigms in Multiple Sclerosis Etiopathogenesis. *Frontiers in Cellular Neuroscience* 2020; **14**.
43. Sen MK, Almuslehi MSM, Shortland PJ, Coorsen JR, Mahns DA. Revisiting the Pathoetiology of Multiple Sclerosis: Has the Tail Been Wagging the Mouse? *Frontiers in Immunology* 2020; **11**.
44. Luchicchi A, Preziosa P, Hart B. Editorial: "Inside-Out" vs "Outside-In" Paradigms in Multiple Sclerosis Etiopathogenesis. *Frontiers in cellular neuroscience* 2021; **15**: 666529-.
45. Zhang Y, Barres BA. Astrocyte heterogeneity: an underappreciated topic in neurobiology. *Curr Opin Neurobiol* 2010; **20**(5): 588-94.
46. Sofroniew MV, Vinters HV. Astrocytes: biology and pathology. *Acta Neuropathol* 2010; **119**(1): 7-35.
47. Kimelberg HK. Functions of mature mammalian astrocytes: a current view. *Neuroscientist* 2010; **16**(1): 79-106.
48. Voigt T. Development of glial cells in the cerebral wall of ferrets: direct tracing of their transformation from radial glia into astrocytes. *J Comp Neurol* 1989; **289**(1): 74-88.
49. Kessaris N, Pringle N, Richardson WD. Specification of CNS glia from neural stem cells in the embryonic neuroepithelium. *Philos Trans R Soc Lond B Biol Sci* 2008; **363**(1489): 71-85.
50. Zhu X, Hill RA, Nishiyama A. NG2 cells generate oligodendrocytes and gray matter astrocytes in the spinal cord. *Neuron Glia Biol* 2008; **4**(1): 19-26.
51. Bushong EA, Martone ME, Jones YZ, Ellisman MH. Protoplasmic astrocytes in CA1 stratum radiatum occupy separate anatomical domains. *J Neurosci* 2002; **22**(1): 183-92.
52. Halassa MM, Fellin T, Takano H, Dong JH, Haydon PG. Synaptic islands defined by the territory of a single astrocyte. *J Neurosci* 2007; **27**(24): 6473-7.
53. Ma B, Buckalew R, Du Y, et al. Gap junction coupling confers isopotentiality on astrocyte syncytium. *Glia* 2016; **64**(2): 214-26.
54. Kiyoshi CM, Zhou M. Astrocyte syncytium: a functional reticular system in the brain. *Neural Regen Res* 2019; **14**(4): 595-6.
55. Halassa MM, Fellin T, Haydon PG. The tripartite synapse: roles for gliotransmission in health and disease. *Trends Mol Med* 2007; **13**(2): 54-63.
56. Perea G, Navarrete M, Araque A. Tripartite synapses: astrocytes process and control synaptic information. *Trends Neurosci* 2009; **32**(8): 421-31.
57. Noriega-Prieto JA, Araque A. Sensing and Regulating Synaptic Activity by Astrocytes at Tripartite Synapse. *Neurochem Res* 2021; **46**(10): 2580-5.
58. Verkhratsky A, Nedergaard M. The homeostatic astroglia emerges from evolutionary specialization of neural cells. *Philos Trans R Soc Lond B Biol Sci* 2016; **371**(1700).

59. Piontek J, Régnier-Vigouroux A, Brandt R. Contact with astroglial membranes induces axonal and dendritic growth of human CNS model neurons and affects the distribution of the growth-associated proteins MAP1B and GAP43. *J Neurosci Res* 2002; **67**(4): 471-83.
60. Barres BA. The Mystery and Magic of Glia: A Perspective on Their Roles in Health and Disease. *Neuron* 2008; **60**(3): 430-40.
61. Domingues HS, Portugal CC, Socodato R, Relvas JB. Oligodendrocyte, Astrocyte, and Microglia Crosstalk in Myelin Development, Damage, and Repair. *Frontiers in Cell and Developmental Biology* 2016; **4**.
62. Abbott NJ, Rönnbäck L, Hansson E. Astrocyte-endothelial interactions at the blood-brain barrier. *Nat Rev Neurosci* 2006; **7**(1): 41-53.
63. Ballabh P, Braun A, Nedergaard M. The blood-brain barrier: an overview: structure, regulation, and clinical implications. *Neurobiol Dis* 2004; **16**(1): 1-13.
64. Daneman R, Prat A. The blood-brain barrier. *Cold Spring Harb Perspect Biol* 2015; **7**(1): a020412.
65. Phelps CH. Barbiturate-induced glycogen accumulation in brain. An electron microscopic study. *Brain Res* 1972; **39**(1): 225-34.
66. Suh SW, Bergher JP, Anderson CM, Treadway JL, Fosgerau K, Swanson RA. Astrocyte glycogen sustains neuronal activity during hypoglycemia: studies with the glycogen phosphorylase inhibitor CP-316,819 ([R-R\*,S\*]-5-chloro-N-[2-hydroxy-3-(methoxymethylamino)-3-oxo-1-(phenylmethyl)propyl]-1H-indole-2-carboxamide). *J Pharmacol Exp Ther* 2007; **321**(1): 45-50.
67. Brown AM, Ransom BR. Astrocyte glycogen and brain energy metabolism. *Glia* 2007; **55**(12): 1263-71.
68. Rouach N, Koulakoff A, Abudara V, Willecke K, Giaume C. Astroglial metabolic networks sustain hippocampal synaptic transmission. *Science* 2008; **322**(5907): 1551-5.
69. Noble M, Murray K, Stroobant P, Waterfield MD, Riddle P. Platelet-derived growth factor promotes division and motility and inhibits premature differentiation of the oligodendrocyte/type-2 astrocyte progenitor cell. *Nature* 1988; **333**(6173): 560-2.
70. Richardson WD, Pringle N, Mosley MJ, Westermarck B, Dubois-Dalcq M. A role for platelet-derived growth factor in normal gliogenesis in the central nervous system. *Cell* 1988; **53**(2): 309-19.
71. Bögler O, Wren D, Barnett SC, Land H, Noble M. Cooperation between two growth factors promotes extended self-renewal and inhibits differentiation of oligodendrocyte-type-2 astrocyte (O-2A) progenitor cells. *Proc Natl Acad Sci U S A* 1990; **87**(16): 6368-72.
72. Sakurai Y, Nishimura D, Yoshimura K, Tsuruo Y, Seiwa C, Asou H. Differentiation of oligodendrocyte occurs in contact with astrocyte. *J Neurosci Res* 1998; **52**(1): 17-26.
73. Bhat S, Pfeiffer SE. Stimulation of oligodendrocytes by extracts from astrocyte-enriched cultures. *J Neurosci Res* 1986; **15**(1): 19-27.
74. Iacobas S, Iacobas DA. Astrocyte proximity modulates the myelination gene fabric of oligodendrocytes. *Neuron Glia Biology* 2010; **6**(3): 157-69.
75. Sorensen A, Moffat K, Thomson C, Barnett SC. Astrocytes, but not olfactory ensheathing cells or Schwann cells, promote myelination of CNS axons in vitro. *Glia* 2008; **56**(7): 750-63.

76. Bush TG, Puvanachandra N, Horner CH, et al. Leukocyte infiltration, neuronal degeneration, and neurite outgrowth after ablation of scar-forming, reactive astrocytes in adult transgenic mice. *Neuron* 1999; **23**(2): 297-308.
77. Faulkner JR, Herrmann JE, Woo MJ, Tansey KE, Doan NB, Sofroniew MV. Reactive astrocytes protect tissue and preserve function after spinal cord injury. *J Neurosci* 2004; **24**(9): 2143-55.
78. Haroon F, Drögemüller K, Händel U, et al. Gp130-dependent astrocytic survival is critical for the control of autoimmune central nervous system inflammation. *J Immunol* 2011; **186**(11): 6521-31.
79. Itoh N, Itoh Y, Tassoni A, et al. Cell-specific and region-specific transcriptomics in the multiple sclerosis model: Focus on astrocytes. *Proc Natl Acad Sci U S A* 2018; **115**(2): E302-e9.
80. Wheeler MA, Quintana FJ. Regulation of Astrocyte Functions in Multiple Sclerosis. *Cold Spring Harb Perspect Med* 2019; **9**(1).
81. Katsouri L, Birch AM, Renziehausen AWJ, et al. Ablation of reactive astrocytes exacerbates disease pathology in a model of Alzheimer's disease. *Glia* 2020; **68**(5): 1017-30.
82. Sofroniew MV. Molecular dissection of reactive astrogliosis and glial scar formation. *Trends Neurosci* 2009; **32**(12): 638-47.
83. Escartin C, Guillemaud O, Carrillo-de Sauvage MA. Questions and (some) answers on reactive astrocytes. *Glia* 2019; **67**(12): 2221-47.
84. Sofroniew MV. Astrocyte Reactivity: Subtypes, States, and Functions in CNS Innate Immunity. *Trends in immunology* 2020; **41**(9): 758-70.
85. Pekny M, Wilhelmsson U, Tatlisumak T, Pekna M. Astrocyte activation and reactive gliosis-A new target in stroke? *Neurosci Lett* 2019; **689**: 45-55.
86. Brosnan CF, Raine CS. The astrocyte in multiple sclerosis revisited. *Glia* 2013; **61**(4): 453-65.
87. Jha MK, Lee S, Park DH, et al. Diverse functional roles of lipocalin-2 in the central nervous system. *Neurosci Biobehav Rev* 2015; **49**: 135-56.
88. Brambilla R, Morton PD, Ashbaugh JJ, Karmally S, Lambertsen KL, Bethea JR. Astrocytes play a key role in EAE pathophysiology by orchestrating in the CNS the inflammatory response of resident and peripheral immune cells and by suppressing remyelination. *Glia* 2014; **62**(3): 452-67.
89. Barres BA, Koroshetz WJ, Chun LL, Corey DP. Ion channel expression by white matter glia: the type-1 astrocyte. *Neuron* 1990; **5**(4): 527-44.
90. Zamanian JL, Xu L, Foo LC, et al. Genomic analysis of reactive astrogliosis. *J Neurosci* 2012; **32**(18): 6391-410.
91. Liddelow SA, Guttenplan KA, Clarke LE, et al. Neurotoxic reactive astrocytes are induced by activated microglia. *Nature* 2017; **541**(7638): 481-7.
92. Escartin C, Galea E, Lakatos A, et al. Reactive astrocyte nomenclature, definitions, and future directions. *Nature neuroscience* 2021; **24**(3): 312-25.
93. Fitch MT, Silver J. Activated macrophages and the blood-brain barrier: inflammation after CNS injury leads to increases in putative inhibitory molecules. *Exp Neurol* 1997; **148**(2): 587-603.

94. Sofroniew MV. Astrocyte barriers to neurotoxic inflammation. *Nat Rev Neurosci* 2015; **16**(5): 249-63.
95. Wanner IB, Anderson MA, Song B, et al. Glial scar borders are formed by newly proliferated, elongated astrocytes that interact to corral inflammatory and fibrotic cells via STAT3-dependent mechanisms after spinal cord injury. *J Neurosci* 2013; **33**(31): 12870-86.
96. Gadea A, Schinelli S, Gallo V. Endothelin-1 regulates astrocyte proliferation and reactive gliosis via a JNK/c-Jun signaling pathway. *J Neurosci* 2008; **28**(10): 2394-408.
97. Rothhammer V, Borucki DM, Tjon EC, et al. Microglial control of astrocytes in response to microbial metabolites. *Nature* 2018; **557**(7707): 724-8.
98. Campos J, Guerra-Gomes S, Serra SC, et al. Astrocyte signaling impacts the effects of human bone marrow mesenchymal stem cells secretome application into the hippocampus: A proliferation and morphometrical analysis on astrocytic cell populations. *Brain Res* 2020; **1732**: 146700.
99. Neary JT, Zimmermann H. Trophic functions of nucleotides in the central nervous system. *Trends Neurosci* 2009; **32**(4): 189-98.
100. Levison SW, Jiang FJ, Stoltzfus OK, Ducceschi MH. IL-6-type cytokines enhance epidermal growth factor-stimulated astrocyte proliferation. *Glia* 2000; **32**(3): 328-37.
101. Colonna M, Butovsky O. Microglia Function in the Central Nervous System During Health and Neurodegeneration. *Annual review of immunology* 2017; **35**: 441-68.
102. Araki T, Ikegaya Y, Koyama R. The effects of microglia- and astrocyte-derived factors on neurogenesis in health and disease. *European Journal of Neuroscience* 2021; **54**(5): 5880-901.
103. Omari KM, John GR, Sealfon SC, Raine CS. CXC chemokine receptors on human oligodendrocytes: implications for multiple sclerosis. *Brain* 2005; **128**(5): 1003-15.
104. Williams A, Piaton G, Lubetzki C. Astrocytes--friends or foes in multiple sclerosis? *Glia* 2007; **55**(13): 1300-12.
105. Bannerman P, Hahn A, Soulika A, Gallo V, Pleasure D. Astroglialosis in EAE spinal cord: derivation from radial glia, and relationships to oligodendroglia. *Glia* 2007; **55**(1): 57-64.
106. Fawcett JW, Asher RA. The glial scar and central nervous system repair. *Brain Res Bull* 1999; **49**(6): 377-91.
107. Silver J, Miller JH. Regeneration beyond the glial scar. *Nature Reviews Neuroscience* 2004; **5**(2): 146-56.
108. Lau LW, Keough MB, Haylock-Jacobs S, et al. Chondroitin sulfate proteoglycans in demyelinated lesions impair remyelination. *Annals of neurology* 2012; **72**(3): 419-32.
109. Clemente D, Ortega MC, Melero-Jerez C, de Castro F. The effect of glia-glia interactions on oligodendrocyte precursor cell biology during development and in demyelinating diseases. *Frontiers in cellular neuroscience* 2013; **7**: 268-.
110. Bannerman P, Horiuchi M, Feldman D, et al. GluR2-free alpha-amino-3-hydroxy-5-methyl-4-isoxazolepropionate receptors intensify demyelination in experimental autoimmune encephalomyelitis. *Journal of neurochemistry* 2007; **102**(4): 1064-70.
111. Anderson MA, Burda JE, Ren Y, et al. Astrocyte scar formation aids central nervous system axon regeneration. *Nature* 2016; **532**(7598): 195-200.

112. Rolls A, Shechter R, Schwartz M. The bright side of the glial scar in CNS repair. *Nature Reviews Neuroscience* 2009; **10**(3): 235-41.
113. Voskuhl RR, Peterson RS, Song B, et al. Reactive astrocytes form scar-like perivascular barriers to leukocytes during adaptive immune inflammation of the CNS. *J Neurosci* 2009; **29**(37): 11511-22.
114. Cui W, Allen ND, Skynner M, Gusterson B, Clark AJ. Inducible ablation of astrocytes shows that these cells are required for neuronal survival in the adult brain. *Glia* 2001; **34**(4): 272-82.
115. Chen Y, Vartiainen NE, Ying W, Chan PH, Koistinaho J, Swanson RA. Astrocytes protect neurons from nitric oxide toxicity by a glutathione-dependent mechanism. *J Neurochem* 2001; **77**(6): 1601-10.
116. Haindl MT, Kock U, Zeitelhofer-Adzemovic M, Fazekas F, Hochmeister S. The formation of a glial scar does not prohibit remyelination in an animal model of multiple sclerosis. *Glia* 2019; **67**(3): 467-81.
117. Alliot F, Godin I, Pessac B. Microglia derive from progenitors, originating from the yolk sac, and which proliferate in the brain. *Brain Res Dev Brain Res* 1999; **117**(2): 145-52.
118. Nimmerjahn A, Kirchhoff F, Helmchen F. Resting microglia cells are highly dynamic surveillants of brain parenchyma in vivo. *Science* 2005; **308**: 5.
119. Davalos D, Grutzendler J, Yang G, et al. ATP mediates rapid microglial response to local brain injury in vivo. *Nat Neurosci* 2005; **8**(6): 752-8.
120. Tremblay M-È, Lowery RL, Majewska AK. Microglial Interactions with Synapses Are Modulated by Visual Experience. *PLOS Biology* 2010; **8**(11): e1000527.
121. Tremblay M, Stevens B, Sierra A, Wake H, Bessis A, Nimmerjahn A. The role of microglia in the healthy brain. *J Neurosci* 2011; **31**(45): 16064-9.
122. Kettenmann H, Kirchhoff F, Verkhratsky A. Microglia: new roles for the synaptic stripper. *Neuron* 2013; **77**(1): 10-8.
123. Umpierre AD, Bystrom LL, Ying Y, Liu YU, Worrell G, Wu LJ. Microglial calcium signaling is attuned to neuronal activity in awake mice. *eLife* 2020; **9**.
124. Kettenmann H, Hanisch UK, Noda M, Verkhratsky A. Physiology of microglia. *Physiological reviews* 2011; **91**(2): 461-553.
125. Verkhratsky A, Parpura V. Store-operated calcium entry in neuroglia. *Neuroscience Bulletin* 2014; **30**(1): 125-33.
126. Brawek B, Liang Y, Savitska D, et al. A new approach for ratiometric in vivo calcium imaging of microglia. *Scientific Reports* 2017; **7**(1): 6030.
127. Eichhoff G, Brawek B, Garaschuk O. Microglial calcium signal acts as a rapid sensor of single neuron damage in vivo. *Biochimica et Biophysica Acta (BBA) - Molecular Cell Research* 2011; **1813**(5): 1014-24.
128. Pozner A, Xu B, Palumbos S, Gee JM, Tvrdik P, Capecchi MR. Intracellular calcium dynamics in cortical microglia responding to focal laser injury in the PC::G5-tdT reporter mouse. *Frontiers in Molecular Neuroscience* 2015; **8**.
129. Hamilton SP, Rome LH. Stimulation of in vitro myelin synthesis by microglia. *Glia* 1994; **11**(4): 326-35.

130. Nicholas RS, Wing MG, Compston A. Nonactivated microglia promote oligodendrocyte precursor survival and maturation through the transcription factor NF-kappa B. *Eur J Neurosci* 2001; **13**(5): 959-67.
131. Nicholas RS, Stevens S, Wing MG, Compston DA. Microglia-derived IGF-2 prevents TNFalpha induced death of mature oligodendrocytes in vitro. *J Neuroimmunol* 2002; **124**(1-2): 36-44.
132. Pasquini LA, Millet V, Hoyos HC, et al. Galectin-3 drives oligodendrocyte differentiation to control myelin integrity and function. *Cell Death Differ* 2011; **18**(11): 1746-56.
133. Bohlen CJ, Bennett FC, Bennett ML. Isolation and Culture of Microglia. *Curr Protoc Immunol* 2019; **125**(1): e70-e.
134. Hanisch U-K, Kettenmann H. Microglia: active sensor and versatile effector cells in the normal and pathologic brain. *Nature Neuroscience* 2007; **10**(11): 1387-94.
135. Hickman SE, Kingery ND, Ohsumi TK, et al. The microglial sensome revealed by direct RNA sequencing. *Nat Neurosci* 2013; **16**(12): 1896-905.
136. Nakamura Y. Regulating factors for microglial activation. *Biol Pharm Bull* 2002; **25**(8): 945-53.
137. Block ML, Zecca L, Hong JS. Microglia-mediated neurotoxicity: uncovering the molecular mechanisms. *Nat Rev Neurosci* 2007; **8**(1): 57-69.
138. Karperien A, Ahammer H, Jelinek H. Quantitating the subtleties of microglial morphology with fractal analysis. *Frontiers in Cellular Neuroscience* 2013; **7**.
139. Li Q, Barres BA. Microglia and macrophages in brain homeostasis and disease. *Nat Rev Immunol* 2018; **18**(4): 225-42.
140. Stence N, Waite M, Dailey ME. Dynamics of microglial activation: a confocal time-lapse analysis in hippocampal slices. *Glia* 2001; **33**(3): 256-66.
141. Holloway OG, Canty AJ, King AE, Ziebell JM. Rod microglia and their role in neurological diseases. *Seminars in Cell & Developmental Biology* 2019; **94**: 96-103.
142. Koss K, Churchward MA, Tsui C, Todd KG. In Vitro Priming and Hyper-Activation of Brain Microglia: an Assessment of Phenotypes. *Molecular Neurobiology* 2019.
143. Hellwig S, Brioschi S, Dieni S, et al. Altered microglia morphology and higher resilience to stress-induced depression-like behavior in CX3CR1-deficient mice. *Brain Behav Immun* 2016; **55**: 126-37.
144. Sierra A, de Castro F, del Río-Hortega J, Rafael Iglesias-Rozas J, Garrosa M, Kettenmann H. The “Big-Bang” for modern glial biology: Translation and comments on Pío del Río-Hortega 1919 series of papers on microglia. *Glia* 2016; **64**(11): 1801-40.
145. Taylor SE, Morganti-Kossmann C, Lifshitz J, Ziebell JM. Rod Microglia: A Morphological Definition. *PLOS ONE* 2014; **9**(5): e97096.
146. Prinz M, Jung S, Priller J. Microglia Biology: One Century of Evolving Concepts. *Cell* 2019; **179**(2): 292-311.
147. Torres-Platas SG, Comeau S, Rachalski A, et al. Morphometric characterization of microglial phenotypes in human cerebral cortex. *J Neuroinflammation* 2014; **11**: 12.

148. Mrdjen D, Pavlovic A, Hartmann FJ, et al. High-Dimensional Single-Cell Mapping of Central Nervous System Immune Cells Reveals Distinct Myeloid Subsets in Health, Aging, and Disease. *Immunity* 2018; **48**(2): 380-95.e6.
149. Krasemann S, Madoe C, Cialic R, et al. The TREM2-APOE Pathway Drives the Transcriptional Phenotype of Dysfunctional Microglia in Neurodegenerative Diseases. *Immunity* 2017; **47**(3): 566-81.e9.
150. Voet S, Prinz M, van Loo G. Microglia in Central Nervous System Inflammation and Multiple Sclerosis Pathology. *Trends Mol Med* 2019; **25**(2): 112-23.
151. Singh S, Metz I, Amor S, van der Valk P, Stadelmann C, Brück W. Microglial nodules in early multiple sclerosis white matter are associated with degenerating axons. *Acta neuropathologica* 2013; **125**(4): 595-608.
152. Zrzavy T, Hametner S, Wimmer I, Butovsky O, Weiner HL, Lassmann H. Loss of 'homeostatic' microglia and patterns of their activation in active multiple sclerosis. *Brain* 2017; **140**(7): 1900-13.
153. Ponomarev ED, Maresz K, Tan Y, Dittel BN. CNS-Derived Interleukin-4 Is Essential for the Regulation of Autoimmune Inflammation and Induces a State of Alternative Activation in Microglial Cells. *The Journal of Neuroscience* 2007; **27**(40): 10714-21.
154. Butovsky O, Landa G, Kunis G, et al. Induction and blockage of oligodendrogenesis by differently activated microglia in an animal model of multiple sclerosis. *The Journal of Clinical Investigation* 2006; **116**(4): 905-15.
155. Yamasaki R, Lu H, Butovsky O, et al. Differential roles of microglia and monocytes in the inflamed central nervous system. *J Exp Med* 2014; **211**(8): 1533-49.
156. Wasser B, Luchtman D, Löffel J, et al. CNS-localized myeloid cells capture living invading T cells during neuroinflammation. *J Exp Med* 2020; **217**(6).
157. Zimmer H, Riese S, Régnier-Vigouroux A. Functional characterization of mannose receptor expressed by immunocompetent mouse microglia. *Glia* 2003; **42**(1): 89-100.
158. Wolf SA, Boddeke HW, Kettenmann H. Microglia in Physiology and Disease. *Annu Rev Physiol* 2017; **79**: 619-43.
159. Perry VH, Holmes C. Microglial priming in neurodegenerative disease. *Nature Reviews Neurology* 2014; **10**: 217.
160. Ramaglia V, Hughes TR, Donev RM, et al. C3-dependent mechanism of microglial priming relevant to multiple sclerosis. *Proceedings of the National Academy of Sciences of the United States of America* 2012; **109**(3): 965-70.
161. Haynes SE, Hollopeter G, Yang G, et al. The P2Y<sub>12</sub> receptor regulates microglial activation by extracellular nucleotides. *Nat Neurosci* 2006; **9**(12): 1512-9.
162. Liddelow SA, Marsh SE, Stevens B. Microglia and Astrocytes in Disease: Dynamic Duo or Partners in Crime? *Trends Immunol* 2020; **41**(9): 820-35.
163. Finsen B, Owens T. Innate immune responses in central nervous system inflammation. *FEBS Lett* 2011; **585**(23): 3806-12.
164. Jo M, Kim JH, Song GJ, Seo M, Hwang EM, Suk K. Astrocytic Orosomucoid-2 Modulates Microglial Activation and Neuroinflammation. *J Neurosci* 2017; **37**(11): 2878-94.



165. Skripuletz T, Hackstette D, Bauer K, et al. Astrocytes regulate myelin clearance through recruitment of microglia during cuprizone-induced demyelination. *Brain* 2013; **136**(Pt 1): 147-67.
166. Tarassishin L, Suh H-S, Lee SC. LPS and IL-1 differentially activate mouse and human astrocytes: role of CD14. *Glia* 2014; **62**(6): 999-1013.
167. Sun M, Yan H, Zou W, Wang Y, Li H, Wang X. [Lipopolysaccharide induces astrocyte activation and downregulates the expression of Kir4.1 channel]. *Xi Bao Yu Fen Zi Mian Yi Xue Za Zhi* 2016; **32**(2): 196-200.
168. Sternson SM, Roth BL. Chemogenetic Tools to Interrogate Brain Functions. *Annual Review of Neuroscience* 2014; **37**(1): 387-407.
169. Roth BL. DREADDs for Neuroscientists. *Neuron* 2016; **89**(4): 683-94.
170. Armbruster BNL, X.; Pausch, M.H.; Herlitze, S.; Roth, B.L. Evolving the lock to fit the key to create a family of G protein-coupled receptors potently activated by an inert ligand. *PNAS* 2007; **104**(12): 5163-8.
171. Guettier J-M, Gautam D, Scarselli M, et al. A chemical-genetic approach to study G protein regulation of  $\beta$  cell function in vivo. *Proceedings of the National Academy of Sciences* 2009; **106**(45): 19197-202.
172. Nakajima K, Wess J. Design and functional characterization of a novel, arrestin-biased designer G protein-coupled receptor. *Mol Pharmacol* 2012; **82**(4): 575-82.
173. Jendryka M, Palchadhuri M, Ursu D, et al. Pharmacokinetic and pharmacodynamic actions of clozapine-N-oxide, clozapine, and compound 21 in DREADD-based chemogenetics in mice. *Scientific reports* 2019; **9**(1): 4522-.
174. Chen X, Choo H, Huang XP, et al. The first structure-activity relationship studies for designer receptors exclusively activated by designer drugs. *ACS Chem Neurosci* 2015; **6**(3): 476-84.
175. Smith KS, Bucci DJ, Luikart BW, Mahler SV. DREADDS: Use and application in behavioral neuroscience. *Behav Neurosci* 2016; **130**(2): 137-55.
176. Shen W, Chen S, Liu Y, Han P, Ma T, Zeng LH. Chemogenetic manipulation of astrocytic activity: Is it possible to reveal the roles of astrocytes? *Biochem Pharmacol* 2021; **186**: 114457.
177. Grace PM, Wang X, Strand KA, et al. DREADDED microglia in pain: Implications for spinal inflammatory signaling in male rats. *Exp Neurol* 2018; **304**: 125-31.
178. Tsai HH, Li H, Fuentealba LC, et al. Regional astrocyte allocation regulates CNS synaptogenesis and repair. *Science* 2012; **337**(6092): 358-62.
179. Bettelli E, Pagany M, Weiner HL, Lington C, Sobel RA, Kuchroo VK. Myelin oligodendrocyte glycoprotein-specific T cell receptor transgenic mice develop spontaneous autoimmune optic neuritis. *The Journal of experimental medicine* 2003; **197**(9): 1073-81.
180. Loschko J, Rieke GJ, Schreiber HA, et al. Inducible targeting of cDCs and their subsets in vivo. *J Immunol Methods* 2016; **434**: 32-8.
181. Zhu H, Aryal DK, Olsen RH, et al. Cre-dependent DREADD (Designer Receptors Exclusively Activated by Designer Drugs) mice. *Genesis* 2016; **54**(8): 439-46.
182. Schindelin J, Arganda-Carreras I, Frise E, et al. Fiji: an open-source platform for biological-image analysis. *Nature Methods* 2012; **9**(7): 676-82.

183. Zhu H, Aryal DK, Olsen RHJ, et al. Cre-dependent DREADD (Designer Receptors Exclusively Activated by Designer Drugs) mice. *Genesis* 2016; **54**(8): 439-46.
184. Gogolla N, Galimberti I, DePaola V, Caroni P. Preparation of organotypic hippocampal slice cultures for long-term live imaging. *Nature Protocols* 2006; **1**(3): 1165-71.
185. De Simoni A, Griesinger CB, Edwards FA. Development of Rat CA1 Neurons in Acute Versus Organotypic Slices: Role of Experience in Synaptic Morphology and Activity. *J Physiol* 2003; **550**(1): 135-47.
186. Delekate A, Füchtmeier M, Schumacher T, Ulbrich C, Foddiss M, Petzold GC. Metabotropic P2Y1 receptor signalling mediates astrocytic hyperactivity in vivo in an Alzheimer's disease mouse model. *Nature communications* 2014; **5**: 5422.
187. Martín R, Bajo-Grañeras R, Moratalla R, Perea G, Araque A. Circuit-specific signaling in astrocyte-neuron networks in basal ganglia pathways. *Science* 2015; **349**(6249): 730-4.
188. Morquette P, Verdier D, Kadala A, et al. An astrocyte-dependent mechanism for neuronal rhythmogenesis. *Nature Neuroscience* 2015; **18**(6): 844-54.
189. Nimmerjahn A, Mukamel EA, Schnitzer MJ. Motor behavior activates Bergmann glial networks. *Neuron* 2009; **62**(3): 400-12.
190. Tischbirek C, Birkner A, Jia H, Sakmann B, Konnerth A. Deep two-photon brain imaging with a red-shifted fluorometric Ca<sup>2+</sup> indicator. *J Proceedings of the National Academy of Sciences* 2015; **112**(36): 11377-82.
191. Schnell C, Shahmoradi A, Wichert SP, et al. The multispecific thyroid hormone transporter OATP1C1 mediates cell-specific sulforhodamine 101-labeling of hippocampal astrocytes. *Brain Structure and Function* 2015; **220**(1): 193-203.
192. Nimmerjahn A, Kirchhoff F, Kerr JN, Helmchen F. Sulforhodamine 101 as a specific marker of astroglia in the neocortex in vivo. *Nat Methods* 2004; **1**(1): 31-7.
193. Elmore Monica RP, Najafi Allison R, Koike Maya A, et al. Colony-Stimulating Factor 1 Receptor Signaling Is Necessary for Microglia Viability, Unmasking a Microglia Progenitor Cell in the Adult Brain. *Neuron* 2014; **82**(2): 380-97.
194. Elmore MR, Lee RJ, West BL, Green KN. Characterizing newly repopulated microglia in the adult mouse: impacts on animal behavior, cell morphology, and neuroinflammation. *PLoS One* 2015; **10**(4): e0122912.
195. Dagher NN, Najafi AR, Kayala KM, et al. Colony-stimulating factor 1 receptor inhibition prevents microglial plaque association and improves cognition in 3xTg-AD mice. *J Neuroinflammation* 2015; **12**: 139.
196. Knapp PE. The cell cycle of glial cells grown in vitro: an immunocytochemical method of analysis. *J Histochem Cytochem* 1992; **40**(9): 1405-11.
197. Sun F, Li N, Tong X, et al. Ara-c induces cell cycle G1/S arrest by inducing upregulation of the INK4 family gene or directly inhibiting the formation of the cell cycle-dependent complex CDK4/cyclin D1. *Cell Cycle* 2019; **18**(18): 2293-306.
198. Kitagawa J, Hara T, Tsurumi H, et al. Cell cycle-dependent priming action of granulocyte colony-stimulating factor (G-CSF) enhances in vitro apoptosis induction by cytarabine and etoposide in leukemia cell lines. *J Clin Exp Hematop* 2010; **50**(2): 99-105.

199. Chehrehasa F, Meedeniya AC, Dwyer P, Abrahamsen G, Mackay-Sim A. EdU, a new thymidine analogue for labelling proliferating cells in the nervous system. *J Neurosci Methods* 2009; **177**(1): 122-30.
200. Stoppini L, Buchs PA, Muller D. A simple method for organotypic cultures of nervous tissue. *J Neurosci Methods* 1991; **37**(2): 173-82.
201. Gerlach J, Donkels C, Münzner G, Haas CA. Persistent Gliosis Interferes with Neurogenesis in Organotypic Hippocampal Slice Cultures. *Frontiers in cellular neuroscience* 2016; **10**: 131-.
202. Hennessy E, Griffin ÉW, Cunningham C. Astrocytes Are Primed by Chronic Neurodegeneration to Produce Exaggerated Chemokine and Cell Infiltration Responses to Acute Stimulation with the Cytokines IL-1 $\beta$  and TNF- $\alpha$ . *The Journal of Neuroscience* 2015; **35**(22): 8411-22.
203. Suzuki T, Sakata H, Kato C, Connor JA, Morita M. Astrocyte activation and wound healing in intact-skull mouse after focal brain injury. *Eur J Neurosci* 2012; **36**(12): 3653-64.
204. Li H, Zhang N, Lin H-Y, et al. Histological, cellular and behavioral assessments of stroke outcomes after photothrombosis-induced ischemia in adult mice. *BMC Neurosci* 2014; **15**: 58-.
205. Choudhury GR, Ding S. Reactive astrocytes and therapeutic potential in focal ischemic stroke. *Neurobiol Dis* 2016; **85**: 234-44.
206. Created with [Biorender.com](https://www.biorender.com).
207. Buffo A, Rite I, Tripathi P, et al. Origin and progeny of reactive gliosis: A source of multipotent cells in the injured brain. *Proceedings of the National Academy of Sciences of the United States of America* 2008; **105**(9): 3581-6.
208. Coleman LG, Jr., Zou J, Crews FT. Microglial depletion and repopulation in brain slice culture normalizes sensitized proinflammatory signaling. *J Neuroinflammation* 2020; **17**(1): 27.
209. Giordano KR, Denman CR, Dubisch PS, Akhter M, Lifshitz J. An update on the rod microglia variant in experimental and clinical brain injury and disease. *Brain Commun* 2021; **3**(1): fcaa227-fcaa.
210. Jha MK, Jo M, Kim JH, Suk K. Microglia-Astrocyte Crosstalk: An Intimate Molecular Conversation. *Neuroscientist* 2019; **25**(3): 227-40.
211. Zuchero JB, Barres BA. Glia in mammalian development and disease. *Development* 2015; **142**(22): 3805-9.
212. Allen NJ, Lyons DA. Glia as architects of central nervous system formation and function. *Science (New York, NY)* 2018; **362**(6411): 181-5.
213. Chen SH, Oyarzabal EA, Sung YF, et al. Microglial regulation of immunological and neuroprotective functions of astroglia. *Glia* 2015; **63**(1): 118-31.
214. Iizumi T, Takahashi S, Mashima K, et al. A possible role of microglia-derived nitric oxide by lipopolysaccharide in activation of astroglial pentose-phosphate pathway via the Keap1/Nrf2 system. *J Neuroinflammation* 2016; **13**(1): 99.
215. Hou L, Zhou X, Zhang C, et al. NADPH oxidase-derived H<sub>2</sub>O<sub>2</sub> mediates the regulatory effects of microglia on astrogliosis in experimental models of Parkinson's disease. *Redox Biol* 2017; **12**: 162-70.

216. Norden DM, Fenn AM, Dugan A, Godbout JP. TGF $\beta$  produced by IL-10 redirected astrocytes attenuates microglial activation. *Glia* 2014; **62**(6): 881-95.
217. Hammond TR, Gadea A, Dupree J, et al. Astrocyte-derived endothelin-1 inhibits remyelination through notch activation. *Neuron* 2014; **81**(3): 588-602.
218. Prajeeth CK, Löhr K, Floess S, et al. Effector molecules released by Th1 but not Th17 cells drive an M1 response in microglia. *Brain Behav Immun* 2014; **37**: 248-59.
219. Prajeeth CK, Kronisch J, Khoroooshi R, et al. Effectors of Th1 and Th17 cells act on astrocytes and augment their neuroinflammatory properties. *J Neuroinflammation* 2017; **14**(1): 204.
220. Trajkovic V, Vuckovic O, Stosic-Grujicic S, et al. Astrocyte-induced regulatory T cells mitigate CNS autoimmunity. *Glia* 2004; **47**(2): 168-79.
221. Le Thuc O, Blondeau N, Nahon JL, Rovère C. The complex contribution of chemokines to neuroinflammation: switching from beneficial to detrimental effects. *Ann NY Acad Sci* 2015; **1351**: 127-40.
222. Xu J, Dong H, Qian Q, et al. Astrocyte-derived CCL2 participates in surgery-induced cognitive dysfunction and neuroinflammation via evoking microglia activation. *Behavioural Brain Research* 2017; **332**: 145-53.
223. Grace PM, Strand KA, Galer EL, et al. Morphine paradoxically prolongs neuropathic pain in rats by amplifying spinal NLRP3 inflammasome activation. *Proceedings of the National Academy of Sciences* 2016; **113**(24): E3441-E50.
224. Yi MH, Liu YU, Liu K, et al. Chemogenetic manipulation of microglia inhibits neuroinflammation and neuropathic pain in mice. *Brain Behav Immun* 2021; **92**: 78-89.
225. Binning W, Hogan-Cann AE, Yae Sakae D, et al. Chronic hM3Dq signaling in microglia ameliorates neuroinflammation in male mice. *Brain Behav Immun* 2020.
226. Saika F, Matsuzaki S, Kobayashi D, et al. Chemogenetic Regulation of CX3CR1-Expressing Microglia Using Gi-DREADD Exerts Sex-Dependent Anti-Allodynic Effects in Mouse Models of Neuropathic Pain. *Front Pharmacol* 2020; **11**: 925-.
227. Franke K, Kalucka J, Mamlouk S, et al. HIF-1 $\alpha$  is a protective factor in conditional PHD2-deficient mice suffering from severe HIF-2 $\alpha$ -induced excessive erythropoiesis. *Blood* 2013; **121**(8): 1436-45.
228. Abram CL, Roberge GL, Hu Y, Lowell CA. Comparative analysis of the efficiency and specificity of myeloid-Cre deleting strains using ROSA-EYFP reporter mice. *J Immunol Methods* 2014; **408**: 89-100.
229. Zhang B, Zou J, Han L, et al. The specificity and role of microglia in epileptogenesis in mouse models of tuberous sclerosis complex. *Epilepsia* 2018; **59**(9): 1796-806.
230. Zhao X-F, Alam MM, Liao Y, et al. Targeting Microglia Using Cx3cr1-Cre Lines: Revisiting the Specificity. *eNeuro* 2019; **6**(4): ENEURO.0114-19.2019.
231. Nimmerjahn A. Two-photon imaging of microglia in the mouse cortex in vivo. *Cold Spring Harb Protoc* 2012; **2012**(5).
232. Huang H, Tohme S, Al-Khafaji AB, et al. Damage-associated molecular pattern-activated neutrophil extracellular trap exacerbates sterile inflammatory liver injury. *Hepatology* 2015; **62**(2): 600-14.

233. Doorn KJ, Goudriaan A, Blits-Huizinga C, et al. Increased amoeboid microglial density in the olfactory bulb of Parkinson's and Alzheimer's patients. *Brain Pathol* 2014; **24**(2): 152-65.
234. Kreutzberg GW. Microglia: a sensor for pathological events in the CNS. *Trends in Neurosciences* 1996; **19**(8): 312-8.
235. Leyh J, Paeschke S, Mages B, et al. Classification of Microglial Morphological Phenotypes Using Machine Learning. *Frontiers in cellular neuroscience* 2021; **15**: 701673-.
236. Ziebell JM, Taylor SE, Cao T, Harrison JL, Lifshitz J. Rod microglia: elongation, alignment, and coupling to form trains across the somatosensory cortex after experimental diffuse brain injury. *Journal of Neuroinflammation* 2012; **9**(1): 247.
237. Ziebell JM, Ray-Jones H, Lifshitz J. Nogo presence is inversely associated with shifts in cortical microglial morphology following experimental diffuse brain injury. *Neuroscience* 2017; **359**: 209-23.
238. Bachstetter AD, Ighodaro ET, Hassoun Y, et al. Rod-shaped microglia morphology is associated with aging in 2 human autopsy series. *Neurobiology of Aging* 2017; **52**: 98-105.
239. Tam WY, Ma CH. Bipolar/rod-shaped microglia are proliferating microglia with distinct M1/M2 phenotypes. *Sci Rep* 2014; **4**: 7279.
240. Williams K, Bar-Or A, Ulvestad E, Olivier A, Antel JP, Yong VW. Biology of adult human microglia in culture: comparisons with peripheral blood monocytes and astrocytes. *J Neuropathol Exp Neurol* 1992; **51**(5): 538-49.
241. Smith D, Brooks D, Wohlgelegen E, Rau T, Poulsen D. Temporal and Spatial Changes in the Pattern of Iba1 and CD68 Staining in the Rat Brain Following Severe Traumatic Brain Injury. *Modern Research in Inflammation* 2015; **04**(02): 9-23.
242. Hoffmann A, Kann O, Ohlemeyer C, Hanisch U-K, Kettenmann H. Elevation of basal intracellular calcium as a central element in the activation of brain macrophages (microglia): suppression of receptor-evoked calcium signaling and control of release function. *The Journal of neuroscience : the official journal of the Society for Neuroscience* 2003; **23**(11): 4410-9.
243. Färber K, Kettenmann H. Functional role of calcium signals for microglial function. *Glia* 2006; **54**(7): 656-65.
244. Korvers L, de Andrade Costa A, Mersch M, Matyash V, Kettenmann H, Semtner M. Spontaneous Ca<sup>2+</sup> transients in mouse microglia. *Cell Calcium* 2016; **60**(6): 396-406.
245. Toulme E, Khakh BS. Imaging P2X<sub>4</sub> Receptor Lateral Mobility in Microglia. *Journal of Biological Chemistry* 2012; **287**(18): 14734-48.

## VIII Appendix

### 1 List of figures

Figure 1: Interplay of CNS resident and invading peripheral immune cells in MS..	2
Figure 2: Diversity of astrocytic triggers and responses.....	5
Figure 3: Diversity of microglia morphologies found in the human CNS .....	10
Figure 4: Microglia function under homeostatic conditions and MS. ....	12
Figure 5: Available DREADD constructs and their ligands.....	17
Figure 6: Ara-C inhibits cell proliferation in all cells in OHSCs. ....	35
Figure 7: Injury size but not depth varies between different laser power settings .....	41
Figure 8: Fluctuation in MP5 laser power output over the experimental time course.....	42
Figure 9: Glial activation increases in response to AFMI in OHSCs .....	47
Figure 10: AFMI induces glial scar formation and increases astrocytic proliferation. ....	49
Figure 11: EdU <sup>+</sup> cells increase in injured slices at 7 dpi. ....	51
Figure 12: Influence of microglia depletion and T cell infiltration on astrocytic proliferation after AFMI .....	53
Figure 13: Astrocytes are not affected by PLX mediated microglia depletion.....	55
Figure 14: EdU <sup>+</sup> cells are increased by Th17 cells and decreased by PLX treatment in OHSCs .....	56
Figure 15: Characterization of a chemogenetic DREADD <sub>Gq</sub> construct expressed under a CSF1R promotor.....	57
Figure 16: Morphological changes in DREADD-activated microglia after CNO treatment...	60
Figure 17: Influence of microglia and astrocyte crosstalk on immune cell invasion and de-remyelination. ....	64
Figure 18: Schematic representations of microglia morphologies observed in health and disease 206 .....	68

## 2 List of tables

Table 1: Laser injury model parameters in published literature .....	14
Table 2: Laboratory equipment.....	20
Table 3: Microscopes.....	20
Table 4: MP5 two photon microscope set up.....	21
Table 5: Laboratory consumables .....	21
Table 6: Chemicals and reagents .....	22
Table 7: Commercially obtained buffers, solutions and media .....	23
Table 8: Custom made buffers, solutions and media.....	23
Table 9: Commercial kits.....	24
Table 10: Magnetic beads .....	24
Table 11: Cell culture cytokines .....	24
Table 12: Immunohistochemistry – primary antibodies .....	25
Table 13: Immunohistochemistry – secondary antibodies.....	25
Table 14: FACS antibodies.....	26
Table 15: Laboratory mouse strains.....	27
Table 16: Software.....	28
Table 17: Keyence microscope settings.....	36
Table 18: Confocal microscope settings .....	37
Table 19: Laser power intensities used in AFMI experiments.. ..	43
Table 20: DREADD microglia morphology frequencies. ....	60

### 3 Curriculum vitae

#### Personal Data

Name: Miriam Johanna Schillner  
Address: Platanenstr. 24, 55129 Mainz  
E-mail: miriamschillner@gmx.de  
Phone: 0176 83084317  
Date of birth: 17.10.1992  
Place of birth: Vorwerk (Ldkrs. Rotenburg an der Wümme)  
Nationality: German

#### Academic Career

Since 11/2017 **JGU Mainz, University Medical Center, Department of Neurology  
Experimental Neuroimmunology, Prof. Dr.Stefan Bittner**  
Doctoral studies on “Microglia activation drives astrocytic response towards  
CNS damage and inflammation”  
Main methods: Organotypic hippocampal slice cultures,  
immunohistochemistry, two photon and confocal microscopy

04/2017-10/2017 **JGU Mainz, University Medical Center, Department of Neurology**  
Master Thesis on: “Characterization of RiboTracker mice crossed with  
different Cre reporter lines to investigate axonal ribosome localization in  
relation to axon injury” (Grade: 1.0)  
Main methods: Immunohistochemistry, confocal microscopy

10/2015-10/2017 **Goethe University Frankfurt am Main**  
International master’s program “Interdisciplinary Neuroscience”  
Practical Courses: Clinical Neuroimaging, Studying Human Cognition with  
MEG, Non-invasive Methods in Human Cognition Research, Brain Damage  
and Neuroprotection  
Graduation: M.Sc in October 2017 (Overall grade: 1.1)

10/2011 – 08/2014 **University of Bremen**  
Bachelor of Science “Biology”  
Bachelor Thesis at the Institute for Theoretical Neurobiology, AG Prof. Dr.  
Kreiter  
Topic: “Training of a macaque monkey on a feature change detection task  
using a Posner Paradigm” (Grade: 1.3)  
Main methods: Behavioral training, MATLAB programming  
Graduation: B.Sc in august 2014 (Overall grade: 2.0)

08/2008 – 08/2011 **Abitur at the Gymnasium an der Hamburgerstraße, Bremen**  
Examination subjects: German, Biology, English, Pedagogy Overall mark:  
1.7

#### Congress participations

11/2021 Neurowind 2021, online conference „Therapeutic Treg transfer shifts CNS  
myeloid cells toward a homeostatic phenotype“

07/2021 Glia 2021, online conference

07/2019 Glia 2019, Porto Portugal

10/2018 ECTRIMS 2018, Berlin Germany

06/2018 rmn<sup>2</sup> 2018, Oberwesel Germany „Axonal ribosome localization and transfer  
in relation to axon injury“



## **Skills**

Language skills:

German: Native language

English: Fluent (Level C1)

IT skills:

Microsoft: Word, Excel, Power Point

Adobe: Photoshop, Illustrator

LAS AF Lite

BZI Analyzer

Fiji

MatLab

Graph Prism

Imaris

Partek Flow

Lab Skills:

Tissue sectioning – Cryotom and Vibratom Immunohistochemistry

Animal handling and experiments (FELASA B equivalent)

Cell Culture

Confocal microscopy

Two-photon microscopy

Fast resonance calcium imaging

RNA sequencing